MODIFICATIONS OF GE DOTS ON SI (001) SUBSTRATES: C-PREDEPOSITION AND SI OVERGROWTH

THÈSE N^{O} 3103 (2004)

PRÉSENTÉE À LA FACULTÉ SCIENCES DE BASE

Institut de physique des nanostructures

SECTION DE PHYSIQUE

ÉCOLE POLYTECHNIQUE FÉDÉRALE DE LAUSANNE

POUR L'OBTENTION DU GRADE DE DOCTEUR ÈS SCIENCES

PAR

Olaf KIRFEL

Diplom-Physiker, Universität Oldenburg, Allemagne
et de nationalité allemande

acceptée sur proposition du jury:

Prof. K. Kern, directeur de thèse
Prof. A. Fiore, rapporteur
Dr D. Grützmacher, rapporteur
Prof. H. von Känel, rapporteur

Lausanne, EPFL
2005

Zusammenfassung

Silizium ist dank seiner besonderen Eigenschaften wie zum Beispiel der guten Wärmeleitfähigkeit und der guten Qualität seines Oxides zu dem wichtigsten Material für die Halbleiterindustrie geworden. Nichtsdestotrotz haben die Einschränkungen, die durch die indirekte Bandlücke bedingt sind, den Durchbruch für optisch-elektronische Anwendungen verhindert. Um die Wahrscheinlichkeit für strahlende Rekombination zu erhöhen, kann man das Heisenberg'sche Unschärfeprinzip ausnutzen. Wenn Ladungsträger in einem Quantentopf eingeschlossen werden, führt dies zu einer Verbreiterung der Wellenfunktion im reziproken Raum, was die Wahrscheinlichkeit für strahlende Rekombination erhöht. Für Silizium erreicht man dies mit dem Wachstum von Germanium, welches im Stranski-Krastanov-Modus auf einer Siliziumoberfläche wächst; wenn die Benetzungsschicht eine Dicke von 3 bis 5 Monolagen übersteigt, formen sich Ge Insel, welche als Quantentöpfen in einer Siliziummatrix dienen können. Während Defektelektronen des Valenzbandes in diesen Quantentöpfen eingesperrt werden, agiert das die Inseln umgebende Silizium, das unter leichter Zugspannung steht, als Quantentopf für die Elektronen des Leitungsbandes.

Entscheidende Parameter für die Beschränkung der Ladungsträger und somit für die Wahrscheinlichkeit der strahlenden Rekombination sind die Dichte, Größe und Zusammensetzung der Inseln. Eine Möglichkeit die Dichte und Größe der Ge-Inseln zu beeinflussen ist das Vorabwachstum von Kohlenstoff. Das Wachsen von Submonolagen von Kohlenstoff führt zu einer c(4x4)-Rekonstruktion derjenigen Teile der Oberfläche, in die Kohlenstoff eingebaut wird. Wenn Ge auf solch modifizierten Oberflächen gewachsen wird, wächst es aufgrund der durch den Kohlenstoff verursachten Spannungsfluktuationen in den Bereichen, die kohlenstofffrei sind. Dies führt von Anbeginn an zu einem dreidimensionalen Wachstum von Germanium, womit kleinere Inseln und eine höhere Dichte erreicht werden können. Da diese beiden Größen von der Dichte und der Größe der Flächen mit c(4x4)-Rekonstruktion abhängen, wurde die Modifikation von Silizium-Oberflächen mit Hilfe der Abscheidung von Submonolagen von Kohlenstoff mit einem Scanning Tunnelling Microscope (STM) untersucht. Als Resultat wurde gefunden, dass die Abscheidung von 0.11 ML bis 0.2 ML von Kohlenstoff den besten Kompromiss zwischen Dichte und Größe der Flächen mit c(4x4)-Rekonstruktion darstellt. Desweiteren wurden

kohlenstoffinduzierte Ge Inseln anhand von Photolumineszenzspektroskopie untersucht. Es wurde gefunden, dass die Wahrscheinlichkeit für strahlende Rekombination im Vergleich zu Inseln auf nichtmodifizierten Oberflächen deutlich erhöht ist.

Wie bereits erwähnt ist neben der Größe und der Dichte die Zusammensetzung der Inseln ebenso von Wichtigkeit. Unsere STM-Untersuchungen ergaben, dass das Überwachsen von Ge-Inseln mit Silizium, um die Ge-Inseln in eine Matrix einzubetten, bei hohen Wachstumstemperaturen zu unerwünschtem Durchmischen und im Falle von Dome-Inseln sogar zu einer Transformation derselben zu Hut-Inseln führt. Diese Beobachtungen sind mit energiegefilterter Elektronen Transmissionsspektroskopie verifiziert worden, wobei zusätzlich die Bereiche der Inseln, die am stärksten durchmischen, bestimmt wurden. Für eine quantitative Analyse wurden Röntgenbeugungsuntersuchungen an den Proben durchgeführt, bei denen die Intensität im reziproken Raum gemessen wurde. Die Simulation der Intensitätsverteilung gab im Rahmen der Beschränkungen des verwendeten Modells einen Einblick in die Zusammensetzung der Inseln.

Um die Durchmischung der Inseln während des Überwachsens zu verringern, wurde die Wachstumstemperatur für die Si-Deckschicht reduziert. Es wurde bei den STM-Untersuchungen dieser Proben keine Transformation von Dome- zu Hut-Inseln gefunden, was eine reduzierte Durchmischung andeutet, jedoch führte die Abscheidung von 3 bzw. 5 Monolagen von Si zur Entstehung von neuen Inseln, deren Ursprung noch nicht vollständig geklärt ist. Um das Konzept der Temperaturabsenkung für die Si-Deckschicht zur Verringerung der Durchmischung für komplette Bauelemente zu überprüfen, wurden zwei Stapel von Inseln gewachsen, einer mit hoher und einer mit niedriger Überwachstumstemperatur, die mit Photolumineszenzspektroskopie charakterisiert wurden. Die Ergebnisse induzieren, dass die Durchmischung der Ge-Inseln mit Si nicht nur während der ersten Schritte des Überwachsen durch ein Absenken der Überwachstumstemperatur verringert werden kann, sonder auch für komplette Stapel von Inseln, wie sie zur Realisierung von Bauelementen notwendig wären.

Abstract

Silicon has become the most important material for the semiconductor industry, due to several advantages like good heat conductance or the high quality of its oxide. Nevertheless, for opto-electronic devices, the limitation of its indirect band-gap has anticipated a breakthrough. To increase the probability for radiative recombination, one way is to use Heisenberg's uncertainty principle. If the carriers are confined in a quantum well, this leads to a broadening of the wave functions in reciprocal space, and a higher probability for recombination processes. For Si, this can be achieved by the deposition of Ge, as this material grows on a silicon surface in Stranski-Krastanov mode. After the formation of a 3-5 monolayer (ML) thick wetting-layer, Ge dots form which can act as quantum wells within a Si matrix. While holes of the valance band are confined in these dots, the silicon surrounding the Ge dots is under tensile strain and therefore acts as a slight quantum well for the electrons of the conductance band. Crucial parameters for the confinement of the carriers and therefore of the probability for radiative recombination are the density, size, and composition of the dots. One way to influence the density and size of Ge dots is to modify the Si surface by the pre-deposition of carbon. The deposition of submonolayers of carbon leads to a c(4x4) reconstruction of those parts of the surface, the carbon is incorporated in. If Ge is deposited on such modified surfaces, it starts to grow on the c(4x4) free areas, due to the strain induced by the carbon. As a result Ge grows directly in a three-dimensional way, and smaller dot sizes and higher densities can be achieved. As these physical values depend on the size and density of the c(4x4) reconstructed areas, the modification of the Si surface by the pre-deposition of carbon was studied by Scanning Tunnelling Microscopy (STM). It was found, that the deposition between 0.11 ML and 0.2 ML of carbon leads to the best compromise between density and size of c(4x4) reconstructed areas. In addition we studied the carbon induced Ge dots by photoluminescence spectroscopy. The intensity of the photoluminescence signal indicates an increase for the probability of no-phonon-assisted recombination.

Besides the size and density, the composition is, as already mentioned, of importance. We found by STM that due to capping of Ge-dots with Si, as it is necessary to embed them in a Si matrix, at high temperatures unwanted intermixing occurs. That can even lead to a shape transformation from dome to hut clusters. This observation was proven by Energy Filtered Transmission Electron Microscopy giving the information, which

parts of the dots intermix strongest. For a quantitative analyses, reciprocal space maps were measured with x-ray diffraction measurement. The simulation of these space maps gave a quantitative insight into the composition of the dots under its restrictions. To prevent the intermixing, the growth temperature for the silicon cap was lowered. Afterwards no shape transformation was found by STM, but during the initial steps of overgrowing (3 ML of Si), another type of cluster appeared, whose origin has not fully been understood yet. To proof the concept of growth temperature reduction for whole devices, two stacks of Ge dots, one overgrown at high temperature and one at low temperature, were investigated by photoluminescence investigations. They gave a hint, that the lowering of the overgrowth not only prevents the intermixing during the initial stages of overgrowth, as investigated before, but also when the dots are completely overgrown.

Table of contents

1 Introduction 3
2 Basic considerations 7
  2.1 Growth modes 7
  2.2 The Si(001) surface 9
  2.3 Ge wetting layer 11
  2.4 Ge islands 13
  2.5 Composition of Ge-dots 15
    2.5.1 Volume interdiffusion 15
    2.5.2 Surface diffusion 17
  2.6 Overgrowth of Ge dots 20
3 Deposition and characterization methods 23
  3.1 Epitaxy system at the Paul Scherrer Institut 23
  3.2 Sample preparation 25
  3.3 Scanning tunnelling microscopy 26
  3.4 X-ray diffraction measurements 30
  3.5 Transmission electron microscopy 35
  3.6 Photoluminescence 38
4 Ge dots on a silicon (001) surface 45
  4.1 Growth parameters 45
  4.2 Reproducibility 49
  4.3 Summary 50
5 Ge dots on carbon modified surfaces 53
  5.1 Pre-deposition of carbon 53
    5.1.1 Calibration of the carbon source 54
    5.1.2 Model of C-induced surface reconstruction 55
    5.1.3 Surface reconstruction depending on amount of deposited carbon 60
  5.2 Ge dots on Si surfaces with carbon pre-deposition 64
  5.3 Conclusions 70
6 Overgrowth of Ge dots 73
  6.1 Initial stage of overgrowth 73
  6.2 High temperature overgrown dots 75
    6.2.1 Analysis by scanning tunnelling microscopy 75
    6.2.2 Transmission electron microscopy 79
    6.2.3 X-Ray diffractometry 82
    6.2.4 Summary 93
  6.3 Overgrowth of Ge dots at low temperatures 93
    6.3.1 STM investigations 94
    6.3.2 Photoluminescence results 98
    6.3.3 Summary 104
7 Summary 105

1 Introduction

Silicon has developed for the semiconductor industry to the most important material for electronic devices, as it has numerous advantages, like e.g. the low density of states [1-3] or the good quality of its oxide, which allows to build high mobility channels [4,5]. Besides this, the high heat conductance and the large knowledge of handling silicon has made it possible to obtain a high integration of transistors with small dimension on silicon wafers, which is a prerequisite for commercial uses.

On the other hand, Si has some limitations, which do hamper the realization of high frequency or optical devices. For optical devices the indirect band-gap is the limitation. Electrons and holes have different momentums at the band-edge and a phonon is needed to balance this momentum difference for the recombination process. The probability for this three particle process is strongly reduced compared to a material with a direct band-gap, which allows a direct electron-hole-recombination, i.e. a two-particle process. The low probability for the recombination process in silicon leads to a long lifetime of free carries up to several milliseconds in pure silicon. As a result, the free carriers have long diffusion lengths and do find defects, so that the recombination processes take place at non-radiative recombination centres. This fact reduces the luminescence of silicon.

To achieve a monolithic integration of optical and electronic devices on Si samples, new concepts are required. One is the use of quantum cascade structures [6], where recombination among quantum levels of the same band within a quantum well are employed. Here, the design and fabrication of the structure is rather complex since it contains a huge amount of different layers. However, quantum cascade lasers have been successfully implemented in the III/V technology [6] and first steps to transfer this concept into the Si technology have been undertaken [7]. Another route to overcome this limitation is to make use of Heisenberg's uncertainty principle. If one localises carriers in quantum wells, i.e. in real space, the wave functions spread in the k-space and their momentum becomes more uncertain. This increases the probability, that an electron finds a hole with the same momentum and a phonon is therefore not necessary. The probability for radiative recombination processes increases.

One way to realize this concept is to confine carriers in Ge quantum dots embedded in silicon. The bulk lattice constant of germanium is by four percent larger than those of silicon. This leads to Stranski-Krastanov growth mode, where after a critical Ge layer

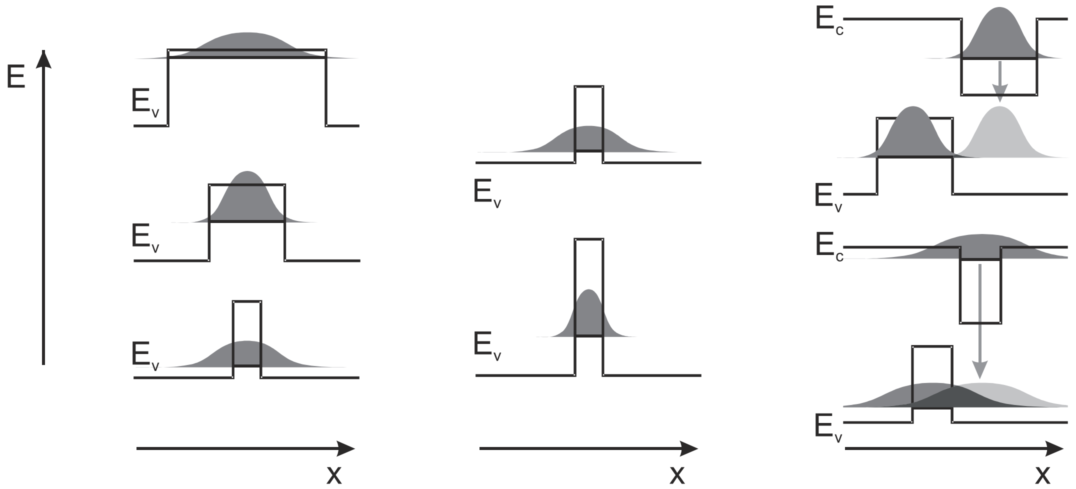

Fig. 1.1: Left: The width of the quantum well depends on the size of the dots. With decreasing size of the dots the width of the well shrinks and the carriers are better confined. On the other hand the energy level, which contains the confined carriers, moves to the valence band and the wave function starts to broaden near the band, leading to a weaker confinement. Middle: With increasing Ge content of the dot the well becomes deeper resulting in an upside shift of the energy level and a better confinement of the carriers. This can antagonize the previous problem. Right: For a good probability of recombination one needs a good overlap of the wave functions in real and in k-space. For this reason one has always to find an optimum in size and composition to maximize the probability.

thickness has been surpassed, Ge dots form on the silicon surface in a self assembled fashion [8]. A Ge-dot embedded in a Si matrix acts then as a quantum well in the valence band, if its dimensions are small enough. Thus a small enough Ge dot is a quantum box for holes. The overgrowth of these dots leads to tensile strained Si that surrounds the dots and forms a quantum well for the electrons [9]. If the spreading of the wave-functions of the holes and electrons leads to an overlap in k-space, the probability for a no-phonon-assisted recombination process increases.

One could think that it is only necessary to grow as small dots as possible, to achieve a strong localisation of the carriers and therefore a large spreading of the wave-functions in k-space. Fig. 1.1.a shows, that the situation is more complicated. Here the wave-function in real-space and therefore the localisation of the holes is indicated for shrinking size of the dot. When the dot is large, the wave-function is broad and no pronounced localisation is achieved. Reducing the size of the dot leads to a better localisation, as indicated in the picture in the middle of Fig. 1.1.a, but also the energy level of the holes, responsible for the recombination, shifts towards the valence band edge of the Si. When the dot becomes too small (bottom picture) the energy level shifts close to the Si valence band edge. In this case the carriers are only weakly localised within the shallow quantum well. The ground state within the quantum well is not only determined by the size of the dot, but also by its composition. When the Ge content within a dot increases the whole well becomes deeper and the relevant energy level shifts closer to the SiGe valence band edge, as indicated in Fig. 1.1.b. If one likes to achieve a good localisation of holes, one must try to grow small dots with a high Ge content. Moreover the situation becomes even more complex, since the holes are localised in the Ge dots and the electrons are localised in the surrounding tensile strained Si, thus they are separated in real-space, as shown in Fig. 1.1.c. When the localisation of the carriers is too strong, no overlap is found in real space and the probability for a recombination process is low, again. For this reason, the localisation of carriers to achieve the best overlap of wave function in real- and in k-space has to be optimised. The size and the composition of the dots have to be controlled exactly.

In our studies, we investigated the formation and the overgrowth of Ge-dots grown by Molecular Beam Epitaxy (MBE) to determine the important parameters for the size and the composition of the dots. It was already shown by Leifeld et al [10], that the pre-deposition of sub-monolayers of carbon influences the formation process and the size of Ge-dots, that were grown on such modified surfaces. The deposited carbon leads to a c(4x4) reconstruction of those areas of the sample surface, where carbon is incorporated into the lattice. Carbon has the same lattice type, but a lattice constant that is by 40 percent smaller than those of Si, leading to a strain variations in the surface of the sample. When Ge grows on such a sample, it tends to avoid the areas with c(4x4) reconstruction due to its larger lattice constant and starts to grow directly in three-dimensions in the carbon free-areas. Smaller Ge dots down to 10 nm in size can be achieved by this method [10]. The size and the density of the Ge-dots are determined by the density and size of the c(4x4) reconstructed areas. For this reason, we investigated (see chapter 5) the influence of the amount of deposited carbon on the surface reconstruction of the sample. These investigations were done by Scanning Tunnelling Microscopy (STM), as this method allows to map the electronic structure of the surface in the sub-angstrom range and therefore gives an inside into the position of the atoms on the surface.

The size and the shape of the dots are not only determined by the formation of the dots themselves. When Ge-dots are overgrown by Si, as it is necessary to embed them in a Si matrix, intermixing of the dots with the capping Si can occur at high overgrowth temperatures. This intermixing changes the strain fields within the dots and has an influence on the size and shape of the dots, as presented in chapter 6. Here we investigated our samples again by STM, as we wanted to determine the size and the shape of the dots before and after overgrowth. In addition, Transmission Electron Microscopy was used, as we got high resolution cross-section through the dots. To determine the second crucial parameter of the dots, the composition, Energy Filtered TEM (EFTEM) was done as this provides elementary maps through the dots. While with EFTEM only single dots can be examined, high temperature capped samples were also investigated by x-ray-diffractometry. This method yields beside the composition of Ge-dots also the strain within the dots, but in contrast to TEM, the values are averaged about all dots.

Finally we saw by STM in chapter 6, that the lowering of the overgrowth temperature prevents changes in shape. As this implies, that the intermixing is reduced due to the lower overgrowth temperature, we also studied the composition of low temperature overgrown Ge-dots by photoluminescence.

2 Basic considerations

For the formation of Ge dots, the specifics of Germanium deposition on silicon play an important role. Both, Si and Ge, crystallize in the diamond lattice, but have a lattice mismatch of about four percent, which limits the hetero-epitaxy growth of Ge on Si. In the following chapters we will therefore briefly recapitulate the fundamental aspects of the epitaxial growth of Ge on Si.

2.1 Growth modes

Bauer has classified three different growth modes in a very often-quoted paper in “Zeitschrift für Kristallographie” (1958) for hetero-epitaxial growth [11]. The first one is a layer-by-layer growth, were material A deposited on substrate B just forms new smooth layers, as indicated in Fig. 2.1.a. This mode is called the Frank-van de Merwe (FM) growth mode. For the second one, the deposition of material A does not lead to a wetting of the surface and direct formation of three-dimensional islands occurs. This mode is called the Vollmer-Weber (VW) growth mode. The third and last one is in-between the two previous ones. Here, material A starts to grow first layer by layer forming a wetting layer and then after a critical thickness has been reached, the growth proceeds in a three-dimensional way forming islands on top of the wetting layer. This is called the Stranski-Krastanov (SK) mode of growth.

Which of the three growth modes is realized, depends on the surface energies. When material A is deposited on material B, layer by layer growth is achieved, if the surface energy γ_A of the deposited material A is smaller than the sum of the surface energy γ_B

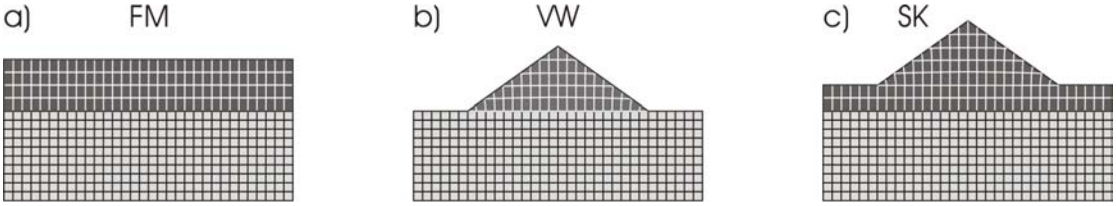

Fig. 2.1 Different growth modes during hetero-epitaxy. a) Frank-van der Merwe mode: The deposited material grows layer by layer on the substrate. b) Volmer-Weber: The deposited material grows directly in three dimensions. c) Stranski-Krastanov: Up to a critical thickness the deposited material grows layer by layer. When the critical thickness is reached, dots form directly on top of the wetting layer and the growth continues in a three-dimensional way. Which type of growth occurs, depends on the surface energies of the material and the interface energy.

of material B plus the interface energy γ_{int}

$$\gamma_A < \gamma_B + \gamma_{\text{int}}$$

In contrast, the formation of islands in the VW growth mode is realized if the increase in surface energy is smaller than the increase due to the interface formation.

$$\gamma_B < \gamma_A + \gamma_{\text{int}}$$

For Stranski-Krastanov growth mode, many factors account, but a certain lattice mismatch between the deposited material and the substrate is most often the reason, as it is the case for Si and Ge. Here, Ge with a four percent larger lattice constant grows up to a critical thickness on the Si lattice. During the initial Ge layer growth, the required deformation of the Ge lattice builds up the strain energy until the critical thickness is reached and three-dimensional islands form. The formation of three-dimensional islands increases the surface energy, but on the other hand, strain can be released within the dots as shown in Fig.2.1.c. This reduction of strain energy within the dot is more efficient, so that the increase in surface energy is overcompensated and the total energy consisting of strain and surface energy is reduced by the formation of islands.

SK-growth is therefore characterised by an energy barrier, which has to be overcome before islands can form. This energy barrier ΔG^* for the formation of pyramids from material in the planar strained layer is given by

$$\Delta G^* = \frac{(4\Gamma)^3}{3(9c)^2} \cot\theta$$

The composition of the material is reflected in the elastic constant $c = \sigma^2(1-\nu)/2\pi\mu$ with ν as Poisson's ration, μ the shear modulus, and σ as strain which is a function of the composition. The energies of the film and surface are reflected in,

$\Gamma = \gamma_f/\sin\theta - \gamma_s\cot\theta$, with γ_s and γ_f surface free energy per unit area for the planar surface and the facets comprising the pyramid and θ the inclination angle. The approach given above was derived by introducing surface energy anisotropy to the Asaro-Tiller-Grinfeld (ATG) instability [12,13] and ignores the influence of deposition on the nucleation process and is therefore only valid for annealing of very low super-saturation deposition.

2.2 The Si(001) surface

Silicon has a face centred cubic lattice, whose base consists of two atoms, which are displaced by (¼, ¼, ¼). Each atom is bonded in a tetrahedron like way to four neighbours as shown in Fig. 2.2. At the Si(001) surface, every atom has two dangling bonds, while it is still bonded by the two remaining bonds to the lattice. As the crystal symmetry is broken at the interface, it is energetically more favourable, to reduce the number of dangling bonds by rearranging the atoms on the surface. The increase in energy gained by the new bond exceeds the energy loss due to the distortion of back-bonds which can reach down several layers and therefore stabilizes the surface.

This rearrangement is called reconstruction and depends on the type of surface. For the Si(001) surface, only the atoms of the topmost layer are displaced. Two neighbouring atoms are moving towards each other and form a new bond. These Si pairs formed by the reconstruction are frequently called dimers and reduce for Si(001) the number of dangling bonds by a factor of two [14]. For this surface three different types of reconstruction exist. They are built by two neighbouring atoms rearranging along the <110> direction. For the first type the rearrangement is within the (001) plane (see Fig.2.2.b). As this two atoms form a new super-cell containing two times one atom, this reconstruction is called (2x1) following the Wood- notation. [15]. When the new dimer is tilted by 16 ° against the (110) plane and one of the atom is 0.6 Å lower than the other, this type is called a buckled dimer. Depending on the

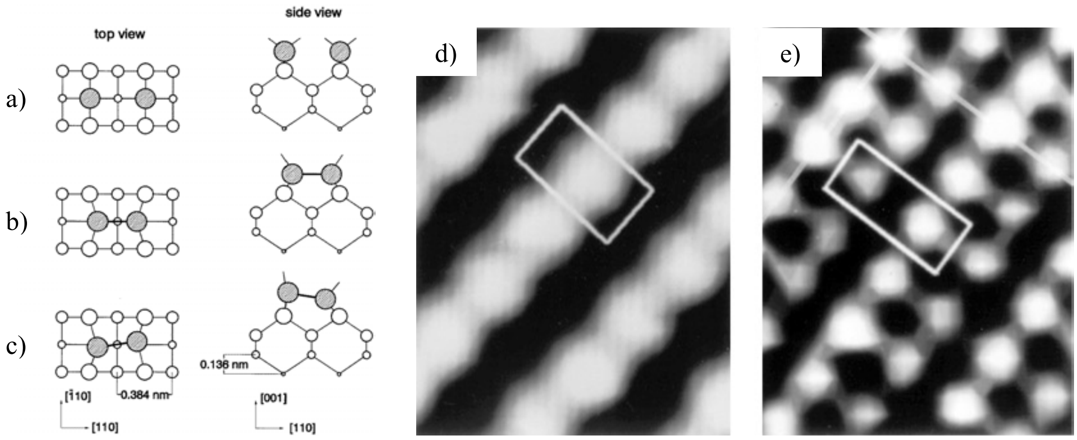

Fig. 2.2 Surface geometry of Si(001) in bulk-like termination (a) and after formation of the (2x1) reconstruction by symmetric (b) and asymmetric (c) dimers (according to Bechstedt and Reichardt (1988)). d) and e) Full and empty-state image of (2x1) reconstructed surface [14].

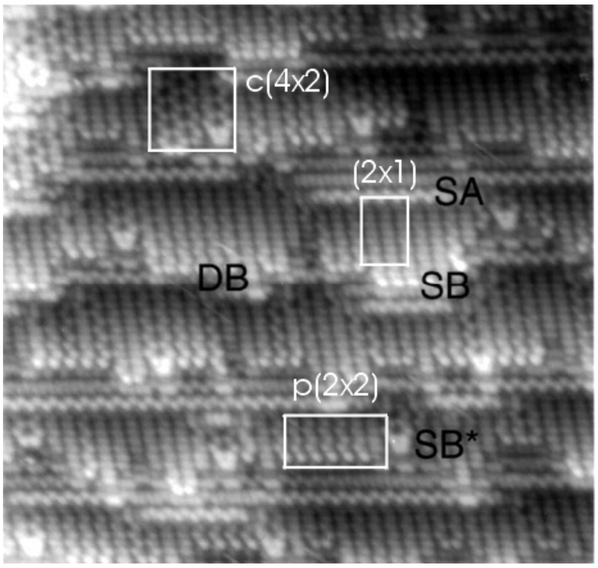

Fig. 2.3 STM picture of terraces, on a Si(001) surface showing the different types of reconstruction. In addition, also the monoatomic and double steps are marked by SA, SB, and DB [14].
Symmetric dimers form a (2x1) surface reconstruction, while for the asymmetric case a c(4x2) and a p(2x2) reconstruction can be built.

correlation between the direction of buckling dimers in adjacent rows, the reconstruction can be either of type c(4x2) or of type p(2x2) as shown in Fig.2.3.
Even though buckled dimers are believed to form the most stable surface due to the lowest energy configuration at zero temperature [16], it is difficult to observe them, as they usually oscillate with high frequency (hν ~ 25 meV) [17] and look therefore symmetric, which then appears as (2x1) reconstruction. One exception is the presence of defects, as they pin the configuration of buckled dimers [18]. As all of the dimers are orientated along rows, the diffusion of atoms on the surface is asymmetric.
Normally, sample surfaces have a certain miscut leading to the formation of terraces separated by steps. Depending on the height of the steps, they can be classified as mono-atomic (S) or double (D) step, according to Chadi [19]. On a terrace, the rows of dimers can be orientated whether perpendicular or parallel to the edge. To

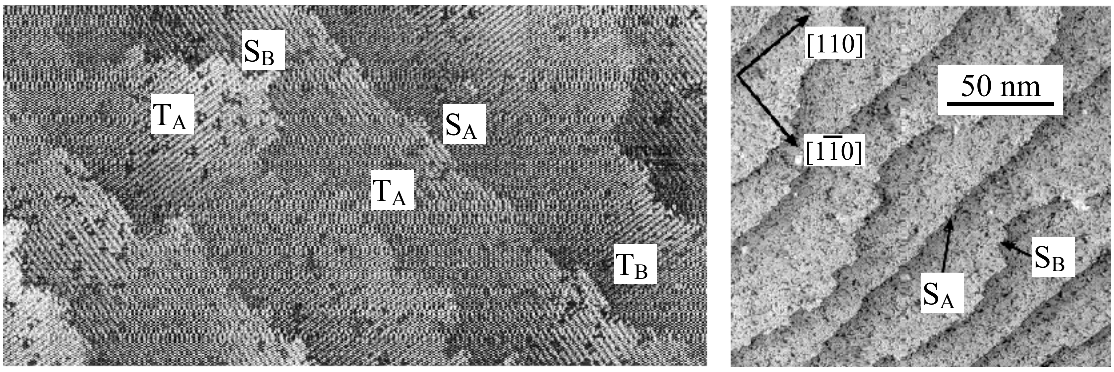

Fig. 2.4 Left: Monoatomic and double step high terraces labelled S and T. Depending on the orientation of the dimers at the edges, a terrace is whether of type A (perpendicular) or B (parallel) [20]. Right: No island-formation can be seen, showing the pure step flow growth mode [21].

distinguish between those terraces they are called T_A and T_B terraces and similar applies to the steps (S_A, S_B, D_A, D_B) (see Fig. 2.4). Typically S_A steps appear to be smoother than S_B steps, which is due to the already mentioned anisotropy. The diffusion of an atom along a dimer row is favoured against the diffusion across a row [22]. For an ad-atom, moving down a S_B step is more likely than moving down a S_A step, as the Schwoebel barrier is lower for a S_B than for a S_A step. In addition, an ad-atom on a lower terrace reaching a S_A step of the higher terrace can diffuse perpendicular to the dimer rows along the S_A step more easily than without the presence of the step and is preferentially incorporated at the end of the S_A step, which has S_B character [23].

Besides this, Fig. 2.4 also shows, that depending on the growth conditions Si can grow in pure step flow mode, i.e. no islands nucleate on the terraces. In this case, the diffusion length of Si must be larger than the width of the terraces.

2.3 Ge wetting layer

When Ge is deposited on a Si surface, one has to take the different lattice constants and surface energies into account. The surface energy of Germanium is lower than that of silicon. As described in chapter 2.1, this leads during the growth of the initial monolayers to a two-dimensional growth. Later on, due to the lattice mismatch, the Germanium starts to form islands. The formation of the wetting layer was already extensively investigated by STM [24-26]. During the initial steps of Ge growth on Si, the Ge is incorporated into the Si terraces by displacing Si atoms [26]. This leads already after the deposition of 0.3 ML of Ge to a disordered structure with lots of missing dimers [28].

When the amount of Ge is increased to 1 ML, the whole surface is Ge-terminated, showing that Ge does not diffuse into the lattice. It forms a (2 x n) reconstruction where every nth dimer is missing. These dimer vacancies arrange into arrays of lines, as can be seen in Fig. 2.5. With an increasing amount of deposited Ge, the n decreases towards its minimum value of eight.

The reason for the formation of dimer vacancies is the relaxation of compressive strain, as the Ge can expand into the vacancies. Tersof showed, that the dimer vacancies are energetically favourable, if the atoms within the trenches consist also of Ge [29]. The bond-configuration was described by Pandey before [30]. It was also shown, that dimer vacancies can relieve elastic strain very efficiently, as they

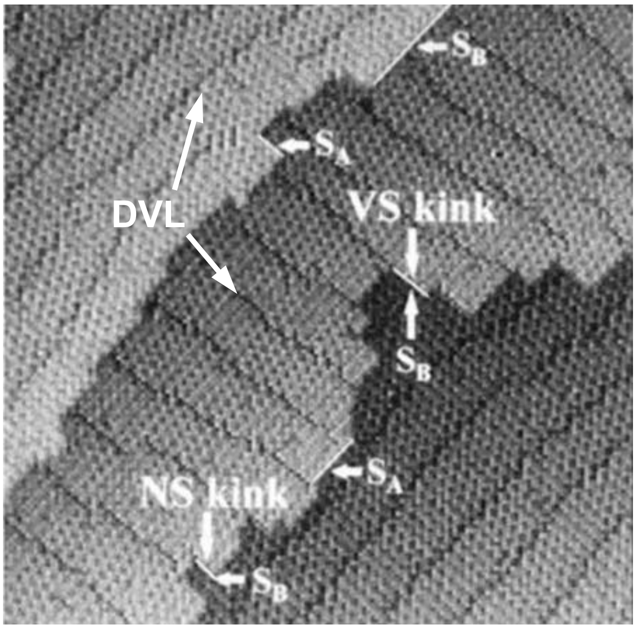

Fig. 2.5 STM image (45x45 nm^2) of the (2xN) reconstruction observed after depositing 1.6 ML of Ge on Si(001). Dimer vacancy lines (DVL's) are visible as dark lines perpendicular to the dimer rows [27].

introduce subsurface rebonding, which introduces tensile strain that will compensate the compressive strain induced by the substrate.

The question of intermixing during the initial stages of growth has been intensively investigated by a couple of researchers [31-33]. It was found, that even at low growth temperatures, Ge intermixes with the Si. Liu and Lagally used molecular simulations and scanning tunnelling microscopy to study the intermixing after the deposition of 2 ML of Ge [34]. They distinguished between two different cases. When no intermixing occurs (this means, the whole Ge is in the two topmost layers) the periodicity of dimer vacancies n should be 6. The second case of strong intermixing was simulated by assuming that the surface layer consists of pure Ge, the second layer of pure Si. The third and forth layer consist of Si and Ge. Si is on the compressed atomic sites (below trenches), while the Ge is on the tensile strained sites, which are below the dimers on the surface. The simulations lead to a periodicity of about 14. As the results received by STM are closer to 8, strong intermixing was excluded [34].

When the amount of deposited Ge is increased to more than 2 ML, Ge forms patches on the surfaces. These patches are bounded in one direction by the dimer-vacancies and perpendicular to the dimer-vacancy-lines by large trenches [35, 36]. These patches have a (m x n) reconstruction, where m gives the periodicity in the direction of the trenches.

2.4 Ge islands

The early stage of Ge growth is a roughening process with a characteristic length scale that depends on strain. The amplitude of roughness increases during the growth, until the critical thickness is reached. For $Si_{1-x}Ge_x$ alloys, the first stage of ongoing growth is the formation of mounds [45]. Afterwards {105} facetted clusters are formed. If pure Ge is deposited, the formation of mounds is not observed and the {105} facetted clusters form directly. This means, the growth mode is of Stranski-Krastanov type as described in paragraph 2.1. With ongoing deposition of Ge, the density of clusters decreases strongly. During this coarsening process, the number of islands varies in that way with time, that is consistent with diffusion-limited Ostwald ripening [37]. The density and volume of the remaining hut clusters depend strongly on the growth temperature and the deposition rate. After the coarsening, the pyramids grow until a critical size is reached, and they start to change their shape. For high temperature grown dots (650°C – 700°C) it was observed by LEED, that the process of shape change can take up to several minutes and involves intermediate stages and ends in the observed dome clusters [38]. For a wide range of conditions, this leads to bimodal distributions in size with pyramids at the lower range and domes at the higher range of the size [38]. One way to explain the bimodal distributions is to assume, that both types of island belong to equilibrium states with minima in energies [39]. The transition from pyramid to dome clusters is a thermal activated process, overcoming the barrier between the two energy minima. This process is a rapid accumulation of atoms with a very short time scale. The observations of Ross et al therefore lead to a more kinetic model, where islands grow by a similar process than Ostwald ripening, but with kinetics modified by an abrupt drop in chemical potential that occurs as islands grow past a critical volume and change their shape [38]. This model has the drop in chemical potential as the driving force for the coarsening of the islands in the beginning of island formation and in the end for the change of shape from hut to dome clusters.

The surface energy anisotropy during the strain-induced roughening plays an important role for the island shape. Fig. 2.6 depicts the different type of clusters, which occur during the different stages of growth. Which of the type is formed, depends on the growth conditions. At low growth temperatures, pyramids with {105} facets are found. These islands bounded by {105} facets are called hut clusters. The

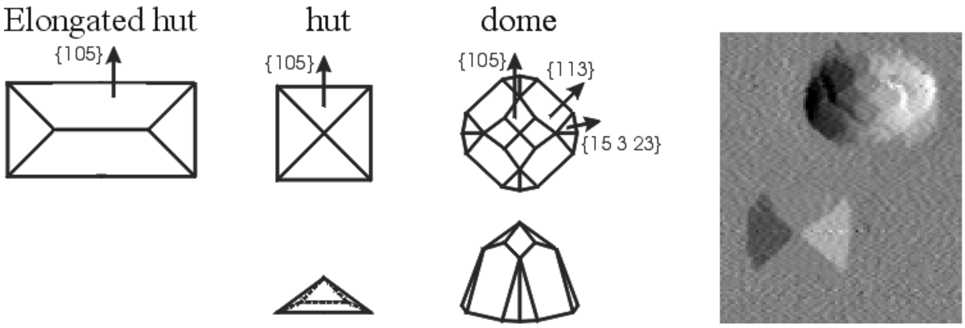

Fig. 2.6 At low growth temperatures elongated hut clusters are found, while the hut cluster have a squared base, if grown at high temperatures. Increasing the amount of deposited Ge leads to the transition from hut to dome clusters.

base of the dots is rectangular and aligned along the <100> direction. A model for the atomic structure has been proposed in [40], which was based on STM-measurements. The elongation of the islands along elastically soft <100> directions is still not fully understood, as the minimum energy would prefer a squared island. The elongation might be driven by kinetics at relatively low growth temperatures. The anisotropy in diffusion along and perpendicular to the dimer rows might be the reason. Beside this, slow mass transport to the island apex [41] and strained facet growth mechanism [42, 43] have been proposed to be responsible for the elongation.

When the growth temperature is increased, the dots tend to form pyramids with a square base. Under these conditions, the limitation of the low growth temperature is overcome, and the islands take the shape for which the model gives the energetic minimum. However, the shape of a dot depends not only on the growth temperature. With increasing amount of deposited Ge, large dots form. These dots have a so-called dome shape, which consists of steeper side facets. These facets are the {15 3 23} and {113} side facets [38]. At the top of the dome are again the {105} facets. Due to the steeper facets, the dome can relax more strain energy than a pyramid of the same volume. Within pyramids about 20 percent of the misfit strain is relieved, whereas dome cluster can release up to 50 percent [44].

For the confinement of carriers, one would like to have dome like clusters, as they have steeper facets and therefore a higher aspect ratio. The aspect ratio of dome clusters is 1:5 (height to diameter) compared to huts of 1:10. The localisation of carriers is therefore easier to achieve for dome than for hut clusters if both would have the same volume. On the other hand, dome clusters only form by a shape transformation from huts, when enough material is deposited. This leads to relatively large clusters of a base diameter of about 40 nm, which is contradicting to a pronounced 0-dimensional confinement. Lowering the growth temperature also decreases the diameter of the dots, but the crystal quality suffers at temperature below 350°C [46]. Thus due to the defect formation at low temperatures, non-radiative recombination processes become more dominant to the expense of the desired radiative recombination processes.

2.5 Composition of Ge-dots

The composition of self-assembled Ge-dots has been the subject of intense research [47-58]. In the literature it is found, that nominally pure Ge islands intermix substantially with Si during growth, if the growth temperature is high, e.g. larger than 550°C. The exact intermixing process is still under investigation. There are two different models, one is based on strain enhanced volume interdiffusion at the basal interface of the cluster and the Si substrate [47,48] while the other assumption is based on surface interdiffusion processes, leading to the observed alloying [54-57].

2.5.1 Volume interdiffusion

Liao et. al. investigated dome clusters, that they grew by molecular beam epitaxy (MBE) on p-type Si(001) substrates [48]. They deposited 0.8 nm resp. 1.2 nm of Ge at 700°C. The obtained diameters of the domes were in the range of 100-200 nm and the typical height to diameter ratio of 1:5 was observed. Due to the large volume of the domes, dislocations within the dots are found. The samples were investigated by Transmission Electron Microscopy (TEM) and Energy Filtered TEM (EFTEM). The latter gives an elementary map of Si and therefore the composition within the dot. They found, that each island of the sample was surrounded by an approx. 7 nm deep trench independently on the relaxation state of the dot, as shown in Fig. 2.7.a-c. The depth of 7 nm is clearly larger than the normal height of a wetting layer which is in the range of 3-5 ML. Also the height of the wetting layer was found to be thicker than expected, which was explained by alloying with Si from the substrate. This assumption was confirmed by Auger electron spectroscopic measurements done by Jiang et al [59] and also by the finding of substantial intermixing during the initial stages of Ge growth on Si(001) [60]. Liao et. al. assumed by the fact that the wetting layer is alloyed, that volume intermixing has occurred during the initial growth of the wetting layer. The EFTEM pictures in Fig. 2.7.e-f show, that Si is found within the

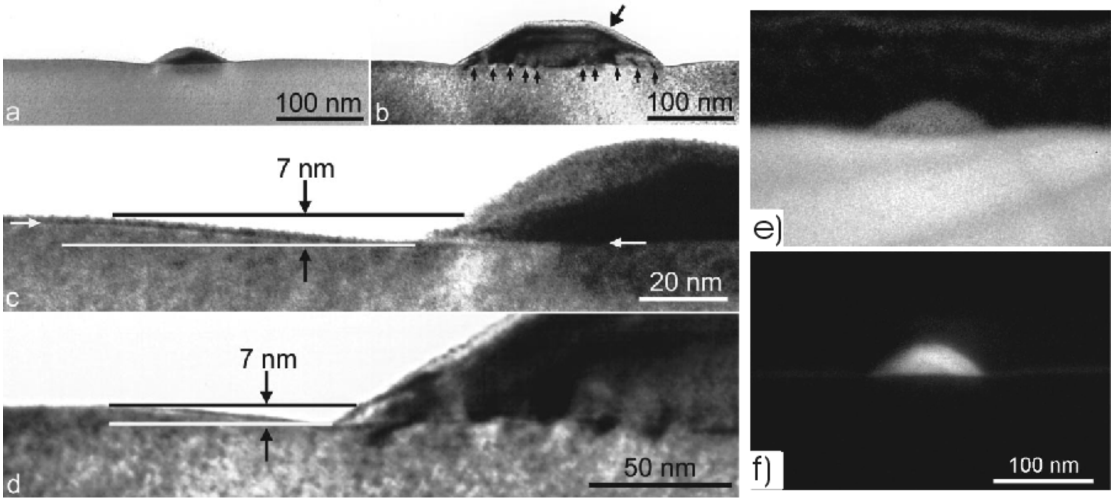

Fig. 2.7 Cross-section bright-field images: (a) a coherent island in sample A; (b) a relaxed island in sample B where misfit dislocations at the island/substrate interface and a stacking fault are arrowed: (c) an enlarged image of a part of (a) showing a clear wetting layer. White arrows at the left and right sides of the image mark the wetting layer/substrate interface and the island/substrate interface, respectively. A white line below the wetting layer represents the depth level of the island/substrate interface. A trench with a depth of about 7 nm at the edge of the island is clearly seen; (d) an enlarged image of a part of (b) where a trench with approximately the same features as the trench in (c) is clearly seen. Cross-section energy-filtered images: (e) an energy-loss (1839 eV) image that represents a Si map. Si is clearly seen within the island; and (f) an energy-loss (1217 eV) image that represents a Ge map. A wetting layer is seen uniformly throughout the entire substrate surface [48].

dots. In addition it is found, that the Si/SiGe interface is below the initial Si-substrate surface. The islands must have sunk into the wetting layer and even into the Si substrate. This let them assume, that also a strong volume intermixing during the growth of the island occurs, which consumes the material below the dot and let the dot sink into the wetting layer and substrate. For this reason, they have suggested a modified Stranski-Krastanov (SK) model for high temperature growth, here 700°C, that is illustrated in Fig. 2.8.

In the first step of the classical SK-model layer by layer growth takes place up to the critical thickness. During this process, Si volume intermixing occurs, as indicate in the figure, which leads to Si uptake in the wetting layer. In the next step, the surface migration of Si and Ge results in the formation of small coherent island. The formation only partially releases the misfit strain. During growth, the misfit strain increases and can be reduced in four proposed ways [48]: I) increasing the height to diameter ratio. As this increases also the surface energy, it only occurs when enough

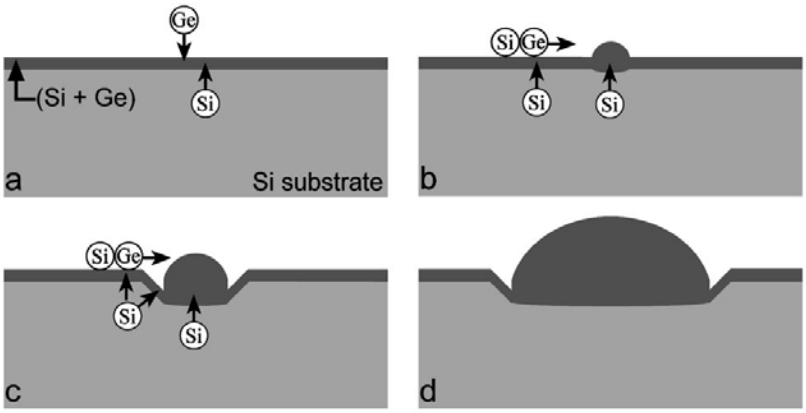

Fig. 2.8 Schematic diagrams of a modified SK growth mode at different growth stages[48].

strain is built up to form dome clusters and a net lowering of the total energy results. II) Introduction of misfit dislocation. This is the case for large domes only, as high strain is needed. III) By reducing the misfit strain in the dots via intermixing with Si. IV) By re-orientating the surface around the dot to permit lateral expansion of the cluster at its sunken base, as illustrated in Fig. 2.8.c.

As the island penetrates into the substrate, the Si below the dot must have gone somewhere else. They assume that it is consumed by the dot, which consequently increases in size and its Ge concentration decreases. It is proposed that the larger dot with the lower Ge concentration can relax the strain energy more effectively via plastic deformation. They admit, that still surface migration can happen, but they stress that some volume intermixing must have occurred. Nevertheless no quantitative investigations were performed, but the EFTEM results clearly show an intermixing of the clusters during high temperature growth. An estimation was performed, that lead to a mean Si content of 30 up to 60 percent of Si, depending on the size of the dots. The difference in Si content for different sizes is explained by the fact, that the volume of the dot increases with the power of three, while the volume of the consumed Si substrate only scales with the power of two (no shape transformation assumed). Similar results, i.e. intermixing leading to a content of about 50 percent was also shown by Kamins et. al. for Ge islands deposited at 650°C by CVD [61].

2.5.2 Surface diffusion

Denker et. al. showed, that intermixing of clusters during the growth at lower temperatures can be explained by surface interdiffusion [57]. They grew Ge clusters in the temperature regime of 560 to 600°C. The dots were formed by the deposition of 6 ML of Ge, which is an amount quite smaller than that used by Liao et. al. After growing the samples, they were cooled down to room temperature and afterwards wet chemical etched in a hydrogen peroxide solution of 31 percent. Etching within such a solution removes the Ge rich parts of a sample, while a Ge concentration of lower than 65% ± 5% acts as etch stop. With this method, the parts of a dot that strongly intermixed during growth are determined. Under the given growth conditions, both types of cluster are found, dome and hut clusters. Due to the etching, only small parts of domes are removed, showing the strong intermixing of the dome clusters with Si. The strong intermixing of dome clusters is in good agreement with the results of Liao, who found a Si content of 30 to 60 percent, which is low enough to prevent the etching. As due to Liao's model the Si content should decrease with an increase in volume, thus it should be possible to grow large enough dome clusters, which can be partially removed by etching due to their low Si content.

For the small huts Fig. 2.9 shows, that only the edges of the huts remained, while the rest and especially the centre of the base is removed. In this case, only the corners intermix strongly. The fact, that the hut clusters of Denker reveal a depression in their centres, implies that volume interdiffusion plays a minor role, as the Ge content stayed high even though the strain should be highest directly above the substrate.

The intermixing of the wetting layer with Si was already shown by Voigtländer, who investigated the periodicity of the (2xN) reconstruction of a Ge wetting layer by STM. As the periodicity also depends on the stoichiometry, it was possible to show the intermixing of the Ge wetting layer with Si by a simulation [62]. The consumption of

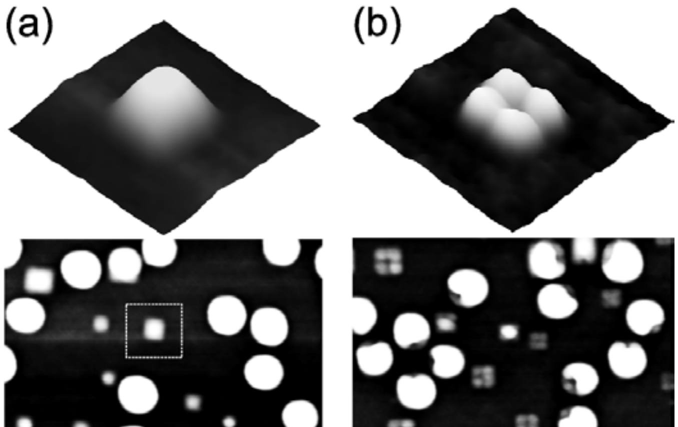

Fig. 2.9 AFM images of domes and pyramids grown at 560 °C (a) before etching and (b) after etching for 2 min in 31% H_2O_2 solution. The etching removes those parts of a dot with a Ge concentration higher than 65 percent. While for domes only small parts are removed, for huts remain only the corners of the pedestals [57].

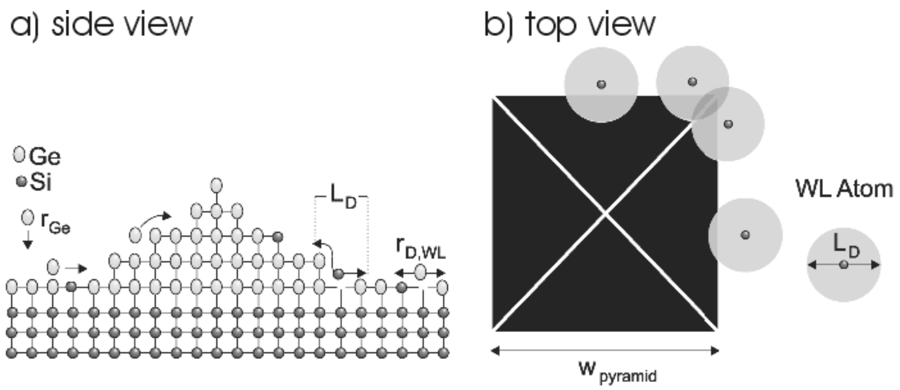

Fig. 2.10 Simulation parameters for the phenomenological growth simulation that includes interdiffusion with a Si intermixed wetting layer. If a short Si diffusion length is assumed, the pyramid corners will be Si enriched because diffusing atoms can reach the island from two sides [57].

the wetting layer during the formation of the dots was proven previously by O.G. Schmidt [63]. The results strongly indicate that the assumption on surface interdiffusion is possible.

The model of Denker is schematically shown in Fig. 2.10 [57]. It is based on two rates. One is the rate r_{Ge} of deposited Ge atoms on the surface which are incorporated into the island, the other is the rate $r_{D,WL}$ at which the atoms from the wetting layer are incorporated into the island. As the wetting layer is intermixed with Si, this also leads to an intermixing of the islands during growth. The results of the model strongly depend on the diffusion length L_D of the Si, however it was possible to simulate even with simple assumptions the composition of the huts. The enrichment of Si in the corners of the dots simply originates from the fact, that the corners can be reached from two sides. This is schematically shown in Fig. 2.10.b by the circles illustrating the area, which can be reached by an ad-atom via surface inter-diffusion.

To determine, if the interdiffusion with a resulting non-uniform distribution profile is driven by the minimization of the elastic strain energy, as predicted by [64], the strain of a free-standing pyramid was simulated by Denker et. al. for three different composition profiles [57]. For all models, the average volume Ge content of 77% was kept constant. The first profile was assumed to be a uniform SiGe alloy throughout the dot, in the second profile the Ge content increased linearly towards the apex, and the last calculation assumed the composition derived from the model shown in Fig. 2.10.

The simulation took the anisotropy of elastic properties into account and based on the finite element method. It was found, that the composition found by the experiment did not had the minimum strain energy, as expected if the interdiffusion would be strain driven. Instead the model with the Ge content that rose towards the apex of the dot was found to have the minimum strain energy. Thus the results imply that the main driving force for intermixing is not strain but surface diffusion.

Thus indications for surface-interdiffusion were found for hut clusters deposited at 560°C – 600°C, while volume-interdiffusion seems to be important for the dome clusters grown at elevated temperatures. None of the models can explain the composition for both types of clusters.

2.6 Overgrowth of Ge dots

The embedding of Ge clusters into a Si matrix, as it is necessary for electronic and opto-electronic devices, may lead to substantial changes of shape, size, and strain of dots, as several investigations have shown [49, 65-68]. These changes strongly depend on the growth temperature of the Si cap layer. Hut clusters which were overgrown at high temperatures, increased in diameter while the height of the huts shrunk due to the formation of a (001) top facet of the hut (see Fig. 2.11) [66]. The process was observed in real time by low energy electron microscopy (LEEM). When the Si flux was interrupted, the growth of the (001) top facet stopped and started again, after restarting the Si flux, showing the relation to the Si deposition. The driving force for this shape change is intermixing of the dot with Si. Whether this intermixing is enhanced by strain or can be attributed solely to thermally activated diffusion is still an open question. However, Si deposited on the island, incorporates into the dot, while Ge segregates to the surface, to lower the surface energy [69, 70] and to minimize the stress in subsurface layers [71]. This change to a more Si rich

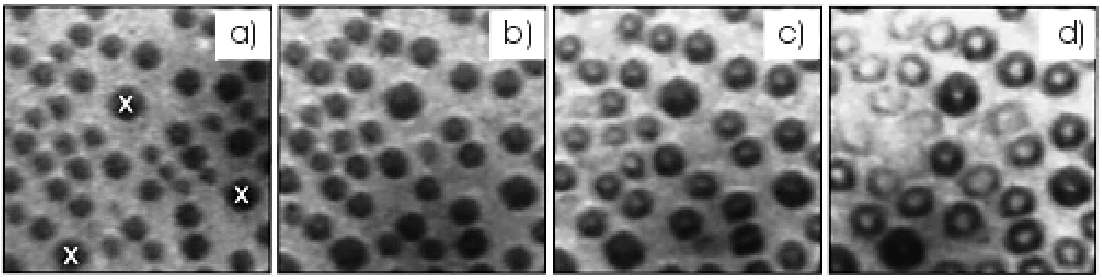

Fig 2.11 Sequence of LEEM images, taken at T = 650 °C and a deposition rate of 2.3 ML/min, illustrating the overgrowth of 3D SiGe islands. (a) SiGe islands prior to Si deposition. Most of the islands are {105} faceted huts, which appear somewhat rounded at this elevated temperature. Three larger, multifaceted dome islands are also present (marked “X”). (b), (c), and (d) Islands during Si deposition, at 4.6, 9.2, and 13.8 ML coverage, respectively. Field of view: 1.5 × 1.5 mm^2 [66].

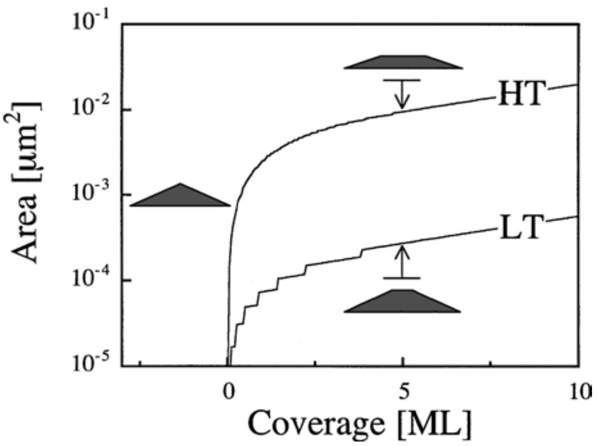

Fig. 2.12 Calculated top facet area on top of a 3D island as a function of Si coverage at high and low temperature. The as-grown 3D island is assumed to be a {105} faceted, square based pyramid (base size 140 nm). The resulting shape after the initial stage of Si overgrowth is shown schematically for capping at low (LT) and high (HT) temperature [66].

composition should be most pronounced at the apex of the island, where the local surface-to-volume ratio is largest. As the lattice constant of the Si is smaller than that of relaxed Ge this intermixing may lead to tensile strain of the SiGe alloy at the apex of the dots as well as to an increase of the compressive strain underneath the intermixed area. Thus it can be assumed that the strain energy increases and it might become more favourable for the alloyed material at the apex of the dot to migrate to the pedestal. This would erase the tensile strain of the apex and in addition would lead to the ability to elastically relax the compressive strain of the Ge dot again. Thus atoms from the apex migrate down the dot walls creating the (001) top facet and also let the dot grow at its pedestal, leading to a larger diameter. For smaller islands with a size close to the critical nucleus, the strain reduction at small Si coverage can already be sufficient to destabilize the entire 3D island. Hence, small islands disappear. Consequently, this process leads to a narrower size distribution, since the small islands dissolve.

The observed behaviour of decreasing in height and increasing in lateral dimensions was simulated by a simple model [66]. The decrease in height was simulated by removing the actual top layer. This means, the decrease in height is layer by layer. Thus, the area of the top facet increases and this increase was estimated to be of constant rate r. The second parameter is the fraction p of atoms, adsorbed on terraces. Therefore it opposes the decay of the island. Under these conditions a fast increase of the top facet area is found in the beginning, which then becomes slower. The different growth temperatures can be taken into account, by keeping the incorporation parameter p fixed and adapting the rate of detachment. This decelerates the process at low temperatures, as shown in Fig. 2.12. For the decay of the islands, there is a kinetic limit. In the beginning, lateral evaporation of the top facet by atom detachment dominates over growth by the incorporation of deposited atoms. When the area of the top (001) facet increases, the lateral growth of the area due to the incorporation of Si accelerates and can eventually outweigh the decay of the island's height. At that point, the island starts to become overgrown.

Not only hut clusters undergo shape transformations. Also dome clusters change their shape, if they are covered at high temperatures. Rastelli et. al. showed, that an initial dome cluster can undergo several intermediate stages and turns finally into stepped mounds, due to the capping with up to 16 ML of silicon. The process for this transformation is the same as for the huts and also leads to shrinkage in height and an increase in diameter. As during the process the cluster intermixes with Si, an increase of volume can be observed. The height to diameter ratio of the uncapped dome clusters shrinks due to the shape change from 0.22 to 0.06, indicating clearly the pronounced shape changes [65].

3 Deposition and characterization methods

As shown in the previous chapters, the composition and size of the dot, as the main important parameters for the realization of opto-electronic devices, are influenced by a wide range of parameters, not only during growth, but also during capping. One of the most important factors for determining this parameter is the interplay of strain within the sample and composition. For this reason, it is desirable to determine the size, the composition and also the strain. Thus a comprehensive investigation was done by scanning tunnelling microscopy, x-ray diffraction measurements, transmission electron microscopy and photoluminescence.

3.1 Epitaxy system at the Paul Scherrer Institut

Growth was performed in a commercial system (Balzers UMS 500). A schematic representation of the UHV epitaxy system is given in Fig. 3.1. It consists of a Molecular Beam Epitaxy (MBE) system of Balzers and a Chemical Vapour Deposition (CVD) system, both designed for four-inch wafers. These systems are combined via a transfer and a plasma chamber. The samples discussed in the present work were only prepared in the MBE chamber. The sample preparation was optimised to avoid contamination of the epitaxial layer interface of the substrate and not to prepare the best atomically flat surface for STM investigations. The goal was to investigate the growth mechanism close to conditions suitable for industrial processing.

The MBE system can be loaded via a self-made load-lock. This load-lock can pick up six four-inch wafers, which lie upside down in silicon rings to avoid contamination by manipulators. The wafers are transferred to the MBE chamber by the manipulator of the central transfer chamber. Its manipulator is fully rotateable and can be extended up to 84 cm. This allows transferring the wafers among all attached chambers (plasma-, MBE-chamber, load-lock, Scanning Tunnelling Microscope). The MBE itself reaches a base pressure of approximately $2 \cdot 10^{-11}$ mbar, pumped by a 330 l/s turbo molecular- and a titanium sublimation pump. A Bayard-Alpert ionisation gauge measures the pressure. A cross-section of the used MBE-chamber is given in Fig. 3.2.

Five evaporation sources are installed at the bottom of the chamber. Two electron beam evaporators (Balzers 200 U) for the growth of Si and Ge, a high temperature effusion cell for p-type doping with boron (HTS 35, MBE-Komponenten), a low

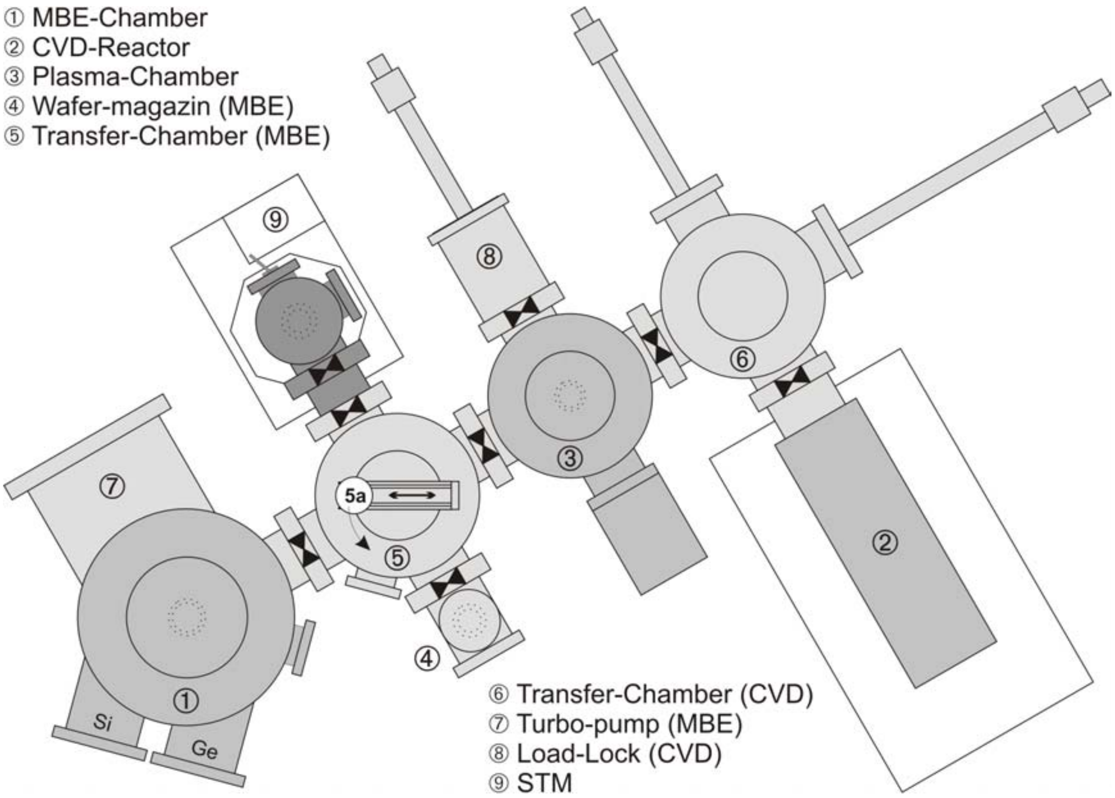
① MBE-Chamber
② CVD-Reactor
③ Plasma-Chamber
④ Wafer-magazin (MBE)
⑤ Transfer-Chamber (MBE)
⑥ Transfer-Chamber (CVD)
⑦ Turbo-pump (MBE)
⑧ Load-Lock (CVD)
⑨ STM
5a
Si
Ge
①
②
③
④
⑤
⑥
⑦
⑧
⑨

Fig. 3.1: Epitaxial-system at the PSI. It consists of a CVD and an MBE, which are connected via a plasma-chamber. Wafers can be exchanged between CVD and MBE. Details of the MBE are shown in Fig. 3.2.

temperature effusion cell for n-type doping by antimony (NTEZ, MBE-Komponenten), and a carbon sublimation source (SUKO 63, MBE-Komponenten), which should deliver a high fraction of monoatomic C into the C flux. The effusion cells are driven at constant temperature using a constant filament current adjusted by Eurotherm controllers (930 series controllers). The Si an Ge flux of the electron beam evaporators are controlled by the emission currents of the filaments as well as by the focus of the e-beams. The fluxes of Si and Ge are permanently recorded by a quadropole mass spectrometer (Balzers QMA 400). These values are used for adjusting the emission current and the focus of the electron beams. The emission current is used to adjust roughly the flux, while the focus of the electron beam is used for fine tuning and stabilization of the fluxes. In this way, very good flux stability and fast flux transients are guaranteed.

The Si and Ge e-beam evaporators with a liquid melt require the upside down mounting of the four-inch wafer. It is just beneath a graphite substrate heater, which allows heating of the wafer during growth and back out up to 950°C. To record the

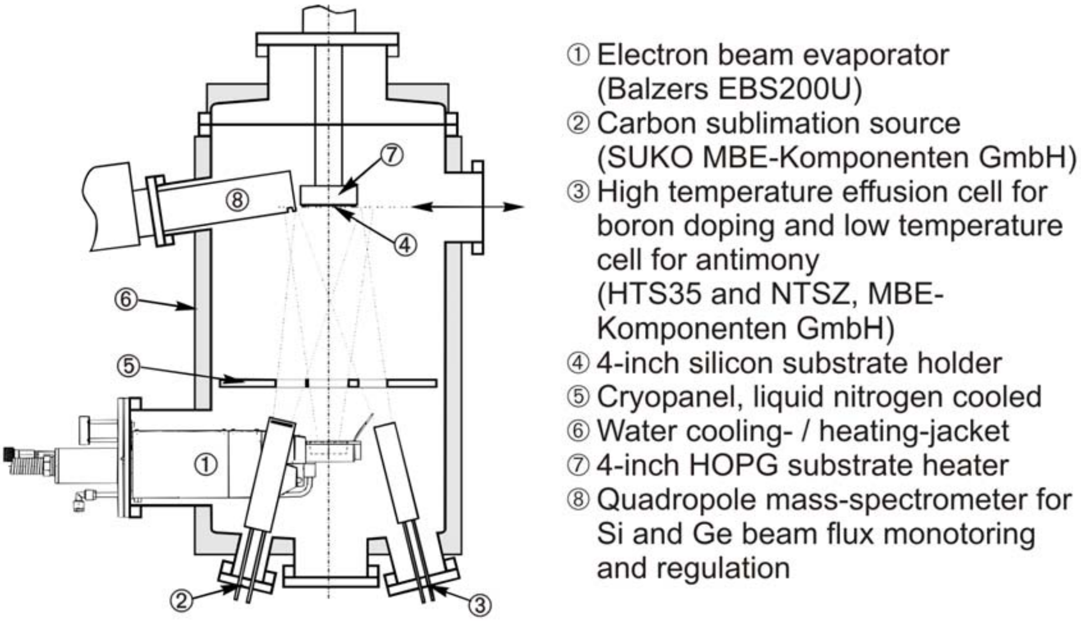
① Electron beam evaporator
(Balzers EBS200U)
② Carbon sublimation source
(SUKO MBE-Komponenten GmbH)
③ High temperature effusion cell for boron doping and low temperature cell for antimony
(HTS35 and NTSZ, MBE-Komponenten GmbH)
④ 4-inch silicon substrate holder
⑤ Cryopanel, liquid nitrogen cooled
⑥ Water cooling- / heating-jacket
⑦ 4-inch HOPG substrate heater
⑧ Quadropole mass-spectrometer for Si and Ge beam flux monotoring and regulation
①
②
③
④
⑤
⑥
⑦
⑧

Fig. 3.2: Cross section of a Balzers UMS 500 Molecular Beam Epitaxy System. It has electron beam evaporators for Si and Ge, effusion cells for boron and antimony, and a carbon sublimation source. The base pressure is 10^{-11} mbar.

temperature, a thermocouple is mounted directly above the heater. During growth, the wafer can be rotated and a bias can be applied additionally.

The sources and the heater are equipped with water cooled shieldings to reduce the heat load of the MBE chamber. The mass spectrometer is cooled by water as well. To improve the pressure during growth, a cryogenic shield cooled by liquid nitrogen is mounted directly above the sources. Holes in the shield confine the atom beams by cutting out the divergent part of the beams and thus minimize the deposition at the chamber ceiling. With very fast pneumatic shutters, which are above the holes in the cooling shield, a quick change of deposited material can be realized during growth.

The MBE system is controlled by a VAX computer system in real time. It allows the independent control of the five evaporation sources. The flux of material during the growth and the growth temperature can be kept constant or ramped. The growth rates are determined by the flux of material from the sources and can be chosen independently from each other and from the growth temperature.

3.2 Sample preparation

A typical sample preparation consists of the cleaning, the loading, the transfer into the MBE-chamber, the growth of a sample, and the transfer of the sample into the STM. The typical 4-inch substrates are polished from one side and have a (001) surface orientation. The miscut angle is below 0.5°. For cleaning, the upper nanometers of the wafers are etched to remove the dirt. In addition, the surfaces of the wafers were passivated to protect them. The etching and passivation is done by oxidizing the wafer surface in a Caros etch (H_2SO_4: H_2O_2 2:1) at 90°C for 10 minutes. Subsequently the wafers are placed into a quick dump rinser to remove the remaining acid. They are rinsed in the water until the resistance of the cleaning water reaches 13 MΩ. The last step is a 2-minute-dip of the wafer in an aqueous hydrofluoric acid solution (5%). The dip removes the silicon oxide from the surface and passivates the dangling Si bonds at the surface with hydrogen. Immediately after the cleaning procedure the substrates are placed into the load-lock of the MBE system. When the pressure in the load-lock decreased below $3 \cdot 10^{-8}$ mbar the substrate was transferred into the MBE-chamber. Afterwards, the substrate is baked in a two step process. In the first step, the temperature is ramped to 650°C within 180 seconds and kept at this temperature for 5 minutes. The temperature is increased slowly and kept below 700°C, as under these conditions the hydro-carbons on the sample surface desorb and a SiC formation which occurs at temperatures above 700°C can be avoided. In the second step, the temperature is raised to 950°C within 180 seconds and kept at this temperature for 30 minutes to desorb silicon-oxide. After the bake-out, the growth temperature is lowered to 750°C and a 1000 Å thick Si buffer is grown at a rate of 1Å/s. The high temperature of 750°C avoids long range undulations, as they typically occur at lower growth temperature [72]. After the growth of the buffer, the preparation of the substrate surface is finished and the desired structure can be grown. When the epitaxial process is finished, the temperature is decreased below 200°C and the sample is unloaded or transferred into the Scanning Tunnelling Microscope.

3.3 Scanning tunnelling microscopy

Scanning tunneling microscopy (STM) was developed and introduced by Binnig and Rohrer in 1982 [73]. A detailed treatment of STM theory and applications can be found in [74]. The basic principle is, that a sharp tip is brought close to a conductive surface, as indicated in Fig. 3.3, until the wave functions of the tip and the surface overlap. If a bias voltage between the tip and the surface is applied, electrons can tunnel from the tip into the surface or vice versa, depending on the sign of the voltage. The correlation between the tunnel current and the electronic structure of the sample is shown in Fig. 3.4. Here, an energy diagram of the tunnel junction between an

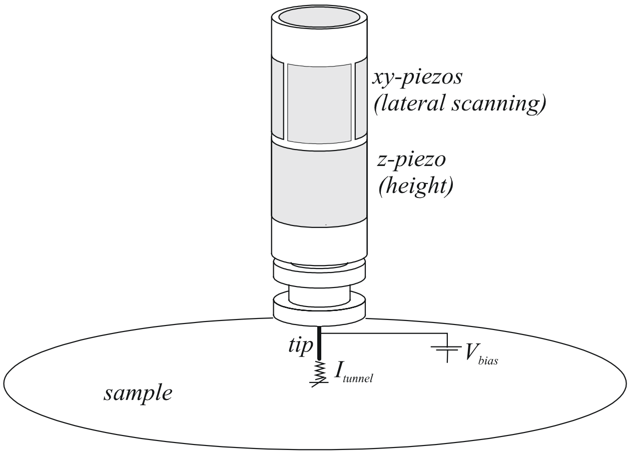

Fig. 3.3 Principle of scanning tunnelling microscopy.
Between a tip and the sample surface a bias voltage is applied. The tip is moved by a piezo towards the sample surface, until a tunnel current occurs. When the tip is scanning horizontal over the surface, I_{tunnel} is kept constant by changing the piezo length. This length changes correspondent to the structure

adsorbate-covered metal surface and a metallic tip is shown. On the left and right side of the picture the density of states (DOS) of the tip are shown for different applied bias voltages related to the sample surface. The density distribution is for simplification reason omitted to be smooth. In the middle, the DOS of the sample surface is indicated. Only electrons from states between the Fermi levels of the tip and the surface can contribute to the tunnel current. This energy window of the two Fermi levels is defined by the applied bias voltage. For a negative bias voltage as shown on the left side, the electrons tunnel from occupied states of the tip into the empty states of the sample surface, while for a positive bias voltage, they tunnel from the occupied states of the surface into the empty ones of the tip. According to the simplified interpretation of STM images by Tersoff and Hamann [75], the tunnel current is proportional to the electron density of the sample at E_f. By scanning horizontal over a

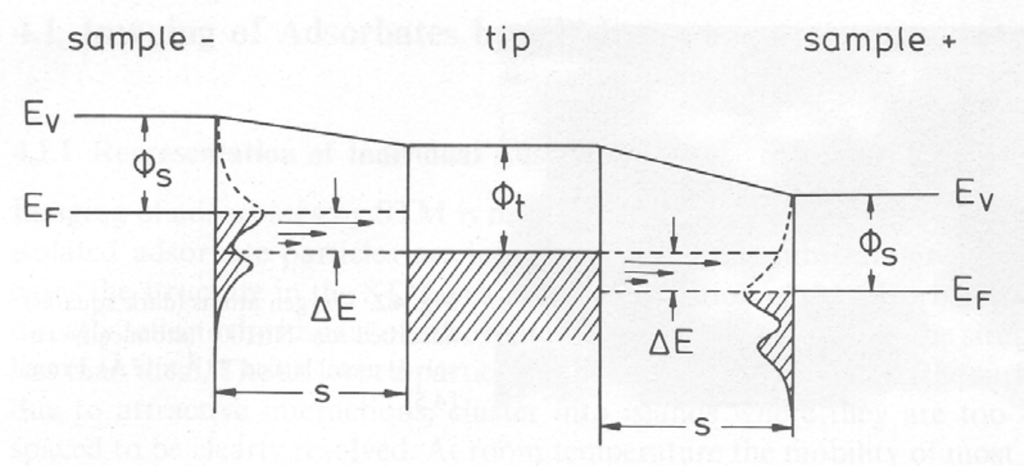

Fig. 3.4 Schematic energy diagram for the tunnel contact between a metallic tip and an adsorbate cover metal surface. Left junction: negative sample bias, right junction: positive sample bias [75]

sample and keeping the tunnel current constant, contour plots of the local density of states at E_f are obtained. In this way an STM maps the electronic structure of a surface. The horizontal scanning and the tracking of the tip to keep the tunnel current constant is done by piezos, as shown in Fig. 3.3.

The importance of STM to determine dimensions and facets of structures was already shown in the introduction and will especially be demonstrated in the chapters 5, 6 and 7. Here, the STM was used to investigate samples in-situ, as they were grown by our Molecular Beam Epitaxy (MBE) system. To realize this, the STM has to fulfil some conditions:

i) Handling of four-inch wafers with their support rings, as used in the MBE-CVD epitaxy system
ii) In situ transfer in vacuum to avoid contamination and oxidation
iii) Damping of vibrations to obtain atomic resolution
iv) Investigation of homogeneity of the whole wafer surface

These requirements are met by our home-made STM shown in Fig. 3.5 [21]. It is fabricated from a DN150CF five ways cross with seven additional DN40CF flanges on the sixth side. To achieve an in-situ transfer, it has in addition a load-lock to realize the connection to the transfer chamber of the MBE system and to a manipulator for loading of tips. The base pressure of the STM chamber is $1 \cdot 10^{-10}$ mbar, while the pressure in the load lock is typically $1 \cdot 10^{-9}$ mbar after a pumping time of about 12 hours. During transfer the pressure is therefore at no time higher than $1 \cdot 10^{-9}$ mbar and in-situ measurements are possible. The low pressure within the STM chamber reduces contamination of the surface, as the number of particles hitting and being absorbed by the sample surface is determined by the pressure. The contamination starts to become important after about eight hours, when too many residual atoms or molecules are absorbed.

As typically one tip is needed for each measurement and the fabrication and loading of tips takes up to 24 hours, an additional tip magazine was mounted to the system. This tip magazine is designed to store up to 10 tips and allows the in-situ change of the tips used for scanning. This can be done with the help of a wobble stick, as the tips are fixed by a magnetic coupling. As loading of new tips is therefore only necessary after every 10th experiment, experimental throughput is substantially improved.

To avoid vibrations introduced by the epitaxy system, e.g. due to the turbo molecular pumps, rotary pumps, or acoustic noise, the STM is disconnected and moved to a more silent room. For this reason, it is placed on a trolley, which also allows vertical movements. The latter allows putting the STM on a damped table (Newport I-2000 series) that suppresses vibrations with a frequency higher than 1 Hz. A second mechanism to avoid vibration is realized with the sample stage of the STM. It hangs on springs and is equipped with magnets that pass a copper stage. This acts as an eddy current brake [103]. Another source of vibrations are the eigen-frequencies of the wafer. To suppress them, the wafer is fixed with clamps on a massive block. This is important, as a beetle STM (developed by Besocke) is placed on the surface of the wafer, which would due to its scanning movements excite these eigen-oscillations.

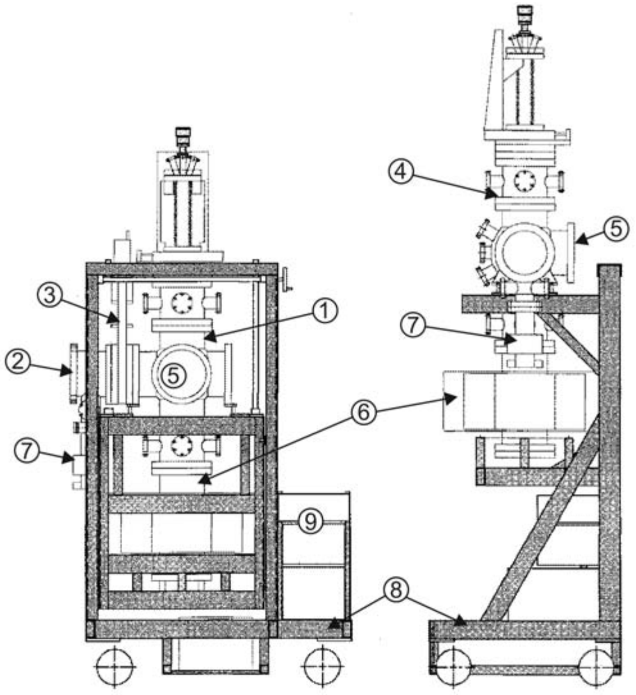

(1) STM main chamber
(2) lock chamber
(3) DN150CF gate valve
(4) flange carrying whole STM assembly
(5) viewports DN150CF
(6) ion getter pump (200 l/s)
(7) turbomolecular pump (50 l/s)
(8) movable trolley with chamber height adjustment
(9) power supplies for pumps and pressure gauges

Fig. 3.5 Scanning tunnelling microscope equipped with a beetle type scanner. The STM is moveable to disconnect it after the wafer transfer from the MBE, as this avoids vibration of the MBE-system.

With these precautions, atomic resolution is achieved. As the wafer is upside down in the MBE and the STM has to be placed on the surface of the wafer, the wafer is rotated by 180° within the sample stage of the STM.

To investigate the whole surface, the STM can be placed with a manipulator on any part of the surface of the sample. The STM itself is placed on three piezo-“legs” with ruby feet onto the surface of the substrate. The inchworm-motor in the centre is used for the tip approach. At the end of the inchworm, the scan-piezo is mounted. The outer piezos allow moving the STM by applying saw tooth voltages. The movement is in the range of micro- to millimetres and is used for the fine positioning. In addition, the STM can be rotated with the piezos. The ruby feet cause some scratches on the surface, but they are never within the scan area, due to the large distance between the scan tip in the centre and the “legs” at the edge.

The tips are self-fabricated by wet-chemical etching of a tungsten wire (∅ 250 µm) with NaOH. When the tip is dipped into the NaOH, a cone is formed. At this cone, the etching is faster and therefore sharp tips with a final diameter smaller than 100 nm are fabricated. The tip approach is done by a combination of inchworm movements and the scan piezo extension. This is not the typically beetle design, but allows to bridge larger distances. The maximum scan size of our STM is 1.5 µm by 1.5 µm. The electronics of the system are a combination of a RHK (model SPM 100) and a self-made Besocke compatible controller. The Besocke controller is responsible for the movements of the beetle STM and the inchworm, while the RHK controller manages the scan piezo, in particular the x-, y-, and z-movement.

3.4 X-ray diffraction measurements

X-ray diffractometry is a good complement to STM. STM measures the size and the shape of single dots. By simulating the data obtained by X-ray diffractometry and using the STM values as input parameter, the average size, shape, strain and composition of the dots is determined. Due to the nature of the samples, as they consist of layers of buried dots or as in our case of a single dot layer on top of a Si buffer, the diffraction measurements underlay certain restrictions.

A scattering experiment can be understood as measurement of intensities along certain paths in reciprocal space, where the scattering is normally of elastic type. This means, that the absolute value of wave-vectors $\mathbf{k_i}$ and $\mathbf{k_f}$ of the incident and scattered waves are the same $|\mathbf{k_i}| = |\mathbf{k_f}| = k$. The resulting momentum transfer $\mathbf{Q} = \mathbf{k_f} - \mathbf{k_i}$, which is

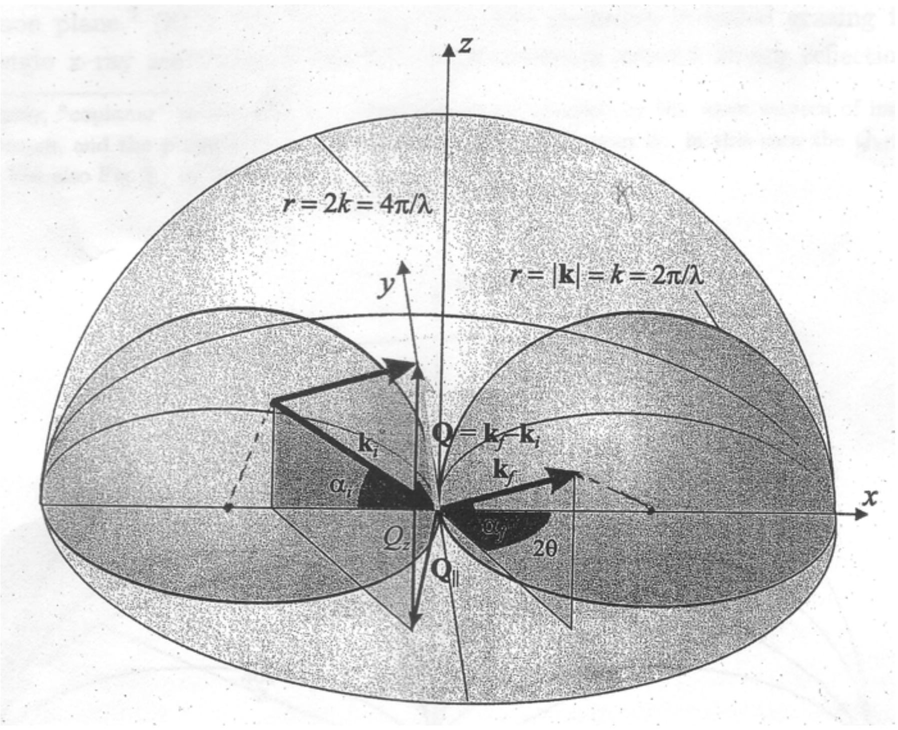

Fig. 3.6 Sketch of the accessible region of the reciprocal space during a scattering experiment. The region beyond the larger half-sphere is not accessible, as the momentum transfer is limited by the incident- and exit-wave-vectors $|\mathbf{Q}| < 2k$. As the incident beam cannot penetrate thought the sample, the so-called Laue zones are also forbidden, indicate here by the smaller half-spheres.

important quantity of the experiments, is therefore limited to $|\mathbf{Q}| = Q = 2k$ and determines the accessible range of the reciprocal space, as indicated by the outer sphere in Fig. 3.6. As the investigated samples have a thickness larger than the absorption length of the x-rays, there is the limitation that the incident and scattered wave-vectors have to be on the same side of the sample. This leads to the restriction that only the upper half-sphere is accessible and in addition, that regions within the two Laue-zones indicated by the two smaller half-spheres in Fig. 3.6 are forbidden, leaving only the region between the outer- and the inner two half-spheres. For Si and a $Cu_{K\alpha}$ source some of the Bragg peaks which lie within the accessible range are shown in Fig. 3.7. The figure is drawn with the crystallographic [001] direction along the z-axis and for a sample azimuth with the [110] crystallographic direction along the incident beam ($\mathbf{k_i}$ || [110]). The relative alignment of the reciprocal space is determined by the azimuth (rotation of the Bragg peaks around the x-axis) and the sample tilt (rotation around the x-axis). The length of the wave-vector influences the accessible range within the reciprocal space.

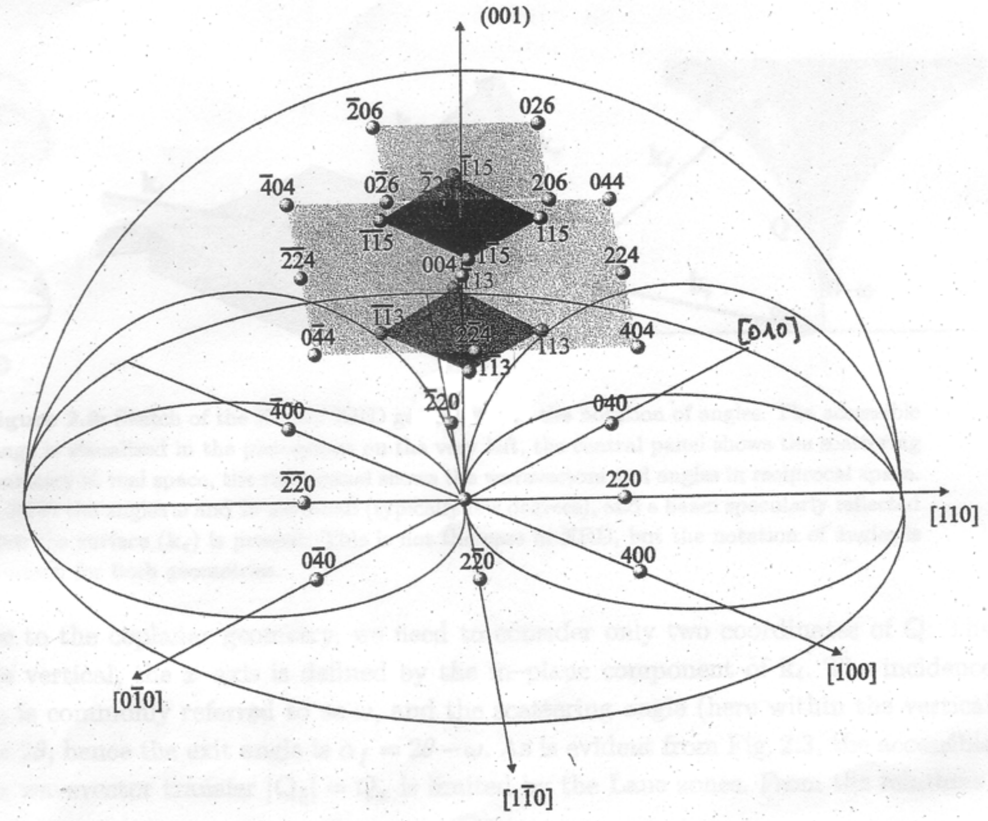
(001)
$\bar{2}06$
026
$\bar{1}15$
$\bar{4}04$
$0\bar{2}6$
206
044
$\bar{1}\bar{1}5$
115
$\bar{2}\bar{2}4$
004
$1\bar{1}5$
$\bar{1}13$
224
$\bar{1}\bar{1}3$
$0\bar{4}4$
$2\bar{2}4$
113
404
$1\bar{1}3$
[010]
$\bar{4}00$
$\bar{2}20$
040
$\bar{2}\bar{2}0$
220
[110]
$0\bar{4}0$
$2\bar{2}0$
400
[100]
$[0\bar{1}0]$
$[1\bar{1}0]$

Fig. 3.7 Position of the most frequently measured Bragg reflections for a particular sample orientation: pole in direction [001] and azimuth in direction [119]. Semi-transparent planes connect reflection of the same Q_z.

Under these restrictions two main groups of possible experiments can be distinguished. One investigates the vicinity of the reciprocal space close to the origin (000), while the other measures Bragg reflections (hkl) outside the origin. For the first group, two different methods exist. One is called coplanar X-Ray Reflectometry (XRR). Here the incident and exiting beam lie together with the surface normal within one plane. When this is not the case, the geometry is called Grazing Incidence Small Angle X-ray Scattering (GISAXS). Both geometries are insensitive to the crystalline state of a sample, e.g. the strain, as only the vicinity of the origin of the reciprocal space is investigated. Only the variation of the averaged electron density in the sample plays a role. Therefore this method is sensitive to structural and morphological properties as layer-thickness, composition, and interface- and surface-roughness as well as their lateral and vertical correlation properties. For XRR, due to the coplanar geometry, the in-plane wave-vector transfer $\mathbf{Q}_{||}$ is limited by the Laue Zone, while there are no restrictions for GISAXS. The advantage of XRR is the high in plane resolution, while GISAXS does not underlie the restrictions of the Laue Zone and can therefore be used for investigating small lateral structures. This is the reason why GISAXS has been used widely to investigate dot samples, e.g. Schmidbauer et al investigated semi-quantitatively the shape and lateral correlation of large freestanding Ge islands on a Si(001) surface by GISAXS and AFM [76]. For $Si_{1-x}Ge_x$ islands that were grown by liquid phase epitaxy at 600°C, they obtained truncated pyramids with {111} facets. Local ordering effects of small numbers of islands were found along the <100> and <110> directions, which was in agreement with the AFM-data. It was assumed, that these ordering is due to strain induced by the islands itself. As the GISAXS and the AFM-data gave similar results, it was expected that this method can be used also for buried islands. This was indeed done by Stangl et. al., who used GISAXS in a semi quantitative study to investigate a stack of buried c-induced Ge dots that were separated by Si spacers. They investigated the shape and size, as well as the lateral and vertical correlations. The shape was found to be lens like with a width of about 12 nm and a height of 1.7 nm. The mean distance was 30 nm. In contrast to normal stacks of Ge dots with Si spacer, no lateral or vertical ordering was found. It is assumed, that this is due to the lower mobility of Ge on the carbon modified surface. With GISAXS the lateral and vertical ordering effects as well as shape and size can be observed, but if the strain and composition is of interest, one has to choose a geometry of the second group of possible investigation methods.

The second main group, that investigates bragg reflections outside the origin of reciprocal space, is divided into three subgroups: X-Ray Diffraction (XRD) again in coplanar arrangement; Grazing Incidence Diffraction (GID) were only small incidence angles are used and therefore only Bragg reflexes with $l = 0$ can be investigated, and non-coplanar XRD. It has not got a name yet, as it is seldom used for investigations.

From the geometrical point of view XRD is similar to XRR, but now the vicinity of a certain reciprocal lattice point (hkl) with $l \neq 0$ is probed. This standard method is sensitive to the crystal lattice, esp. its vertical component, and can therefore be used to determine lattice strain, composition and relaxation of epitaxial layers, layer thickness etc. The steep incident angle is the main disadvantage. The beam penetrates deeply into the substrate and the reflected beam has therefore a large contribution from the bulk crystal. Nevertheless Wiebach et al employed coplanar x-ray diffraction to study the interdiffusion of large $Si_{0.75}Ge_{0.25}$ islands grown by LPE on Si(001) [77]. In these studies, x-ray diffraction experiments that are sensitive to shape and strain were performed. A "brute-force" method was used to calculate the strain field by using the finite element method based on elastic theory and assuming well defined values for the shape, size, and composition of the dots. In a second step, the strain field is used to simulate the x-ray scattering intensity. Next one has to compare the simulation with the measured reciprocal space map and adjusting the size, shape, and composition. This way, the shape, size, composition and the strain are determined. As a result, a vertical Ge concentration gradient inside the island was obtained with 25 percent of Ge near the wetting layer, which increased after one third of the height abruptly to 30 percent. Here, the composition and besides this the strain of uncapped clusters were determined.

For GID the momentum transfer Q_Z in vertical direction (along growth direction) is virtually zero. Only lattice strain parallel to the sample surface can be determined by this method, but there is no information on strain in growth direction. The main advantage is the sensitivity to thin layers near the surface. The penetration depth of the beam depends sensitively on the incident angle of the beam. Whether chosen properly, the contribution to the signal can be restricted to a layer depth of 5 nm. The disadvantage of the method is: A big portion of the beam is specularly reflected and only a small portion contributes to the diffraction. Nevertheless, for some applications like the investigation of Ge-dot layers, there is no other way than using small incidence geometry. This method was used by Kegel et al, who performed grazing-incidence diffraction investigations to determine the relaxation and interdiffusion of free-standing InAs dots on GaAs (001) [78].

Another method combines the advantages of XRD and GID. It is surface-sensitive asymmetrical x-ray diffraction (GICE). Due to the small incident angle, it is like GID sensitive to the surface of the sample, but in addition, it has a finite vertical momentum transfer Q_z, making this method also sensitive to vertical strain components. The scattering experiment is described by four angles, the in-plane-angles 2θ and ω, and the incidence and exit-angles α_i and α_f, as can bee seen in Fig.3.8.a. The geometry in reciprocal space is shown in Fig. 3.8.b. The momentum transfer $\mathbf{Q} = \mathbf{k_f} - \mathbf{k_i}$ can be achieved with different combinations of the wave vectors of the incident and scatter beams $\mathbf{k_{i,f}}$. As the experiment has four degrees of freedom,

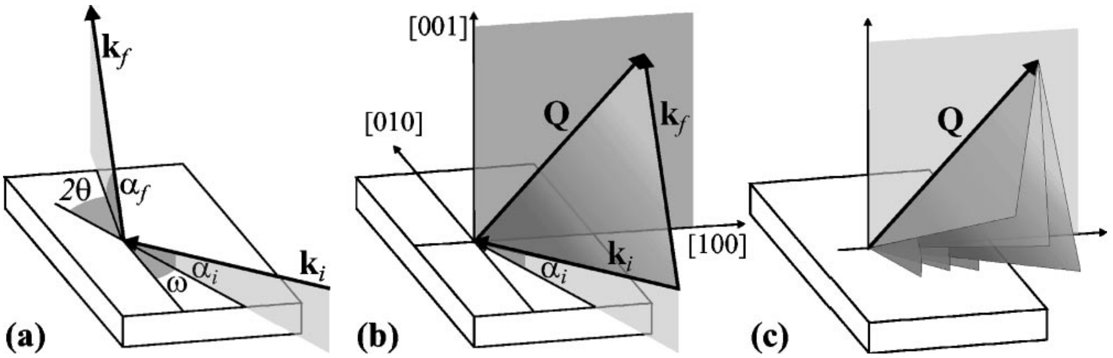

Fig. 3.8 Sketch of the scattering geometry in real (a) and reciprocal space (b) for the GICE-geometry. The scattering plane can be rotated around Q to tune the incidence angle (c) [52]

one of the angles can be determined independently, allowing to rotate the scattering plane stretched by $\mathbf{k}_{\mathbf{i,f}}$ around **Q**. This allows to keep α_i at a fixed value and preserve the surface sensitivity. In addition, Bragg reflexes are accessible, which could not be reached in the coplanar geometry of XRD. The disadvantage is, that the detector angles 2θ and α_f have to be varied for each measured point and it is impossible to use a position sensitive detector. Because we were interested in the lateral strain, the vertical one, and the composition of the dots, we chose the GICE-method for our investigations. The experiments were performed in cooperation with the group of Prof. Bauer from the university of Linz at the synchrotron source ESRF, in Grenoble (beamline ID10B). Because of the rather small scattering volumes, x-ray diffraction experiments were carried out at a high brilliance undulator beamline.

3.5 Transmission electron microscopy

Transmission Electron Microscopy (TEM) is a tool to investigate slices of samples. By thinning a sample either parallel or perpendicular to its surface, one can gather planar or cross-sectional views through the epitaxially grown layers and Ge dots. The formation of TEM-images can be understood from an optical ray diagram with an optical objective lens, as shown in Fig. 3.9. When a crystal is irradiated by electrons and the Bragg condition is full-filled, diffracted waves can be observed. In the back focal plane diffraction spots are then formed by the diffracted waves. The space is called reciprocal space. The transformation from real to reciprocal space is given by the fourier transformation. If the transmitted and diffracted beams interfere on the image plane, a magnified image of the sample can be obtained. The lateral point to

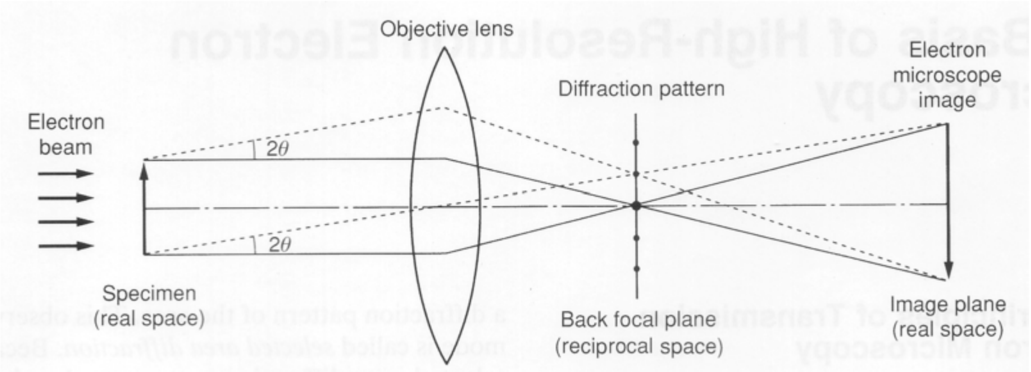

Fig. 3.9 Optical ray diagram with an optical objective lens showing the principles of imagine process in a transmission electron microscope [79]

point resolution of the TEM is determined by the spherical aberration coefficient C_s of the objective lens and the wavelength λ of the used electrons

$$d_s = 0.65 C_s^{1/4} \lambda^{3/4}.$$

Usually one is only interested in the elastic part of the scattered electrons, but when a high energy electron beam traverses a sample, the electrons of the beam interact with the electrons of the sample and lose a certain amount of energy. The energy loss is characteristic for the element, at which the interaction took place. By applying energy filters, electrons are selected that have only interacted with a special element e.g. Si, and an elementary map of this element can be obtained. As most of the electrons scatter elastically, the signal is very low and a special resolution in the range of 1 nm can be achieved, while the accuracy of the chemical composition is between 5 and 10 percent.

Our TEM samples consist of cross-sections through dots. They were investigated by High Resolution Transmission Electron Microscopy (HRTEM) and Energy Filtered TEM (EFTEM). The former gives cross-sections through the sample and allows insight into the facets, dislocations, and the roughness of interfaces and surfaces. The latter is sensitive to the composition of the samples and therefore provides information on the composition profile through the sample.

For both techniques, the specimens were mechanically pre-thinned and subsequently milled to electron transparency by Ar ions in a Precision Ion Polishing System from Gatan at an acceleration voltage of 4.3 kV and an edging angle of 4°. HRTEM and EFTEM were performed along the Si [110] direction in a Philips CM30ST TEM, shown in Fig. 3.10, at an acceleration voltage of 300 kV, leading to a point to point

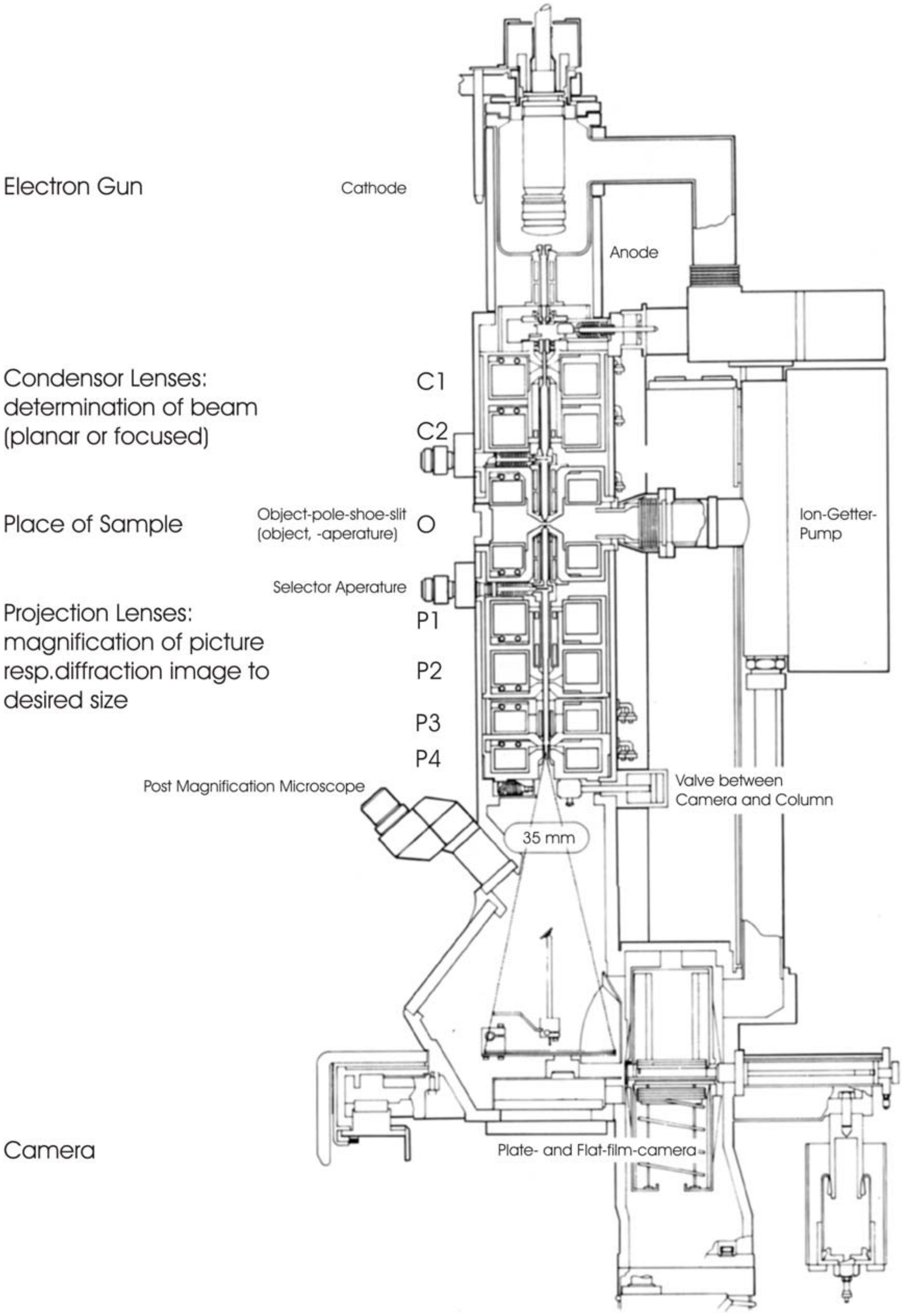
Electron Gun
Cathode
Anode
Condensor Lenses: determination of beam (planar or focused)
C1
C2
Place of Sample
Object-pole-shoe-slit (object, -aperature)
O
Ion-Getter-Pump
Selector Aperature
Projection Lenses: magnification of picture resp.diffraction image to desired size
P1
P2
P3
P4
Post Magnification Microscope
Valve between Camera and Column
35 mm
Camera
Plate- and Flat-film-camera

Fig. 3.10 Cross-section through the column of the Philips EM 400 Electron Transmission Microscope.

resolution of 0.19 nm, and in a Philips Tecnai ST (300 kV) equipped with a Gatan Imaging Filter, respectively. The three windows technique [80] was applied to the Si L-edge.

3.6 Photoluminescence

If a Ge dot is embedded in a Si matrix it forms a quantum box in the valence band, as schematically illustrated in Fig. 3.11. The shape of the dot and also its composition determines the position of the energy levels within the dot. Using photoluminescence measurements, the relative position of the energy levels of the involved hole and electron can be determined. The energy level of the hole is mainly determined by the size and the composition of the dot. The electron is also confined in a quantum well, which is built by the strained Si surrounding the dots [81]. The energy level of the electron depends therefore also on the composition of the dot, as this determines the strain within the silicon surrounding the dot. We used photoluminescence measurements to determine the variations in size and shape of Ge dots during the capping process of the dots. As previously indicated, this is a difficult task, since many factors interplay, but relative changes should be detectable.
To interpret the data correctly a deep understanding of band structure and the impact of strain and quantum structures on it is required. Hence, we briefly introduce the band structure, and the phonon dispersion of Si and Ge.

The reciprocal lattice of Si and Ge is body-centred cubic. Its first Brillouin zone is shown in Fig. 3.12 together with important symmetry axes, to help identifying important points, given in the band-diagram of Fig. 3.13. The maximum of the valence-band is for both materials at the centre of the Brillouin zone (k=0) and it is fourfold degenerated. The corresponding point in the centre of the Brillouin zone is

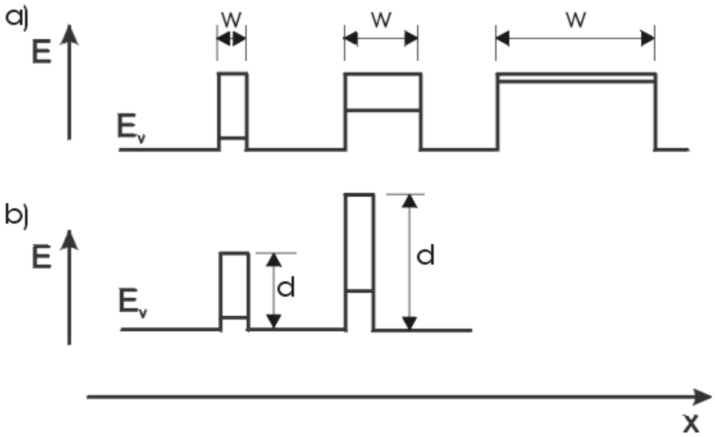

Fig. 3.11 Ge quantum wells within a Si matrix. a) If the size w of a Ge dot increases, the energy level responsible for the photoluminescence shifts closer to the conduction band.
b) With increasing Ge content within the dot, the well becomes deeper and therefore the energy level also shifts to higher energies.

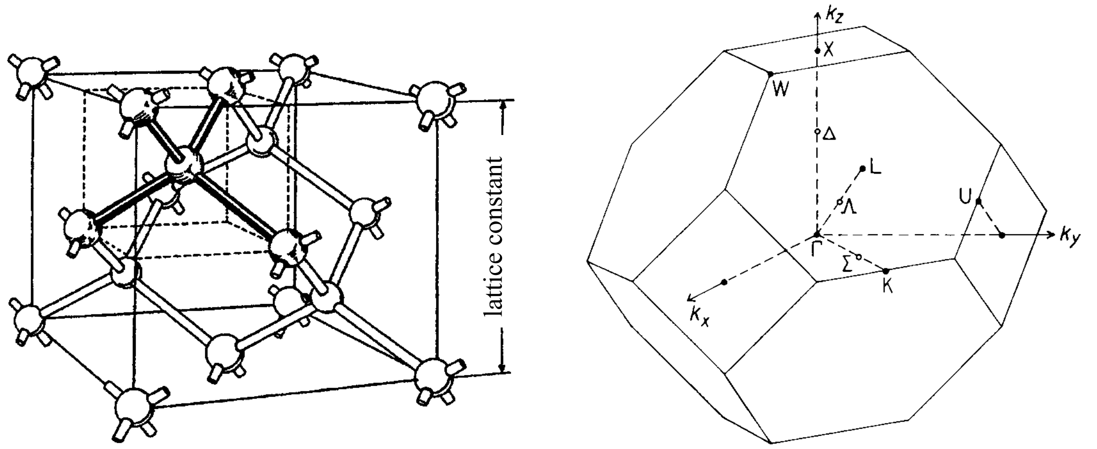

Fig. 3.12 Left: lattice structure of Si and Ge. The lattice consists of two bases, which are face centred cubic. One is shifted by (¼,¼.¼). Right: Brillouin zone of Si and Ge together with important symmetry axes and points.

called Γ. The four energy states differ by spin and by effective mass. For this reason, two of them are called heavy and two are called light holes. At Γ there are two further hole states, which have a slightly higher energy due to spin-orbit-coupling. For Si, the energy difference is 0.04 eV and for Ge it is 0.30 eV [82].

The minima of the conduction band for Si and Ge are not in the centre of the brillouin zone. For this reason, Si and Ge are indirect semiconductors. For Si the minimum is often called Δ and it is found on the symmetry-axes Δ between the points Γ and X in [100] direction in reciprocal space. As shown in Fig. 3.12, there are six equivalent X points, making the minimum of the conduction band six fold degenerated for Si. For Ge the minimum is found at the L point at the edge of the brillouin zone in [111] direction. There are eight equivalent L points, making the conduction-band-minimum of Ge eightfold degenerated.

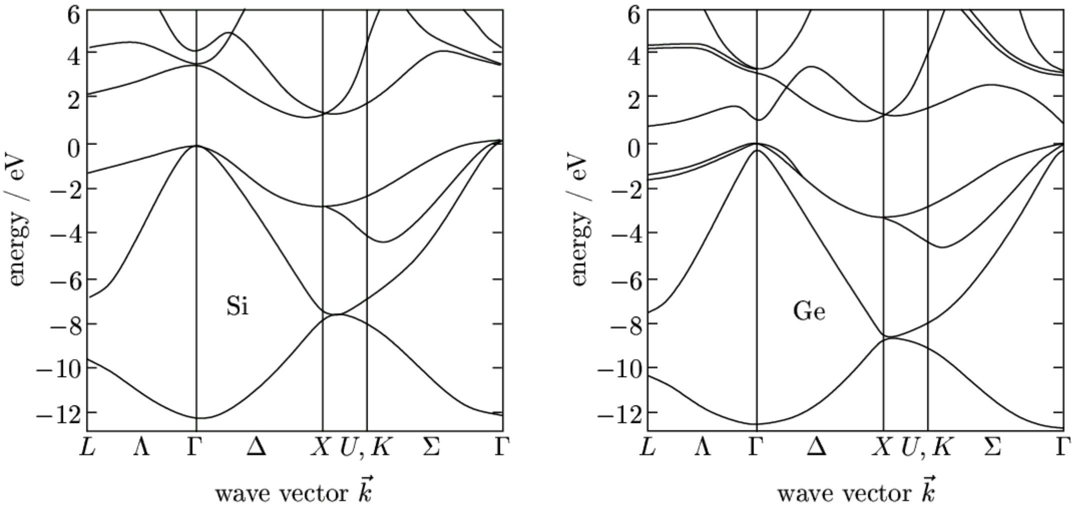

Fig. 3.13 Band structure of Si (left) and Ge (right) [83,84]. The energy states of the most important symmetry axes of the Brillouin zone were calculated by non- and local pseudo-potential.

The excitonic band-gap of Si, Ge, and its alloys was determined by photoluminescence measurements and is shown in Fig. 3.14 [87]. For the excitonic-band-gap the different positions of the conduction-band minima for Si and Ge play an important role. For low concentration of Ge, the band-gap is composed via the Δ point, which belongs to the Si conduction band minimum, while it is composed via the L point for high Ge concentrations. The switching is at a Ge concentration around 85 percent, where both minima for the electrons at Δ and L have the same value, and which splits the curves in Fig. 3.14 into two branches. For both ranges of the Ge concentration, x<0.85 and x>0.85, analytic expressions with a good agreement to the measured band gap energies can be given and are shown as lines in Fig. 3.14:

$$E^{\Delta}_{g,exciton}(x) = (1.155 - 0.43x + 0.206x^2)\ \mathrm{eV}\ \text{for}\ 0 < x < 0.85 \quad \text{(1a)}$$

$$E^{L}_{g,exciton}(x) = (2.010 - 1.27x)\ \mathrm{eV}\ \text{for}\ 0.85 < x < 1 \quad \text{(1b)}$$

The fundamental energy-gap has to be calculated by adding the binding energy of the free exciton to the given expressions. This binding energy is 14.7 meV for Si resp. 4.15 meV for Ge. For strained $Si_{1-x}Ge_x$ alloys on Si usually a simple interpolation of the values for pure Si and Ge is applied [88]. The fundamental band-gap turned out to be 1.170 eV resp. 0.744 eV for Si and Ge.

The indirect nature of Si and Ge requires, that a radiative recombination is a three-particle process with an electron, a hole and a phonon to compensate the momentum

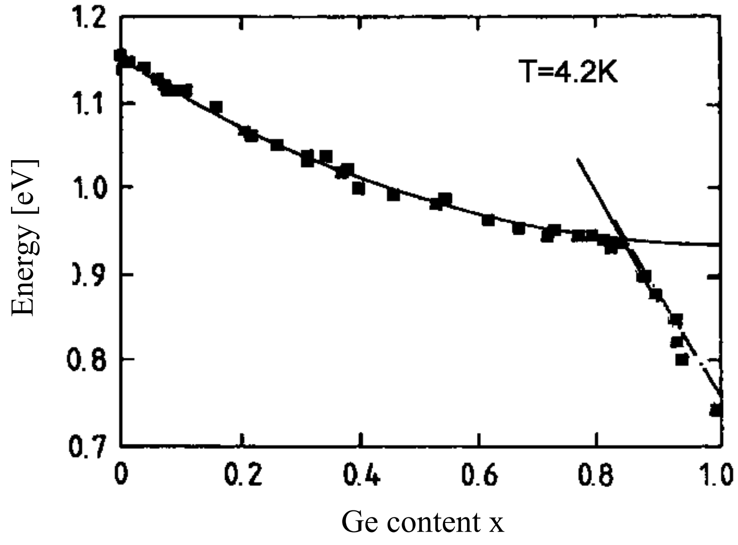

Fig. 3.14 Exciton band gap determined by photoluminescence measurements [87]. The measured values are shown as rectangles, while the equations 1a,b are shown as straight lines. Older values determined by absorption measurements, are shown as triangles.

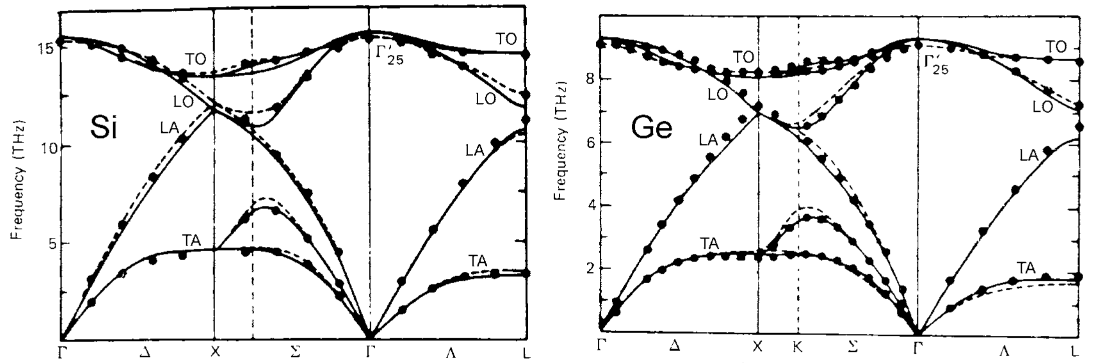

Fig. 3.15 Phonon-dispersion-relation for Si (left) and Ge (right) for important symmetry axes of the brillouin zone [85]. Experimental determined values are given as circles. The values of two different models are given as lines. A phonon-frequency of 1 THz equals a phonon-energy of 4.14 meV.

difference between the valence-band maximum and the conduction band minimum, as the momentum of the generated photon is negligible compared to momentum difference. Due to the fact, that the recombination is a three-particle process, its probability is clearly smaller than for a direct semiconductor where only two particles are involved.

The energy of the photon created during the recombination process is reduced by the energy of the necessary phonon. As the valence-band maximum is in the centre of the brillouin zone, its moment equals zero and therefore the momentum of the necessary phonon is equal to the momentum of the conduction band minimum position. The energy of the phonon can easily be determined by the phonon-dispersion-curve given in Fig. 3.15. Due to the degree of freedom of the two atoms of the primitive unit cell, six different phonons with partly different energies exist for every momentum. They belong to the three optical- and acoustical branches of the dispersion-relation. Two of the transversal optical-branches, resp. two of the acoustical branches of the dispersion relation have the same values for the symmetry axes on which the conduction band minima of Si and Ge lie. The dispersion relation for Si and Ge looks qualitative more or less the same, but the energies strongly differ.

For Si it is deduced from the dispersion relation, that the phonons can have energies of 58.0 meV (TO), 56.2 meV (LO), and 18.4 meV (TA) [90]. Fig. 3.16 shows a typical photoluminescence spectrum, which was detected with different slit sizes to determine also the less pronounced signals. Due to the imperfections of the sample, also the direct recombination, which should be normally forbidden, can be detected. This peak, which belongs to the excitonic band-gap, is marked with an NP as no-

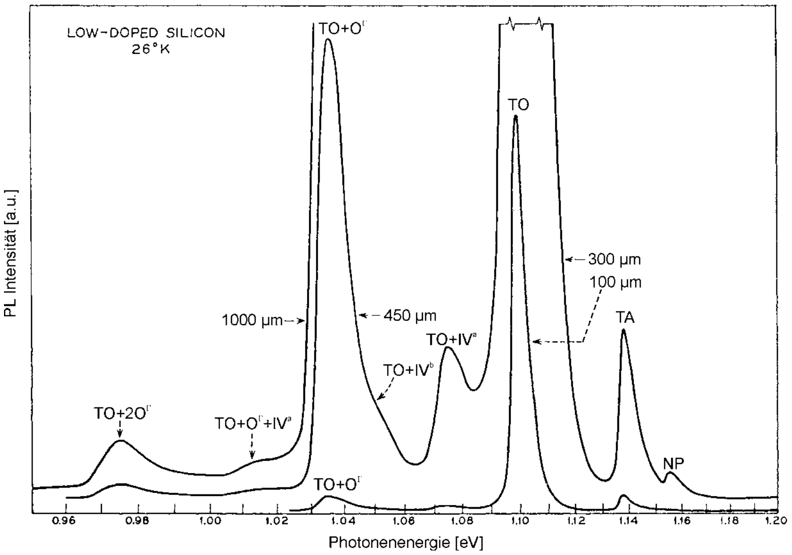

Fig. 3.16 Photoluminescence spectrum of a Si sample with $2{\cdot}10^{14}$ phosphor atoms. The spectrum was measured at 26 K with a slit size of 1 mm and 0.1 mm [89].

phonon in the diagram. The next two peaks with a strong signal are found at positions with an energy difference of 18 meV and 58 meV. These peaks belong to the TA and TO phonon. All other peaks belong to multiple phonon processes, where the TO and TA phonon have the necessary momentum.

For the Ge, the conduction band minimum is found at the L point of the brillouin zone. The corresponding energies of the phonons are 35 meV (TO), 30 meV (LO), 27 meV (LA), and 8 meV (TA) [82]. For $Si_{1-x}Ge_x$ alloys, the phonons belong to oscillations between Si-Si, Ge-Ge, and Si-Ge atoms. The phonons of the Si-Si and Ge-Ge phonon are the same as for pure Si and Ge, while the Si-Ge phonon has an energy of 49 meV and belong to the TO branch of the dispersion relation [91].

When Ge dots are embedded in a Si matrix, in addition to the photoluminescence

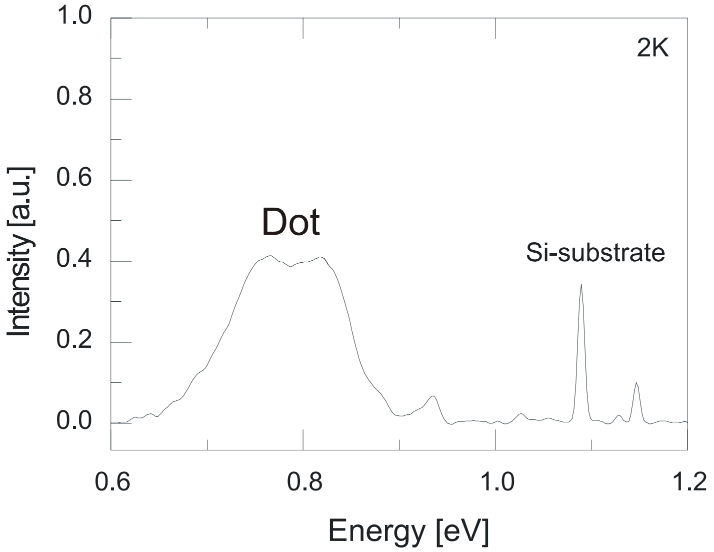

Fig. 3.17 Photoluminescence signal of a Ge dot stack. The broad double peak around 0.8 eV belongs to the Ge dots, while the peaks above 1 eV belong to the Si substrate, as shown in Fig. 3.16.

which originates from the Si spacers and substrate, the photoluminescence from the Ge dots is found as indicated in Fig. 3.17. Here, the PL energy depends on the size and the composition of the dot, as mentioned in the introduction.

In our photoluminescence experiments the energy of the exciting photons is larger than the band gap of the investigated material. An argon laser with photon energy of 2.54 eV (≡ 488 nm) and an output power of 12 mW was chosen. The set-up is sketched in Fig. 3.18. The spot size of the beam is about 1 mm^2. It was focused under an angle of 45° with a convex-planar lens on the sample. The size of the illuminated area of the sample surface was not measured, but can be estimated to be about 7000 μm^2. The luminescence was collected with a lens, covering the light under an angle of 90° with respect to the surface. A fourier-transformation-infrared spectrometer (Bruker Equinox 55) was used, to measure the luminescence. To be sensitive to the near infrared spectrum an InSb-detector (Bruker D413) and a beam splitter with a Si coating of CaF_2 (Bruker T401/3) was used, permitting to measure the PL signal between 0.5 eV and 1.3 eV. To distinguish between the luminescence signal and background illumination a lock-in technique was applied, using an amplifier (EG&G Parc model 5210) and a chopper positioned between the laser and the first lens. The temperature could be varied, as the sample was mounted in a bath cryostat (Janus SVT-300). By cooling the sample with helium and using an additional heater, measurements between 2.7 K and room temperature are possible.

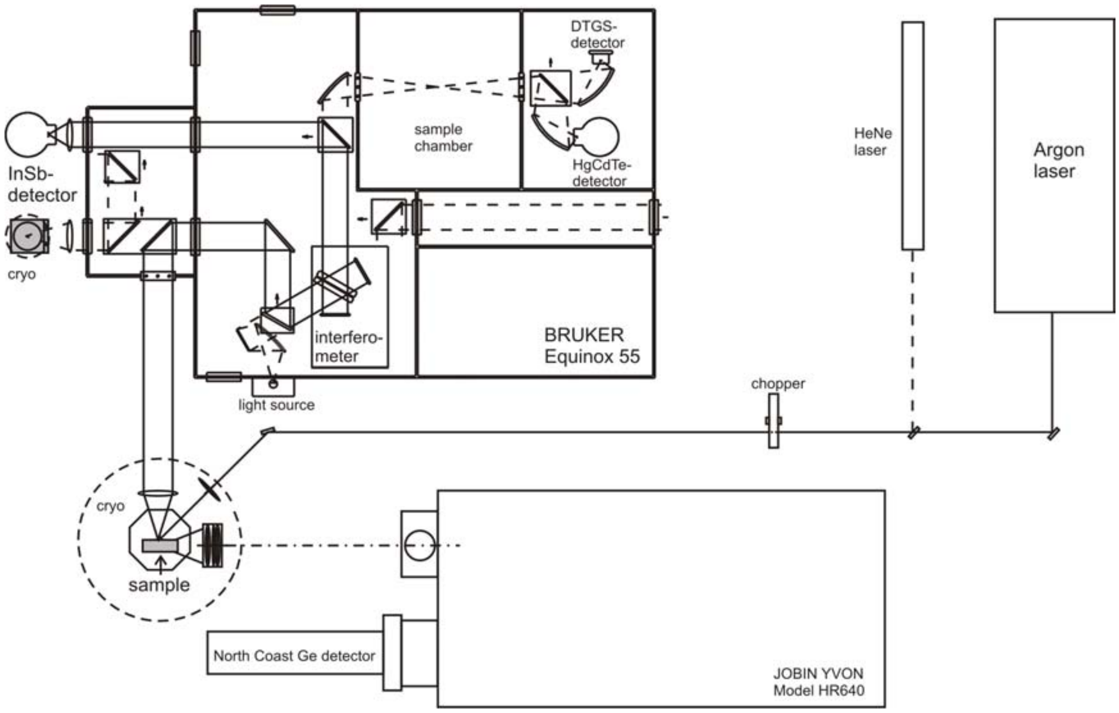
DTGS-detector
sample chamber
HgCdTe-detector
InSb-detector
cryo
interfero-meter
BRUKER Equinox 55
light source
HeNe laser
Argon laser
chopper
cryo
sample
North Coast Ge detector
JOBIN YVON Model HR640

Fig. 3.18: Photoluminescence set-up

4 Ge dots on a silicon (001) surface

A good confinement of carriers is needed and therefore the dots have to be small and with a high Ge content to improve radiative recombination efficiency (as described in the introduction). For this reason, in a first step, we studied the growth of Ge dots on a pure silicon surface to see, if the prerequisite can be fulfilled. Therefore we investigated the influence of the growth parameters, i.e. the growth temperature and the amount of deposited material, on the shape and size of the Ge dots and the reproducibility.

4.1 Growth parameters

The samples were prepared as described in paragraph 3.2. The shape and the size of the dots were determined for four different growth temperatures in the range between 550 °C and 820 °C. For the low temperature grown dots at 550°C and 580°C, the amount of deposited material was kept constant at 6.2 ML. Both samples have so called elongated hut clusters that were described in paragraph 2.4 and are shown in Fig. 4.1. As described in paragraph 2.4, normally squared hut clusters should be energetically more favourable and the kinetics at low growth temperature might be responsible for the elongation. A hint for this assumption might be, that on one side the dot density ($4.7\cdot10^{10}$ cm^{-2}) for the sample grown at 550°C is about a factor of five higher compared to the density of the sample grown at 580°C ($1\cdot10^{10}$ cm^{-2}). On the other hand the average length of the diagonal (48.1 nm) is about 10 nm longer

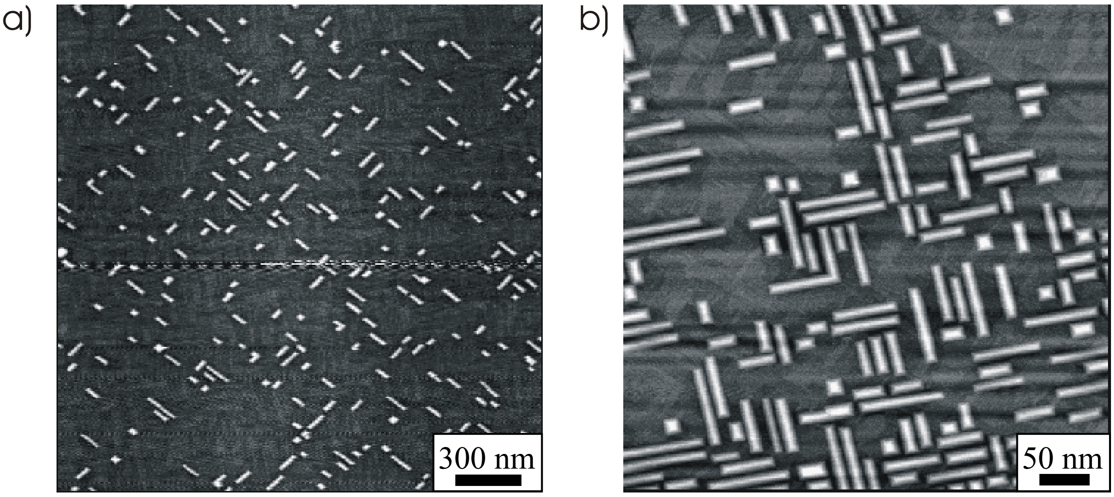

Fig. 4.1 Dots formed after the deposition of 6.2 ML of Ge. The sample on the left side (a) was grown at 550 °C, while the growth temperature for the right sample (b) was 580°C. Both samples have elongated hut clusters due to the low growth temperature.

compared to that of the sample grown at 580°C (38.6 nm). This indicates that for a growth temperature of 580°C, the Ge diffusion length is larger and the material is consumed from larger areas for a single dot, leading to the lower density. Also, as indicated by the smaller diagonals, the hut clusters base become more square like, as seen by the ratio of side length, which is 1 : 3.6 for the dots grown at 550°C, and 1 : 2.5 for the islands grown at 580°C.

For the samples grown at 820°C, at high temperature, the amount of deposited Ge was varied. For the first it was 7 ML, while for the second one 14 ML were deposited. As shown in Fig. 4.2, even though 7 ML is a high amount of deposited material, only hut clusters were found. In addition, the mean base length of the squared hut cluster is very large (184 nm). The increase to 14 ML leads to the formation of hut and dome clusters. The averaged size of huts with 151 nm base length and domes with a mean diagonal of 168 nm are again quite large. In addition, the size of the dots is reflected in the low densities of dots for the two samples, which are just $5 \cdot 10^8$ cm^{-2} (7ML of Ge) and $7 \cdot 10^8$ cm^{-2} (14 ML of Ge). Here the high growth temperature has two effects. One is the high surface diffusion length, which leads to a similar but stronger pronounced effect as already seen for the low temperature grown islands, the decrease in density of dots as material from larger areas is consumed for a single dot. The second one is stronger intermixing with Si from the substrate. Due to the reduced Ge content, less strain is built up in a dot compared to one with the same volume but

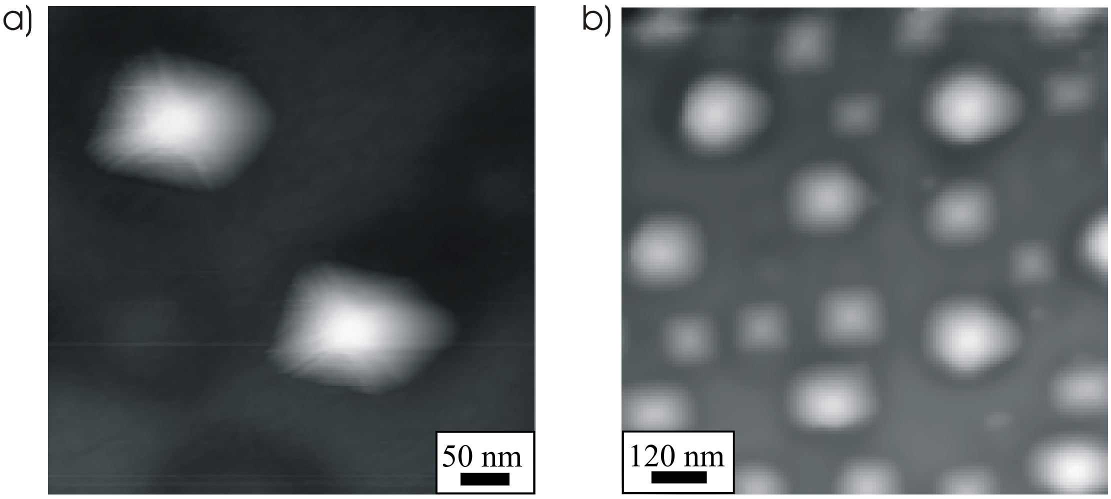

Fig. 4.2 The dots were grown at 820°C. 7 ML of Ge were deposited for the sample on the left side (a), while 14 ML of Ge were deposited for those on the right side (b). While on the sample on the left side only hut clusters were found, for the sample with a higher Ge deposition also dome cluster are visible. All clusters are quite large with mean diameters of more than 150 nm.

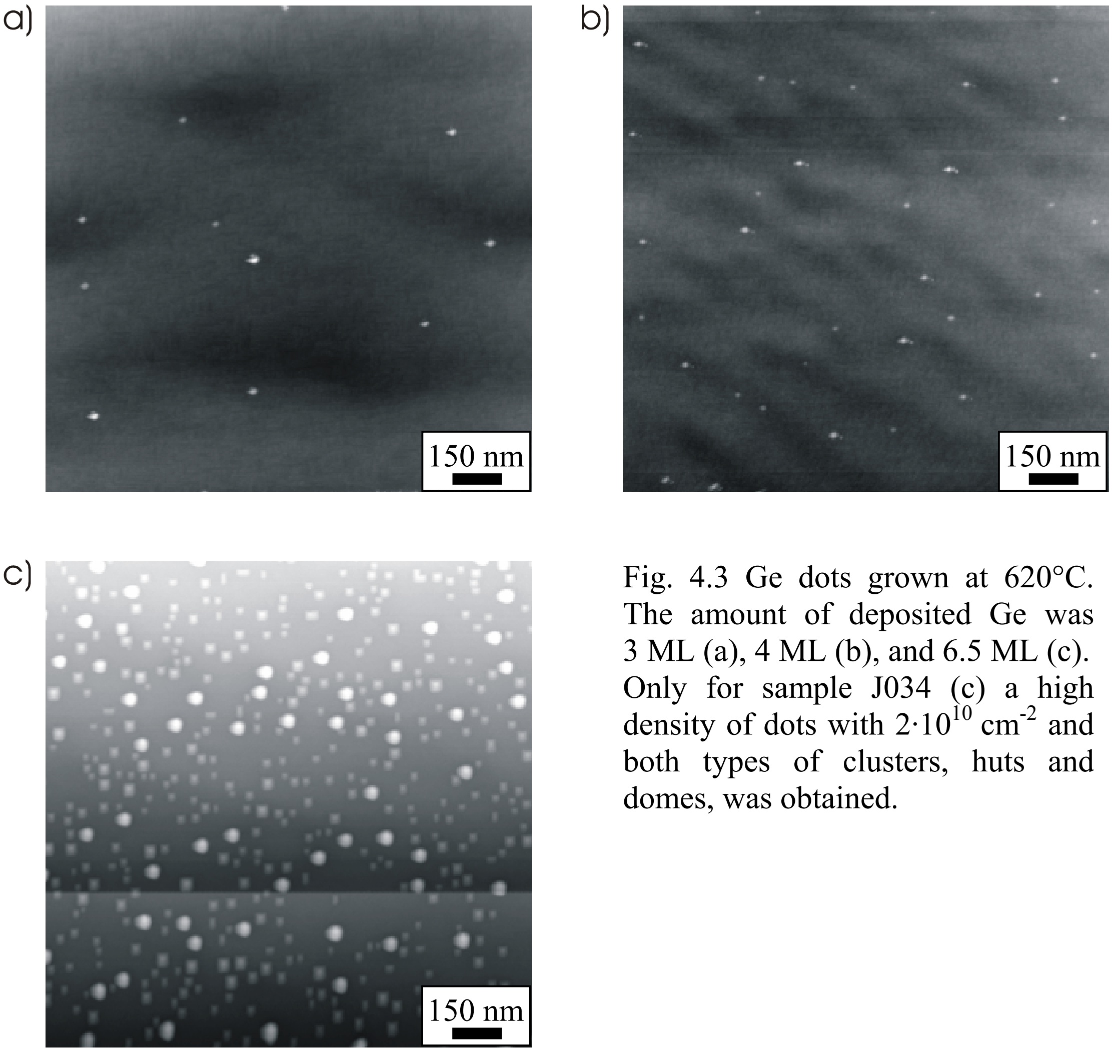

Fig. 4.3 Ge dots grown at 620°C. The amount of deposited Ge was 3 ML (a), 4 ML (b), and 6.5 ML (c). Only for sample J034 (c) a high density of dots with $2\cdot10^{10}$ cm^{-2} and both types of clusters, huts and domes, was obtained.

higher Ge content. As the shape of the dot is determined by the minimum of the sum of strain- and surface-energy, as described in paragraph 2.4, larger hut clusters can be grown before it becomes more favourable (from the energetic point of view) to increase the surface energy by a shape transition to a dome cluster.

To achieve a high density of clusters on one side and to keep the intermixing with Si from the substrate low on the other, lower growth temperatures were chosen than for the previous samples. On the other hand, when the growth temperature is too low, the diffusion anisotropy comes into account as described in chapter 2.4 and elongated hut clusters form. Therefore it is difficult to achieve 0-dimensional confinement. Elongated hut clusters were observed for the samples grown at 550°C and 580°C. To obtain small squared hut clusters, we chose a growth temperature slightly higher (620°C) and varied the amount of deposited material. Three samples were grown with 3, 4, and 6.5 ML of Ge. For the two samples with 3 and 4 ML of Ge, only a small

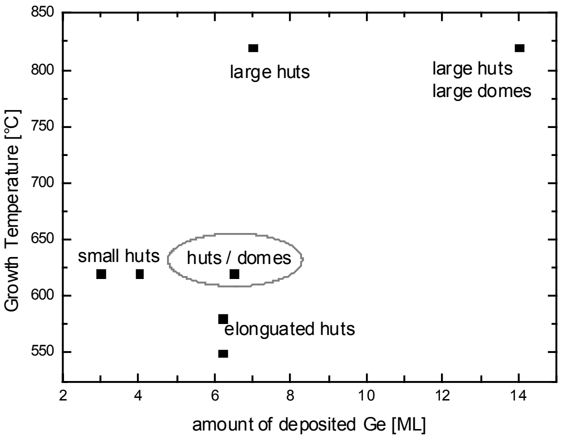

Fig. 4.4 No optimum of growth parameters can be found. The smallest clusters are found at a growth temperature of 620°C, but the density is to low. Below 580°C the clusters become elongated and zero-dimensional confinement can not be achieved. The conditions marked by a circle were chosen in chapter 6.1 to study the influence of capping.

number of hut clusters were obtained, as the deposited amount is close to the critical thickness. Here, densities of $5\cdot10^{8}$ cm^{-2} and $1\cdot10^{9}$ cm^{-2} respectively were achieved. However, the huts have a square base with a small length of 20 nm, as can be seen in Fig. 4.3. Here smaller clusters were obtained than for the samples grown at 550°C and 580°C, but for any kind of optical device, the density of clusters would be too low. To increase the density of clusters, a sample with 6.5 ML of Ge was grown. Fig. 4.3 shows that a high density of dots was achieved, but two types of clusters (huts and domes) were found. The density of dots is $1.7\cdot10^{10}$ cm^{-2} while the ratio of hut to dome cluster is 5:1. The mean base width of the huts is 32.5 nm, while the mean diagonal of the domes is 60 nm. Here, a higher density of dots is found, but the clusters are again quite large. As the formation of dome clusters occurred for a smaller amount of deposited material than for the samples grown at 820°C, a reduced intermixing with the Si from the substrate can be assumed. The growth conditions and the obtained cluster types are summarized in in Fig. 4.4. For a high growth temperature of about 820°C, the intermixing is strong leading to large clusters with a high Si content and a low density of dots. For low growth temperatures between 550°C and 580°C the density of dots is high and the intermixing should be reduced, but one obtains elongated hut clusters due to the anisotropy in diffusion at this low growth temperatures. At the growth temperature of 620°C the diffusion anisotropy is overcome, but hut and dome clusters were formed with a base length of about 35 nm resp. 60 nm, which is still to large for a good confinement. For low amounts of deposited Ge (3,4 ML), even though small huts are achieved, the density of islands is too low.

4.2 Reproducibility

As seen in the previous paragraph, small changes in temperature and the amount of deposited Ge can lead to strong changes. For this reason, we grew three samples under the same growth conditions, where we could study the influence on both types of clusters. Those three samples were grown at 620°C and with 6.5 ML of Ge. In Fig. 4.3.c one of those samples was already shown, while the two other are shown in Fig. 4.5. For both samples hut and dome clusters are found. The obtained results for the ratio of hut to domes clusters, the density of clusters and the mean diameter are given in table 4.1.

The ratio of the clusters, the density and their size varies within some limits. The ratio of dome to hut clusters is quite similar for all samples. The largest differences are found for the density of cluster, differing with a factor of four, while the mean diameter for the hut and dome only differ by a factor of 1.5. These differences are also reflected in the total volume of hut and dome clusters, as can be seen in Tab. 4.2. The volumes differ by a factor of 2.7 and even 5.2. For the variation of total volume there

Sample	***ratio huts to domes***	***density [cm^{-2}]***	***mean diameter huts [nm]***	***mean diameter domes [nm]***
J034	5 : 1	$1.7 \cdot 10^{10}$	32.4	60.3
H030	4.5 : 1	$5.3 \cdot 10^{9}$	45.0	57.7
J044	3.7 : 1	$2 \cdot 10^{10}$	53.1	79.5

Tab. 4.1 Comparison of samples grown under the same growth conditions

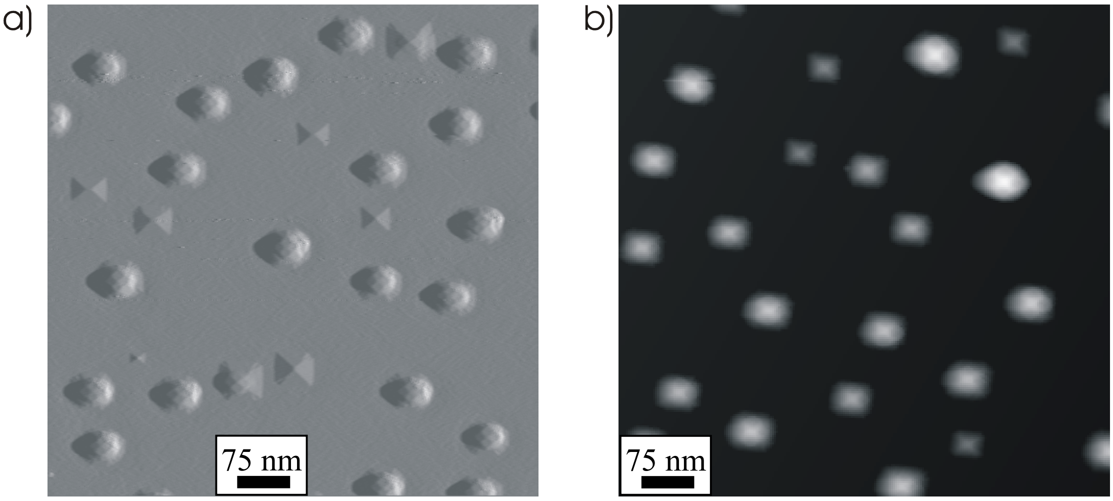

Fig. 4.5 Both samples grown at 620°C and 6.5 ML of Ge were deposited. For the samples H030 (a) and H044 (b) similar Ge dots were obtained, showing the reproducibility of the growth.

might be two possible reasons. One is a slight difference in growth temperature, which leads to higher intermixing and therefore to larger clusters. This could be the case for sample J044, where the highest density and the largest clusters were obtained. Another reason might be, that the wafers were not rotated during the growth, to avoid an electrostatic charging due to friction. This can lead to fluctuations in the growth temperature even on a single sample, resulting in the observed variation of size and density. For sample J034 the size of huts clusters is the smallest and stronger intermixing did therefore not occur, so that in this case the last explanation is more probable.

Sample	V_{total} ***[nm³]***
J034	$1.8 \cdot 10^{14}$
H030	$6.6 \cdot 10^{13}$
J044	$3.4 \cdot 10^{14}$

Tab. 4.2 Total deposited volume V_{total} of dome and hut clusters

Changes in density of the dots and therefore also in the size of the dots might also be attributed to differences in the used substrates. If the miscut of the substrate is different, the diffusion is effected and the densities and sizes of clusters vary. But this can not explain the differences in total volume. Nevertheless, the reproducibility is still good enough for a qualitative and also a quantitative analysis, even though variations are found.

4.3 Summary

Ge dots grown on pure Si(001) surfaces are mainly determined by the growth temperature and the amount of deposited material. If the growth temperature is to high, strong intermixing with Si from the substrate occurs, leading to large clusters and a low density of islands. For to low growth temperatures, smaller than 580°C, we obtained elongated hut clusters showing the limited growth kinetics at this temperature. Increasing the temperature to 620°C leads to the formation of small and medium size clusters, but without the kinetically limitations leading to elongated huts at 550°C and 580°C. At 620°C the growth of small hut clusters with a size of 20 nm is obtained, however the density is too low for opto-electronic devices. For this reason, another method to reduce the size of dots is investigated in the following chapter. Increasing the amount of deposited Ge to 6.5 ML results in a high density of dots, but they are larger and have a bimodal diameter and height distribution, containing squared hut and dome clusters. These growth conditions were chosen for the STM-reference samples of chapters 6, since they permit to study the influence of a Si cap layer on the composition of Ge dots for both types of dots, huts and domes.

5 Ge dots on carbon modified surfaces

For opto-electronic devices a small size, high Ge content, and good crystal quality of the dots are important to get high luminescence intensity. The size of the dots is predominantly determined by the amount of deposited Ge and the growth temperature, as Ge grows on Si in Stranski-Krastanov (SK) mode. In the previous chapter we saw, that at low growth temperatures the diffusion length is reduced on the surface and therefore the area or volume, that can contribute to a single dot is small. But those dots are elongated and zero-dimensional confinement can not be obtained. If one increases the temperature the anisotropy of diffusion is overcome and squared hut clusters can be obtained, but the dots become too large for a good confinement. For this reason, a way has to be found to modify the growth of Ge on Si surfaces to grow small dots at relatively high temperatures of more than 580°C. It was previously shown and explained by a model and will be readopted in the next subparagraph, that the deposition of carbon on Si(001) leads to a c(4x4)-surface-reconstruction in these areas, where carbon is incorporated [92]. Since the surface separates into areas with and without carbon incorporation, an undulating strain field is formed on the surface, which yields to “selective” growth of Ge on “strain modified” areas in a Volmer-Weber like mode, resulting in higher densities of clusters and smaller dots.

5.1 Pre-deposition of carbon

As the size and density of carbon free regions determine the size of the Ge dots, we studied the influence of carbon incorporation on Si surfaces in a first step. Up to now, during the last years other groups have had the aim to achieve high quality $Si_{1-x}C_x$ films with high content of substitutional carbon on Si(001) substrates [12,93]. On one hand there is the problem of the small equilibrium solubility of C in Si of the order of 10^{-4} atomic percent, due to the very large lattice mismatch between Si and C of about 40 percent. To achieve a carbon content up to a few percent, one has to operate far from the thermal equilibrium. On the other hand, the solubility on a surface might be quite different. The co-evaporation of Si and C by MBE, or the deposition of 1-2 ML of C by a subsequent overgrowth of Si were used for realising C-rich $Si_{1-x}C_x$ films [13,93].

So far only the pre-deposition in the range of 0.05-0.11 ML was investigated [40]. The deposition of 0.05 ML carbon leads mainly to the incorporation of carbon at step edges. At 0.11 ML about 10 percent of the surface is covered by a c(4x4) reconstruction, which is not present on clean Si surfaces and must form due to the deposition of carbon (Details are given in chapter 5.1.2). Therefore we investigated additionally the sub-monolayer C deposition in the range between 0.2 and 0.3 ML, as this should lead to smaller C free areas and thus leading to smaller Ge nucleation sites, which could lead in the end to smaller Ge dots.

5.1.1 Calibration of the carbon source

Especially if small amounts of a material have to be deposited, in this case between 0.05 and 0.3 ML, the growth rate and calibration of the source is important. Due to the opening and closing of the shutter, the temperature of the carbon source and therefore the carbon flux can change, as the shutter reflects heat and the shutter position therefore correspondents to different thermal equilibriums. To minimize this influence, a carbon source has to be chosen that allows low growth rates, as the resulting growth time has to be longer than the time to establish the new equilibrium after opening the shutter. The carbon source (MBE Komponenten: SUKO 63) used in these studies contains a meander-shaped filament machined from a highly orientated pyrolithic graphite plate. A DC current heats the filament, leading directly to the sublimation of carbon. The flux i.e. the sublimation rate is just controlled by the current, which is adjusted to achieve the necessary high source-temperature of 2000-2200 °C. At typical conditions, e.g. at a current of 103 A and an applied voltage of 13.6 V, a carbon growth rate of $2.3\cdot10^{-4}$ ML/s is established. This leads to growth times for carbon in the range of 208 up to 1250 s for 0.05 ML and 0.3 ML. The time in which the source temperature changes due to the opening and closing of the shutters was estimated by SIMS investigations analysing the amount of C deposited in samples with different thick $Si_{1-x}C_x$ layers. It was found to be in the range of 20 s leading to negligible errors for typical deposition times.

For the calibration of the carbon source a sample with a stack of carbon and Si layers was grown. The carbon layers are separated by 60 nm thick Si spacers. The growth time for the carbon layers was always 500 s, while the filament current changed for each single layer from 90 ampere for the first layer to 106 ampere for the last layer. The amount of deposited carbon atoms was determined by SIMS. A typical profile through a calibration sample is depicted in Fig. 5.1.a. A peak with a width of several nanometers can be found for each layer. The width depends on the depth resolution of SIMS. An area density of carbon results from the integration over each peak.

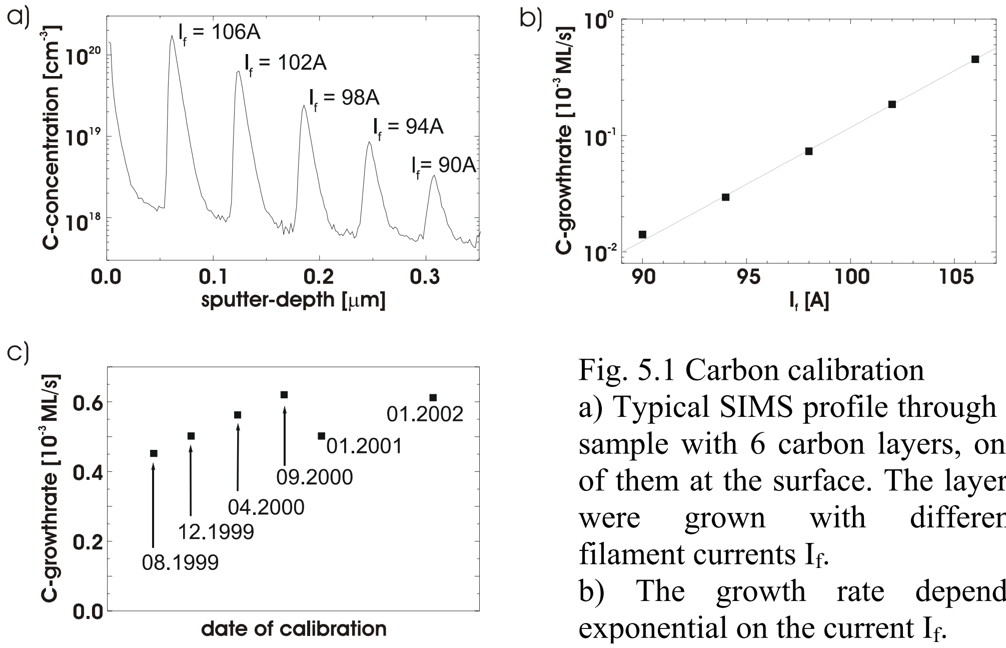

Fig. 5.1 Carbon calibration
a) Typical SIMS profile through a sample with 6 carbon layers, one of them at the surface. The layers were grown with different filament currents I_f.
b) The growth rate depends exponential on the current I_f.
c) As the filament becomes thinner in time, the resistance and therefore the temperature for a given I_f increases, which leads to an increase of the growth-rate. In January of 2001 the SIMS-set-up was changed, which explains the jump in the growth rate and gives an estimation for the error bars of this method.

Applying this to the surface density of Si, one gets the amount of deposited monolayers of carbon on a Si surface. The dependence of the resulting C-deposition rate and filament currents obeys an exponential law, as shown in Fig. 5.1.b. The growth rate slightly increases within time, since the diameter of the filament becomes smaller, leading to an increase in resistance and in turn a higher voltage is required to maintain the same current, leading to a hotter source and higher growth rates. This is demonstrated in Fig 5.1.c. The jump to smaller growth rates between September 2000 and January 2001 in this figure is related to a change of SIMS set-ups, as the calibration was done after January 2001 by another institute. This shows the limitations of the calibration, as obviously the different SIMS set-ups are not calibrated in the same way.

5.1.2 Model of C-induced surface reconstruction

For small amounts of carbon, hints were found e.g. by XPS, that carbon could be incorporated into the Si lattice down to the fourth layer [94]. STM investigations showed, that the deposition of small amounts of carbon leads to a change of the surface reconstruction. The main features are short chains of paired bright spots, which occur on top of terraces after the deposition of 0.05 ML of carbon as shown in Fig. 5.2.a. For 0.11 ML of carbon, small patches of single monolayer heights were

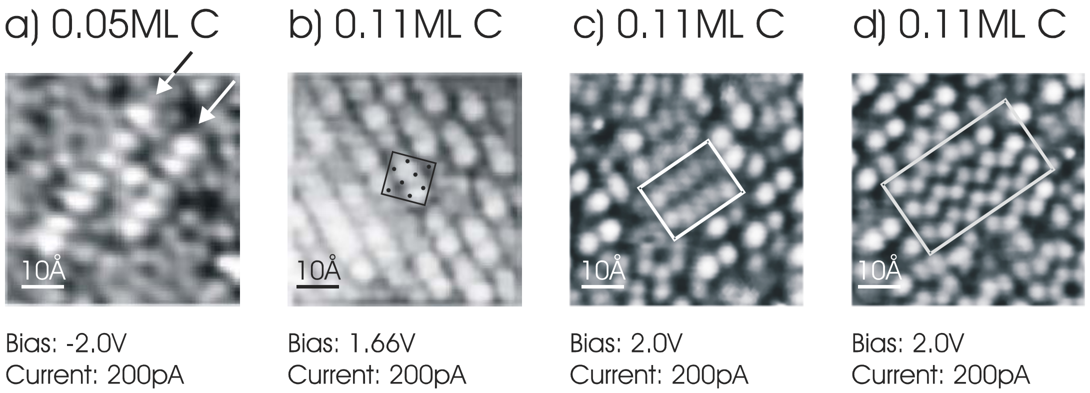

Fig. 5.2: Modified surface after the deposition of carbon. Short chains of bright spots are the striking feature (a), forming single step high islands with a c(4x4) reconstruction when the amount of carbon is increased to 0.11ML (b). Besides normal Si dimers (c) so called buckled dimers are found (d), which are normally present when impurities are incorporated [8].

formed from these chains, as can be seen in Fig. 5.2.b. Besides this main feature, also so called buckled Si dimers were found (see. Fig. 5.2.c-d) [95], which typically occur when the dimer rows are pinned by the presence of impurities at the surface and which are normally an indicator for the presence of impurities.

The patches exhibit a c(4x4) reconstruction. The unit cell includes two paired spots. The intra distance of the centres is 5.9 Å; the periodicity of the spots is 15.5 Å. This value is close to 15.4 Å, which is the fourfold distance of normal Si dimers. Therefore the dimers are in the same direction as normal Si dimers, it was assumed, that the paired spots belong to two visible dimers with a missing or invisible dimer located in-between. The visible dimers must have moved together, due to the strain introduced by the incorporated carbon, as the distance of 5.9 Å is 23 percent smaller compared to the distance of 7.7 Å of an unperturbed Si surface (Fig.5.3.a).

In former investigations, eight models, containing carbon on lattice sites in the position labelled A to J in Fig. 5.3.b and c, were investigated [21]. The total energies and the thermodynamic stability of the models were predicted. In addition calculations of the electronic charge density of the structures in the bulk and on the surface have been performed based on pseudo-potential density functional calculations. More details can be found in [21]. Among these models, one was found, that could explain the displacements of dimers by 1.8 Å of the c(4x4) surface reconstruction, observed by STM. The model consists of six carbon atoms in the positions B, E, and F and a missing dimer releasing the strain (Configuration 6B in

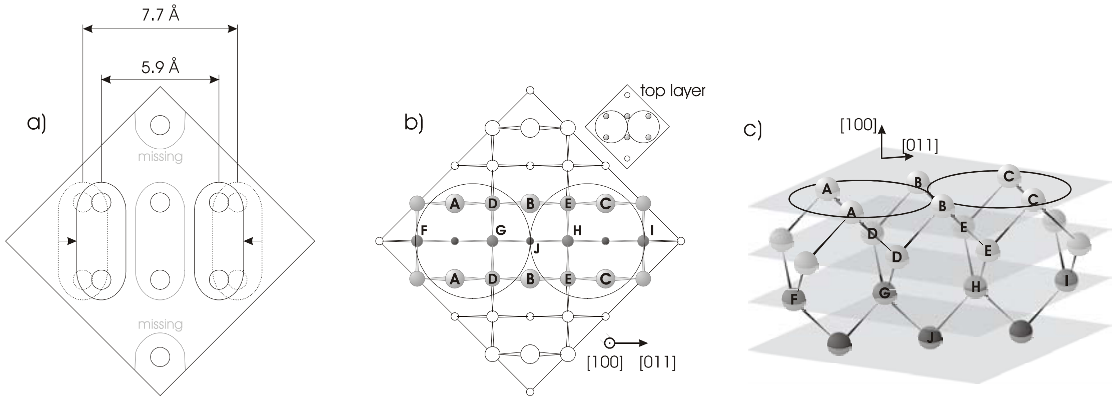

Fig. 5.3 a) Unit cell of a c(4x4) surface reconstruction. The visible dimers are shown in black. The distance between them is smaller compared to a pure Si surface. b) Si atom position within the unit cell down to the fourth layer in the case where no carbon is present. The grey atoms were taken into account for the model, while only the labelled atoms were expected to be replaced by carbon. c) A three-dimensional view of the atoms consider within the model.

Fig. 5.4). But this model is not accounting for the presence of C in the third and fourth subsurface layers, as indicated by XPS [96, 97] experiments.

To account for this discrepancy, another possible configuration was evaluated [98] and compared to model 6B (Fig. 5.4). The possible configurations are named NA or NB (with N the number of carbon substituting Si atoms). In addition, the configurations B have a missing dimer vacancy. The model of Kaxiras is in accordance with configuration 6B. While the models 6A and 6B contain C-C dimers, the models 5A and 5B consist of five C atoms positioned at second nearest neighbour arrangements in the first and third sub-layer, forming a cubic β-SiC cluster below the surface. Ab initio density functional theory calculations to obtain the relative energies, simulation of STM images of considered structures, and Monte Carlo simulations to study their stability and thermo dynamical properties were performed. Table 5.1 shows the relative and formation energies for the ab initio

Configuration	***0A***	***0B***	***6A***	***6B***	***5A***	***5B***
$E_{r,ab\ initio}$	0.00	0.25	7.94	6.99	*3.16*	3.75
$E_{f,\ ab\ initio}$	0.00	0.00	7.94	6.74	*3.16*	3.51
$E_{r,MC}$	0.00	1.39	10.1	8.84	*4.02*	4.12
$E_{f,\ MC}$	0.00	0.00	10.1	7.45	4.02	*2.73*

Table 5.1 Relative and formation energies for the various configurations. $E_{r,\ MC}$ is the free energy difference at 900 K [98].

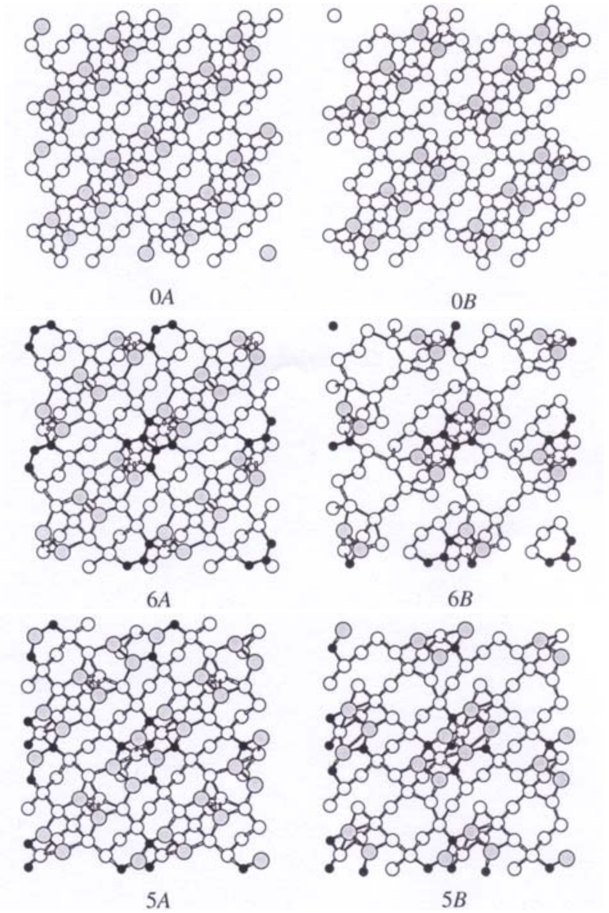

Fig. 5.4 Relaxed geometries (top views, topmost four layers shown) of possible configurations explaining c(4x4) reconstruction. A supercell four times the c(4x4) unit cell is shown. The configurations on the right column, marked B, contain a dimer vacancy defect. Si surface atoms are shown as grey circles, Si atoms of the 2nd, 3rd, and 4th layer are shown as smaller, white circles. C atoms are represented by black circles [98].

calculations and the Monte Carlo simulations of the different models. Comparing the configurations without carbon (0A, 0B), only a small difference in relative energy is found. In the configuration with a dimer vacancy (0B), there are two competing effects. One is the reduction of dangling bonds from 8 to 6 per unit cell and the restoration of bond angles, which lowers the total energy. The other effect is the distortion of bond lengths, which raises the total energy. This competition results in the small relative energy.

For the configurations with six carbon atoms per unit cell (6A, 6B), it is found that the configuration with a dimer vacancy has a lower relative energy. Due to the high number of carbon atoms per unit cell and the large difference in bond length between Si and C, a lot of strain is introduced. In configuration 6B, the structure can relax due to the missing dimer, which leads to the lower relative energy of this structure. For the

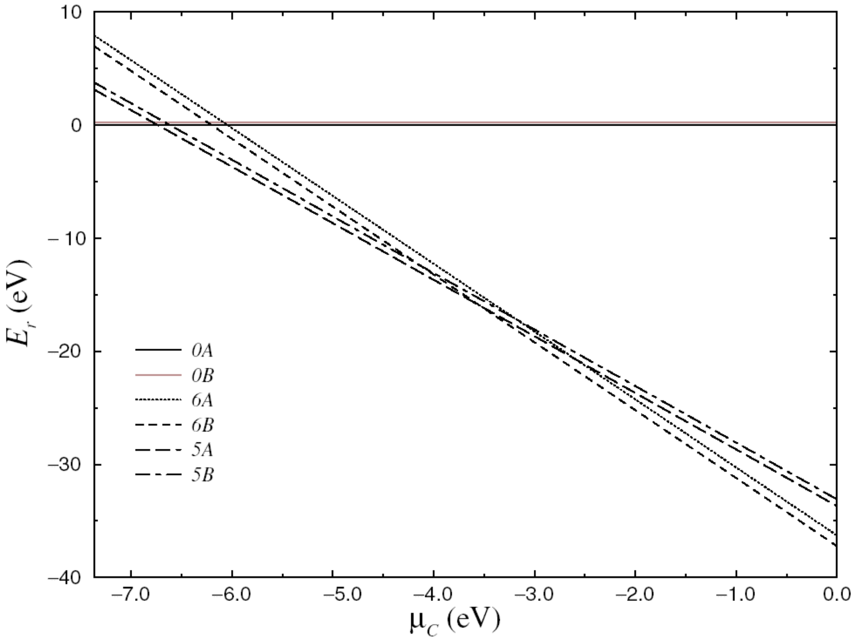

Fig. 5.5 Relative energies of the considered structures as a function of the chemical potential, as derived from the ab initio calculations at zero temperature. Energies are given in eV per c(4x4) unit cell [98].

configurations with 5 carbon atoms per unit cell it is found, that the presence of a missing dimer is not lowering the energy of the system. It turns out, that configuration 5A has the lower relative energy compared to 5B. Three different ranges can be distinguished for the relative energy as a function of chemical potential μ_C as shown in Fig. 5.5. At low μ_C the configuration 0A is the preferred one. In the range -6.8 eV < μ_C < -3.6 eV the configuration 5A has the lowest relative energy, while above -3.6 eV, again the configuration 6B is favored. During MBE growth, the number of atoms per cluster is small (one or two), leading to chemical potentials of above -6 eV. Here, the configurations 5A and 6B can coexist. The values in table 5.1 were calculated in the zero temperature picture. Accounting the Monte Carlo simulations that were done for 900 K, the ranges shift to higher chemical potentials and for MBE configuration 5A becomes more probable, but 6B can still coexist [98].

The calculated STM pictures of model 5A match better to the high resolution STM-pictures of the c(4x4) reconstruction, comparing to those of model 6B. Together with the fact, that in configuration 6B no carbon is in the third or forth layer in contradiction with results obtained by XPS and XPD analysis, the new model 5A seems to fit best to the observed experimental observations.

5.1.3 Surface reconstruction depending on amount of deposited carbon

As introduced in the previous subparagraph, for the deposition of 0.05 to 0.11 ML, bright-paired spots were observed which could form single step high terraces as demonstrated in the overview pictures of Fig. 5.6. A model taking relative energies and the simulation of STM pictures into account explained this feature. A goal is to vary the size and density of the areas with and without c(4x4) reconstruction. So the amount of deposited carbon was increased up to 0.3 ML. For the investigations, the preparation of the substrate was in analogy to the procedure described in paragraph 3.2. After the growth of the 200 nm thick buffer, as a next step the substrate was cooled down to 550°C within 3 minutes and the carbon sub-monolayer was deposited. The deposition rate was adjusted to $2.4 \cdot 10^{-4}$ ML/s. This deposition rate leads to growth times in the range of 840 s for 0.2 ML of carbon, thus the error due to the temperature change of the source related to the shutter movements is less than 10 percent. When the C deposition was finished, the samples were cooled down to room temperature and were transferred to the STM without breaking the vacuum.

For the samples shown in Fig. 5.6, the deposition of 0.05 ML only lead to single lines of paired bright spots, while after the deposition of 0.11 ML of carbon, ten percent of the surface is covered by a c(4x4) reconstruction. Line-scans along edges of those paired spots including areas with buckled Si dimers show that the spots are of single

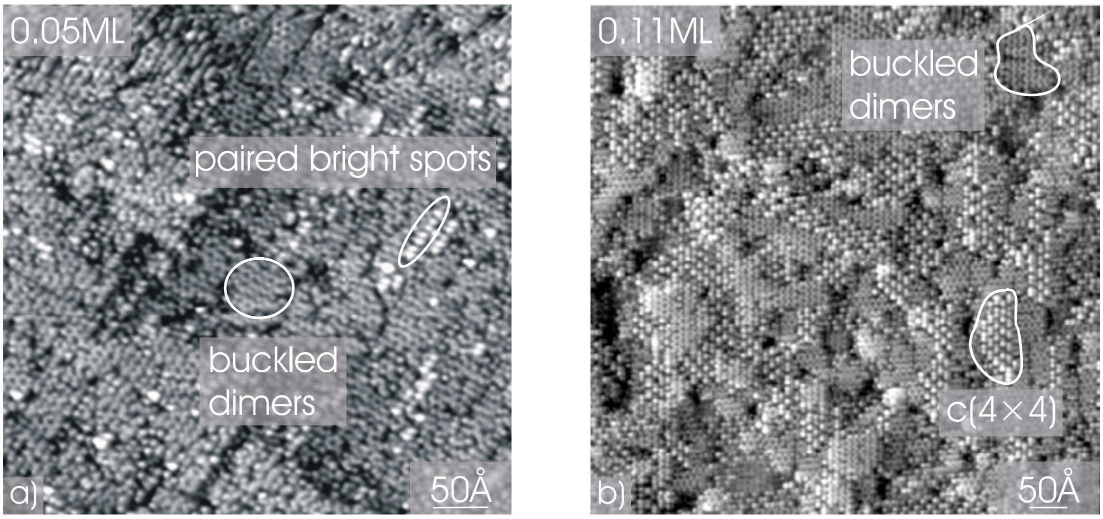

Fig. 5.6 a) After depositing 0.05 ML of carbon, bright paired spots are visible, which form chains on top of the Si surface. b) With 0.11 ML of Si, the chains form islands with a c(4x4) reconstruction and single step height. Buckled Si dimers are found between the islands [8].

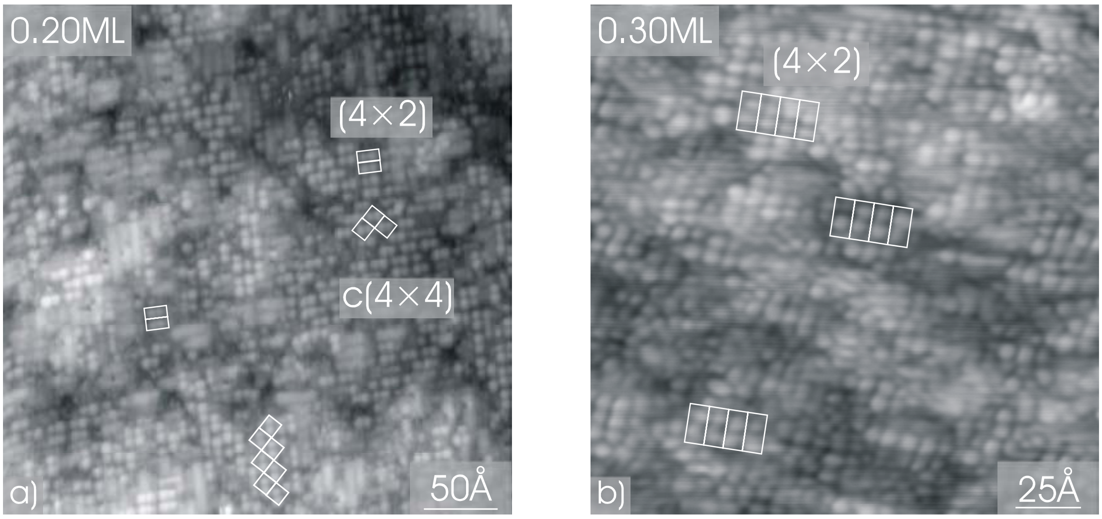

Fig 5.7 a) After depositing 0.2 ML of carbon most of the area has a c(4x4) reconstruction. A new (4x2) reconstruction is found at island boundaries. b) If the amount of carbon is increased to 0.3 ML, the new (4x2) reconstruction expels the c(4x4) reconstruction.

step height. Already after the deposition of 0.2 ML of carbon, most of the surface has a c(4x4) reconstruction, and some small areas exhibiting a (4x2) reconstruction. The (4x2) reconstruction still consists of the observed chains of paired bright spots, but now the neighbouring chain is not shifted by half of the length of a paired spot. As these areas with the new reconstruction are very small and only consist of a few spots, it might be a border effect between domains of c(4x4) reconstruction.

When the amount of carbon is increased to 0.3 ML of carbon, the c(4x4) surface reconstruction is expelled and only the (4x2) reconstruction can be found. This shows, that at high carbon concentrations this reconstruction becomes more favourable compared to the c(4x4) reconstruction.

The changes in reconstruction are best seen, if one takes the line-scans of Fig. 5.8 into account. There, the typical distances between the chains of 7.7 Å are found, while the intra- and inter-distances of 5.9 Å and 9.6 Å were only found for the samples with up to 0.2 ML of carbon deposited on top of them. At already 0.2 ML of deposited carbon, the inter-distance between the bright spots along a chain changes to 7.7 Å for most of the parts of the sample, indicating the lost of the pairing effect. And at least after 0.3 ML, only the (4x2) reconstruction is found. One cannot speak any longer of chains, as the distance to a neighbouring spot is always 7.7 Å, as presented in Fig. 5.8. Using the model of Remediakis, five carbon atoms are needed per unit cell, to form the c(4x4) reconstruction. As the unit cell contains eight lattice sites at the surface, the deposition of 0.11 ML, 0.2 ML, and 0.3 ML of carbon should lead to a portion of

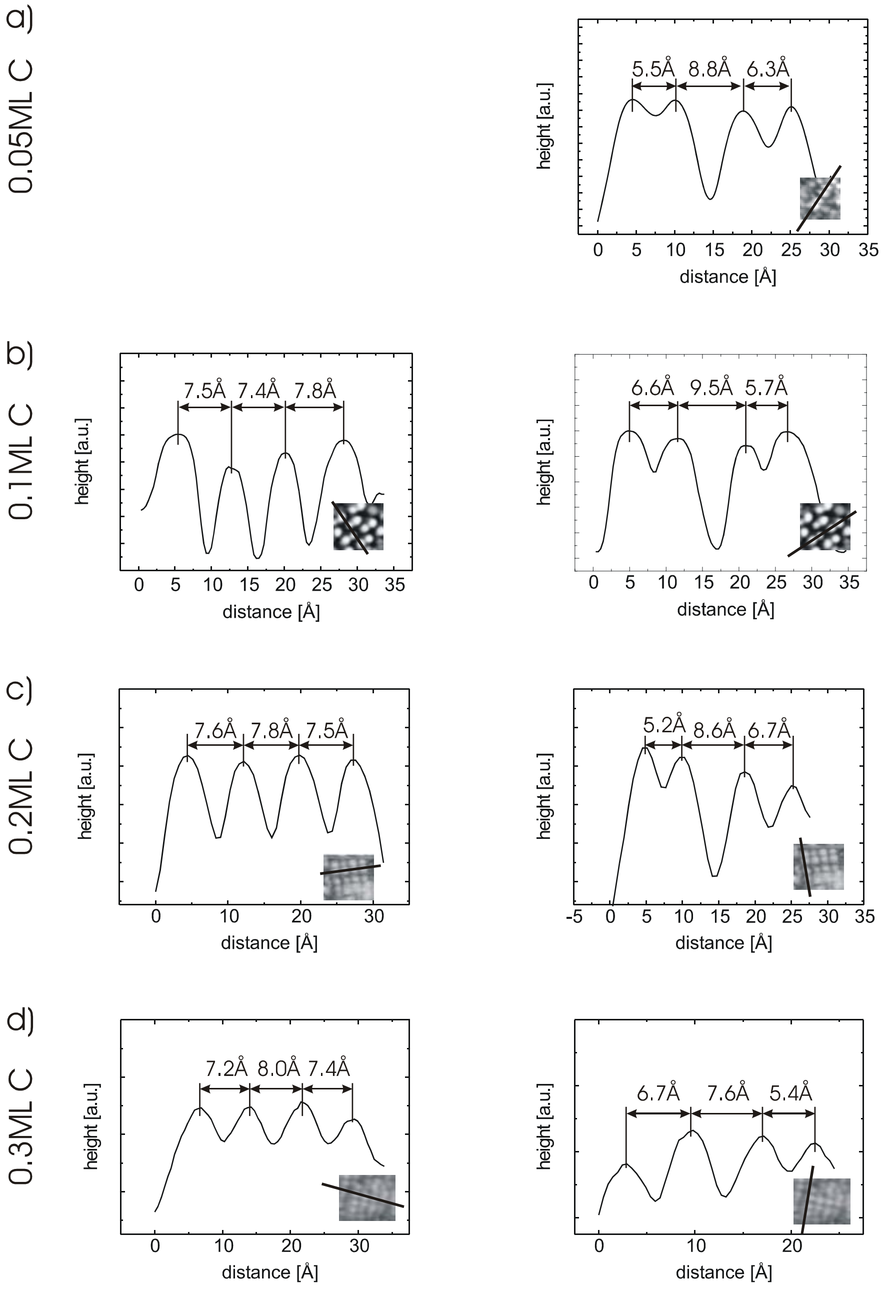

Fig. 5.8. Line-scans for samples after the deposition in the range of 0.05 to 0.3 ML of carbon. While for samples with up to 0.2 ML of carbon chains with paired spots are found, indicated by the inter- and intra-pair distances of 5.9 and 9.6 Å, the pairing starts to be lost at 0.2 ML and is totally lost after 0.3 ML, as shown by the change in spot distances. The distance between the chains remains always at about 7.7 Å.

17%, 32%, and 48% of the surface with a c(4x4) reconstruction. The presented results strongly differ. For the deposition of 0.11 ML of carbon, Leifeld found that ten percent of the surface were covered by c(4x4) reconstruction. The difference can be explained with carbon that is incorporated at interstitial sites and might lead to the observed buckled Si dimers. The fact, that the islands are of single step height, can be explained by assuming, that the carbon drives out the Si atoms at those lattice site, where it is incorporated. These Si atoms form the dimers and therefore the islands on the surface. The amount of out driven Si would only suffice for single step high islands. But already after the deposition of 0.2 ML of carbon, most of the surface is covered by the c(4x4) reconstruction. This would mean, that assuming a homogenous distribution of carbon only one up to two carbon atoms are needed per unit cell to form the c(4x4) reconstruction, or that different configurations leading to the observed c(4x4) reconstruction coexist. One of the configurations cannot contain carbon and would only be built by missing dimers and or strain introduced due to the carbon deposition in the other regions. Missing dimers are very unlikely, as Remediakis investigated one model (0B), that contains one missing dimer. The simulated STM picture looks like normal Si surfaces, with a missing spot at the dimer vacancy, which is quite different to the observed experimental results. In addition, if in some parts of the surface the c(4x4) reconstruction is built by including missing dimers, the strain introduced by the carbon in the other c(4x4) reconstructed areas could be released and no driving force for the formation of this different c(4x4) reconstruction remains. In the end, assuming the coexistence of two configurations (one of them without carbon), only the strain introduced by the carbon containing areas can build up this second configuration. But this would mean, that the configuration 5A for the carbon contain areas is more probable, as configuration 6B of Kaxiras model releases its strain at missing dimers.

The second possibility is, that due to the high amount of strain, the configurations 5A becomes instable and another configuration with less carbon can build up the new c(4x4) reconstruction. Kaxiras also investigated a model, containing only carbon atoms at the position B of Fig. 5.3. This model was favoured at high chemical potentials and was also able to lead to the observed c(4x4) reconstruction [21].

Another indication for the reconfiguration is the appearance of the new p(2x4) reconstruction. It is already visible after depositing 0.2 ML of carbon and starts at domain borders of c(4x4) reconstructions. When 0.3 ML of carbon are deposited, the whole surface has this new reconstruction, even though the amount of deposited carbon would only be enough to reconstruct 48 percent of the surface by c(4x4) in the 5A configuration. Obviously, the c(4x4) reconstruction became instable. The configuration 5A is not containing missing dimers and for this reason the accumulated strain increases fast when the amount of carbon is increased. After the deposition of 0.3 ML of Si, the strain might be that high, that the configuration 5A becomes instable and the carbon is redistributed over the whole surface and forms the new reconstruction.

5.2 Ge dots on Si surfaces with carbon pre-deposition

When Ge is deposited at 350°C on pure Si, the growth is kinetically limited by diffusion on the Si(001) surface. Under this condition, Ge would form elongated pyramids on non-modified Si due to the diffusion anisotropy on Si(001), when the critical thickness is reached [99] . If, at 350°C, Ge is grown on a Si surface modified by the pre-deposition of 0.11 ML of carbon, single-step high islands are found on terraces already after the deposition of 0.1 ML of Ge. The islands are surrounded by buckled Si dimers, as shown in Fig.5.9.a. Diffusion anisotropy seems to be reduced, due to the presence of regions with c(4x4)-reconstruction. Also, no Ge is detected on the c(4x4)-reconstructed areas, while about 50 percent of the Ge seems to be incorporated in step edges.

The observation that Ge is not nucleating on the C-rich c(4x4) reconstructed areas correspondents well with the predicted repulsive interaction of Ge and C atoms in this SiGeC material system [91], taking the different lattice- and bond length into account.

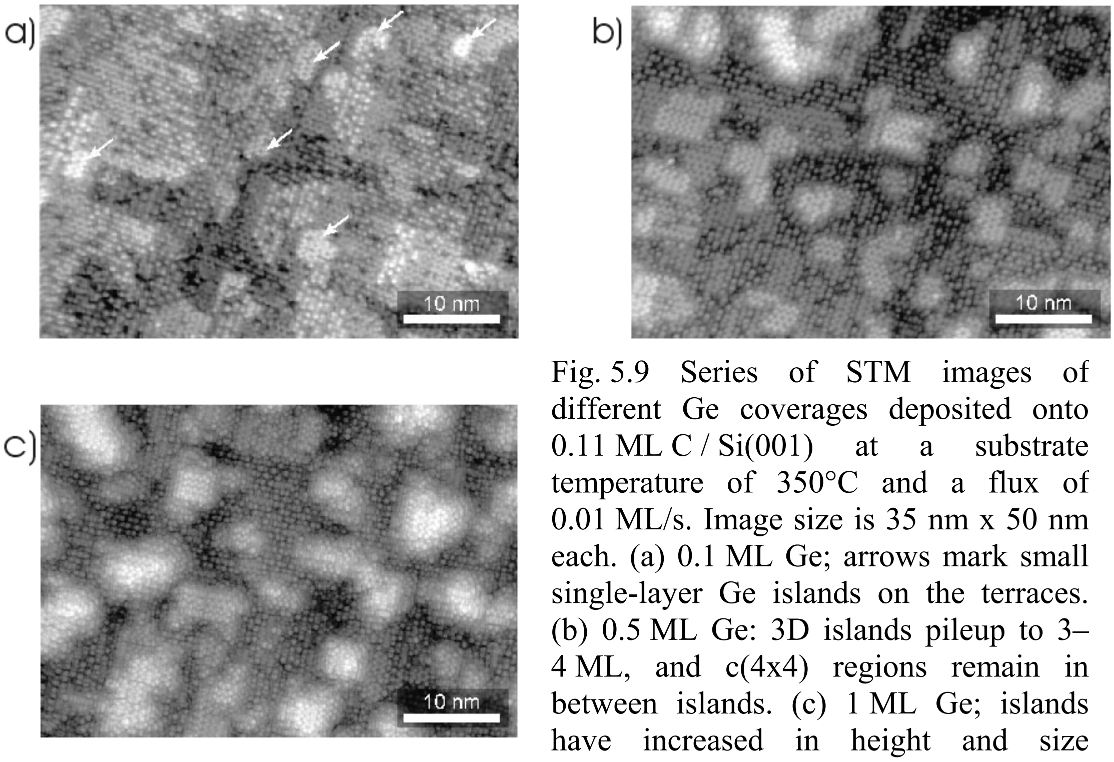

Fig. 5.9 Series of STM images of different Ge coverages deposited onto 0.11 ML C / Si(001) at a substrate temperature of 350°C and a flux of 0.01 ML/s. Image size is 35 nm x 50 nm each. (a) 0.1 ML Ge; arrows mark small single-layer Ge islands on the terraces. (b) 0.5 ML Ge: 3D islands pileup to 3–4 ML, and c(4x4) regions remain in between islands. (c) 1 ML Ge; islands have increased in height and size compared to (b) [81].

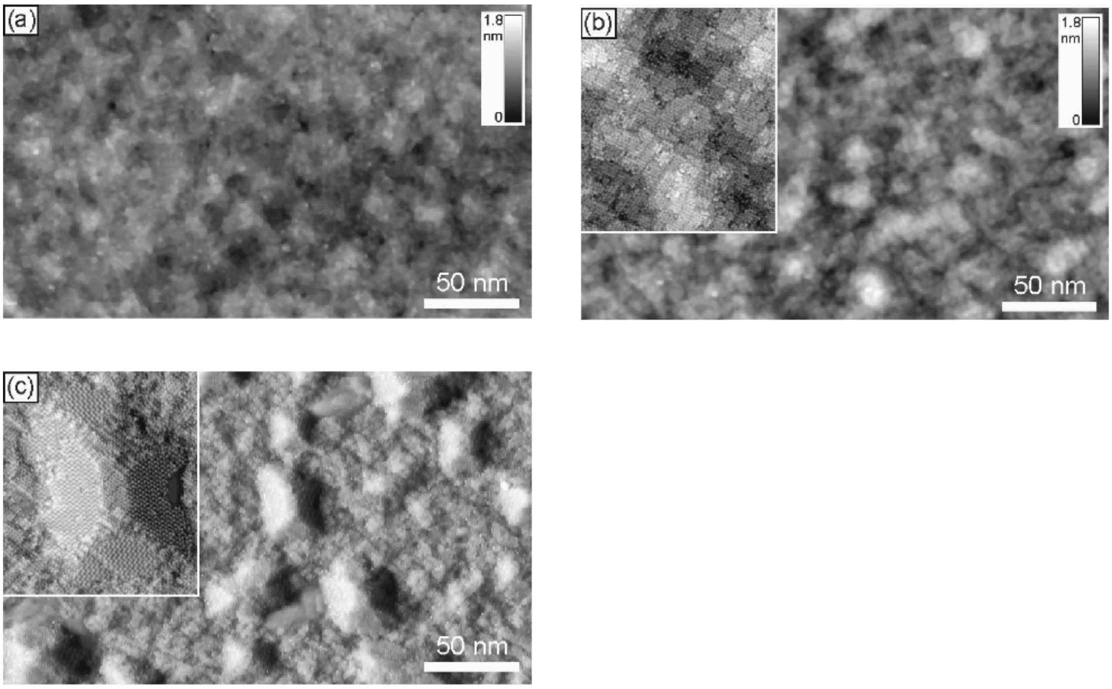

Fig. 5.10 Comparison of surface morphologies of different Ge coverages on Si(001) precovered with 0.11 ML C. For (a) 2.5 ML and (b) 4 ML Ge coverage irregularly shaped islands with stepped terraces are obtained on C-precovered Si. Their height increases with the Ge coverage. At 5.8 ML Ge {105} faceting of the Ge island occurs at the expense of island density, as depicted in (c). The size and height (about 3 nm) of the faceted island exceeds that of the stepped ones [100].

Carbon has a lattice constant of about 40 percent smaller than silicon. This means, that the c(4x4) reconstructed areas are under tensile strain. Ge has the largest lattice constant of these three materials and therefore tends to grow on the areas, which are closer to its own lattice constant. Thus Ge prefers to grow on the surface areas which are free of C.

Increasing the amount of deposited Ge from 0.1 to 0.5 ML leads to larger islands (see Fig. 5.9.b). Ge still avoids to attach to the c(4x4) reconstructed areas. It is adsorbed on the islands, which increase in height. Hence, the growth mode changes due to the strain incorporated by the carbon to a Volmer Weber mode, which means that the islands start to grow directly in three dimensions. The areas between the islands are mainly c(4x4)-reconstructed, and the islands most frequently have a rectangular shape and a low aspect height to diameter ratio. The edges are aligned along the <110> direction, which is by 45° rotated compared to huts on pure silicon.

Most of the Ge islands are at step edges, where no c(4x4) reconstruction is found. This might indicate that the growth is still in a kind of step flow mode, where the Ge atoms migrate on the upper terraces along dimer rows towards the step, descend, and are incorporated there. The ongoing growth is just intercepted by the repelling character of the c(4x4) reconstruction, which straitens the lateral growth of the Ge and let the islands grow in three dimensions. This means, that the three-dimensional growth is driven by the strain undulations at the surface, and the energy built up to form islands is lower than it would be necessary to incorporate Ge into the c(4x4) regions.

Fig.5.9.c shows, that still after the deposition of 1 ML of Ge, the Ge avoids to grow on the c(4x4) regions, as these are still unperturbed. The island slightly increases in diameter, but they reach a height of 4-5 ML. They still do not have facets and look more round shape than those, which have formed after the pre-deposition of only 0.5 ML of carbon. So far, it has been demonstrated that at a substrate temperature of 350°C the Ge is completely repelled by the incorporated carbon, and that therefore no wetting layer is formed, which leads to a change in growth mode.

When the growth temperature during the Ge deposition is raised to 530°C, the growth is no longer kinetically limited by diffusion. At this temperature, indications for intermixing exist, but still c(4x4) reconstructed areas can be found. Ge still avoids to grow on these areas. For a deposition amount of up to 2.5 ML of Ge, the islands have a diameter of up to 20 nm and are rather isotropic in shape. There density is in the range of 10^{11}cm^{-2}. In this regime of up to 2.5 ML of Ge, there exist two types of islands. One consists of islands having a height of 3 ML, which are very seldom, and the other one of islands, whose height can reach up to 6 ML [100]. When the amount of Ge is increased up to 4 ML, still three-dimensional growth of irregular shaped Ge islands is found, as indicated for 2.5 ML and 4 ML in Fig. 5.10.a and b. The height of the islands increases to 7 resp. 12 ML, while the density stays constant at ~10^{11}cm^{-2}, again showing the repelling character of the c(4x4) reconstruction. These reconstructed areas are more and more disturbed with increasing amount of deposited Ge. When the amount of Ge is increased to 5.8 ML, faceted hut cluster occur. These clusters have again {105} side facets and a (001) top facet. At the same time, the surface between the clusters smoothes and the irregular shaped clusters from lower deposition amounts die out. Also the density of clusters decreases by a factor of four.

Again, even at high growth temperature of 530°C, no wetting layer is found as this was the case for the dots grown at 350°C. The growth mode of Ge under these conditions is of Volmer-Weber type, leading from the beginning to three-dimensional islands of Ge [47]. The diameters of high temperature grown islands are larger

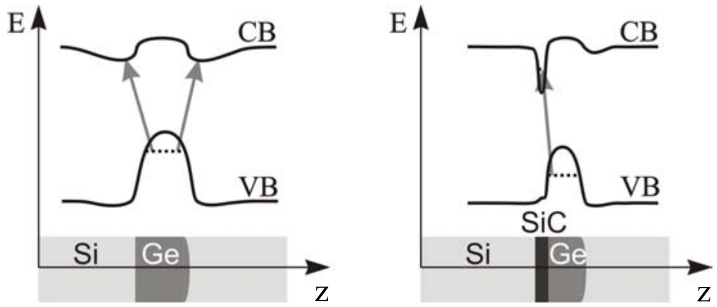

Fig. 5.11 Left: Band diagram of Ge cluster on pure Si. The Ge dot is surrounded by strained silicon, that can act as a quantum well. Right: The regions with incorporated carbon lead to a deeper quantum well in the conduction band and therefore to a better confinement of the carriers.

compared to the low temperature grown dots, but a better crystal quality might be achieved by the increase in growth temperature. Compared to clusters on pure silicon, the irregular shaped islands are still smaller and their density of islands is by a factor of 10 higher. For the island that have already facets, the density is comparable to the density of Ge dots grown on pure Si, but even though these huts are formed by a similar mechanism than it occurs for clusters grown on pure Si, their size is still smaller. This might be the case, as the diffusion length on the surface is reduced due to the roughness of the surface.

The obtained results indicate that the pre-deposition of submonolayers of carbon is a promising route for the control in size and density of islands.

Besides the size control of the Ge cluster, the pre-deposition of C has another advantage. The carbon incorporates leads to the formation of a quantum well in the conduction band, where also electrons can be confined. As shown in Fig. 5.11, this quantum well for the electrons in the conduction band is deeper than one built by the strained Si that surrounds Ge dots on a pure silicon surface. The better confinement of the electrons in reciprocal space can also increase the probability for radiative

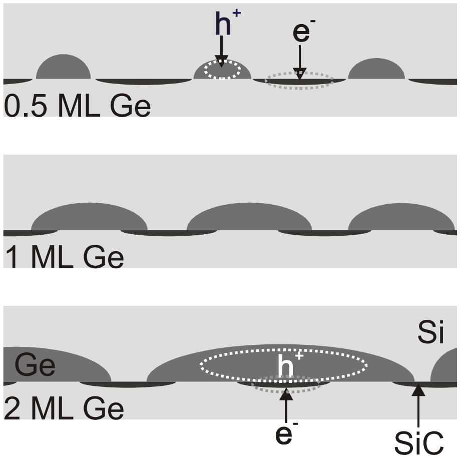

Fig. 5.12 When only small amounts of Ge are deposited, the electrons in the SiC regions are separated from the holes in the Ge dots. With increasing amount of deposited Ge, the Ge dots overgrow the SiC regions and the overlap of the wave functions in real space increases.

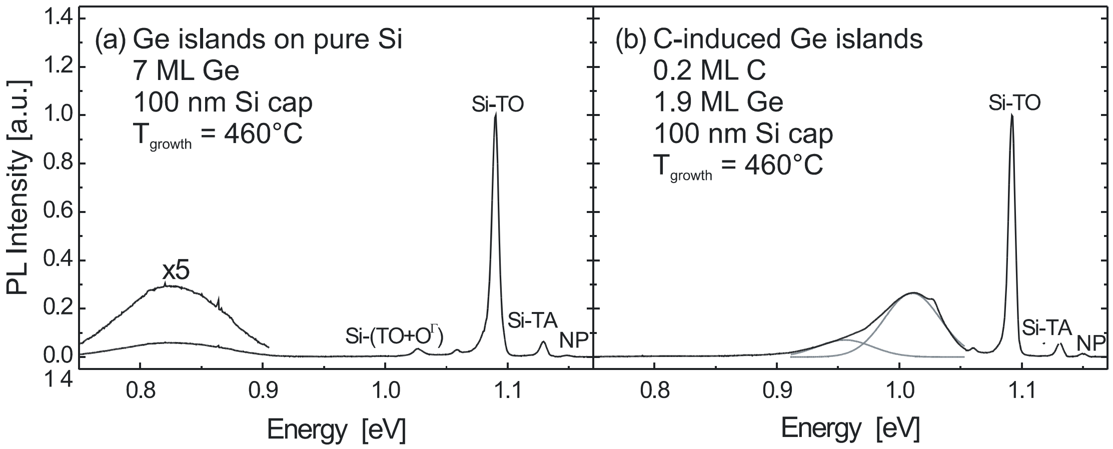

Fig. 5.13 Photoluminescence spectrum of Ge islands on pure Si and (a) and a Si surface, that was modified by the deposition of 0.2 ML of carbon (b). The dots on pure Si have a weak PL signal at 825 meV which arises from the Ge dots, while the intensity for the C-induced Ge dots is by a factor of five higher.

recombination, but the separation of carriers in real space (electrons in the carbon enriched areas and holes in Ge dots) has to be taken into account, too, as illustrated in Fig. 5.12. When the Ge dots overgrow the SiC regions, the overlap of the wave functions in real space increases and besides the better confinement in k-space, a good confinement in real space can also be achieved. That is why we studied carbon induced Ge-dots, that were grown on Si surface, which had been modified by a pre-deposition of about 0.2 ML of carbon. Here the carbon free areas are small so that small Ge dots have already overgrown SiC regions. The photo-luminescence spectrum of Ge dots grown on pure Si shows a weak intensity of the Ge dot signal at about 825 meV, as can bee seen in Fig. 5.13.a. The additional peaks in the range from 1.05 to 1.16 eV belong to photo-luminescence of the Si substrate, as described in chapter 3.4. The effect of better confinement and smaller dot sizes due to the C-predeposition leads to a higher peak intensity as illustrated in Fig. 5.13.b. In addition, as the ground level of smaller quantum wells move to the band edge, also the energy of the PL-peaks moved to higher energies.

To study the influence of the size of the Ge dots, photoluminescence-spectroscopy was performed for a series of samples with stacked Ge dots. Each stack consists of 10 layers of C-induced Ge dots (the amount of deposited carbon was always 0.2 ML). To change the sizes of the dots, the amount of deposited Ge was increased from 0.4 ML up to 3.4 ML. Each layer was separated by a 8 nm thick Si spacer. As the dots were grown at 460°C, the samples were annealed in a 4% H_2/N_2 gas mixture at 650°C for 10 minutes to heal up point defects. Fig. 5.14 shows that the increase of deposited Ge

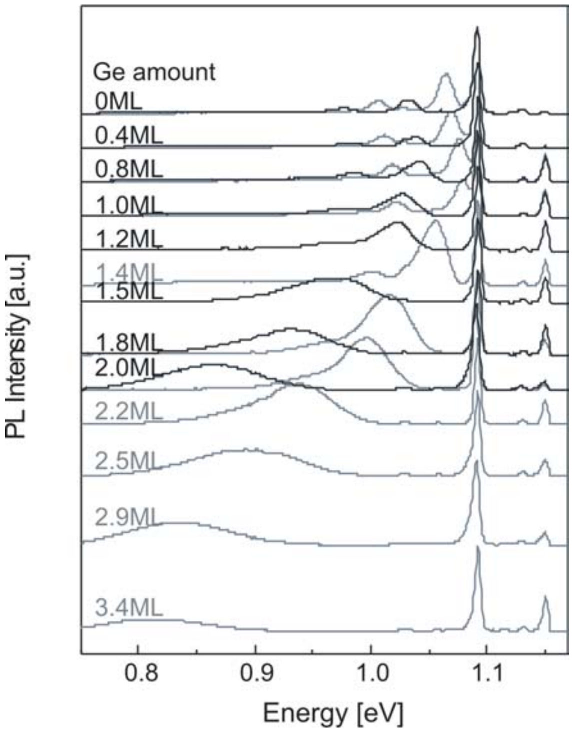

Fig. 5.14 1.8 K spectra of C-induced Ge dots deposited on Si(001) substrates at 460°C. The number of Ge MLs was increased from 0.4 to 3.4 ML within this series of samples. The samples were annealed in 4% H_2/N_2 gas mixture for 10 minutes.

leads to a red shift of the PL-signal of about 250 meV in the range from 1 ML to 3.4 ML. The red shift can be explained by the increase in dot size. As the dots become larger, the ground state, responsible for the radiative recombination, moves away from the valence band edge and therefore reduces the PL energy. In addition, the dots grow not only by the absorption of deposited Ge, but also by the coalescence of islands. This leads to a broader size distribution and in the end to an increase of PL-linewidth. In the range between 0.4 ML and 1 ML of deposited Ge, a blue shift of the PL energy

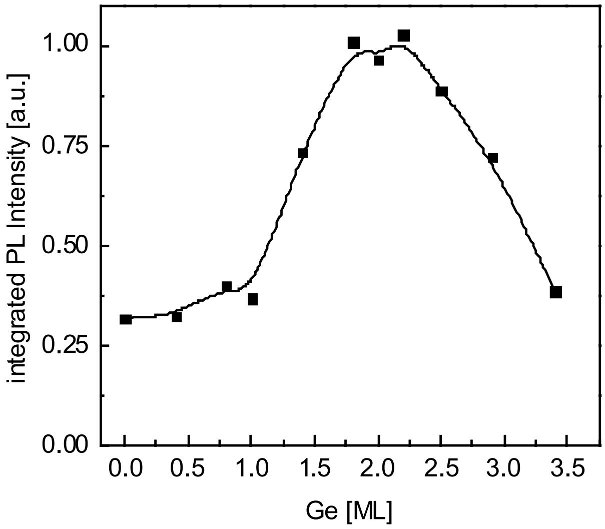

Fig. 5.15 Dependence of the integrated dot-related PL intensity on the Ge coverage

can be observed with increasing amount of deposited material. Here the deposited Ge starts to overgrow the carbon containing regions which leads to a partial strain compensation, as carbon has a smaller bond length than Si and Ge. The decrease in strain reduces the depth of the quantum wells and therefore leads to larger PL energies. This effect must overcompensate the effect by the increase in size of the dots. Fig. 5.15 shows the integrated dot-related photoluminescence intensity depending on the amount of deposited Ge. For a coverage of 2 ML the intensity is best. Here the overlap of the wavefunctions due to the confinement of the electrons in the carbon rich regions and the holes in the Ge dots must be the best one. For lower coverages, the overgrowth of the carbon rich areas is too small, so that the indirect recombination process in real space reduces the probability for radiative recombination. For coverages above 2 ML the confinement of the holes becomes weaker, resulting in the decrease of intensity.

5.3 Conclusions

The deposition of carbon on a Si(001) surface changes the surface reconstruction. For an amount of up to 0.11 ML, only buckled Si dimers and a c(4x4) reconstruction is found. Different models were taken into account in collaboration with Kaxiras and Remediakis. The most promising candidate at least for low amounts of deposited carbon is a sub-surface β-SiC-cluster with 5 carbon atoms. This model is able to simulate the observed STM pictures and the configuration is also stable. When the amount of carbon is increased to more than 0.11 ML of carbon, the situation is different. At 0.2 ML most of the surface is covered by the c(4x4) reconstruction, while also some small areas with a p(4x2) reconstruction are now observed. They often occur at domain boundaries of the c(4x4) islands. As the amount of deposited carbon would not be enough to cover the hole surface by a c(4x4) reconstruction in the configuration 5A, the former configuration may have become instable and another configuration including only up to two carbon atoms, as it was e.g. suggested by Kelires for high amounts of carbon, must have become more favourable from the energetic point of view. One possible reason for the reconfiguration can be the strain, as the configuration 5A for low amounts of carbon does not contain missing dimers and therefore no strain can be released. Finally, after the deposition of 0.3 ML of carbon, the c(4x4) reconstruction becomes instable and only the new p(4x2) reconstruction is found.

The pre-deposition of carbon leads to strain modifications in the surface. As a consequence, Ge grows in Volmer-Weber mode within the carbon free areas up to a critical thickness. For higher coverages, the dots start to overgrow the carbon rich areas. As these areas act as quantum well for electrons, the separation of electrons and holes in real space is then reduced and radiative recombination becomes more probable. The intensity of the photoluminescence signal was found to be highest, when 2 ML of Ge were deposited on a Si surface that had been modified by the pre-deposition of 0.2 ML of carbon. The integrated signal is higher by more than one order of magnitude than that of Ge dots grown on pure Si.

6 Overgrowth of Ge dots

The overgrowth of Ge dots is necessary for the realisation of dot devices. Besides the problems of the dot formation, discussed in the previous chapter, one has to investigate the impact of the overgrowth on the shape and composition of the dots themselves. Ge dots on pure Si surfaces can relax due to their three dimensional structure. When a Ge dot is overgrown, it is embedded in a Si matrix and the Ge dot has to fit again into the surrounding Si lattice. Thus the embedding of Ge dots into the Si system will increase the strain energy in the system again. The compressive strain in the Ge dot will increase and tensile as well as compressive strain will be found in the surrounding Si matrix [104]. It can be expected, that the system tries to avoid this increase in strain energy during the initial stages of overgrowth. Here we study the impact of deposition of 1-5 ML of Si on the shape and composition of Ge dots by means of STM, (EF)TEM, and x-ray diffractometry measurements. STM allows investigating the size and facets of a large number of dots at the same time. With TEM it is only possible to look at a few dots, but if energy filters are applied, an elementary map of e.g. silicon can be obtained, leading to qualitative distribution profiles. Changes in strain energy are expected and therefore x-ray diffraction measurements were performed to simulate the composition and the strain within a dot. Here, especially the temperature during the overgrowth should have a strong influence, as segregation and thermally activated processes like interdiffusion might occur.

6.1 Initial stage of overgrowth

The initial stage of overgrowth is expected to have a strong impact on the final composition and shape of the dot. During this phase, the system tries to minimize its energy by redistributing the strain and surface energy. For simplicity, three basic scenarios can be considered. In the first scenario shown in Fig. 6.1.a, the Si arriving at the surface covered with Ge dots and the wetting layer, is only incorporated on the wetting layer and not on the dot. Neglecting the relaxation of the wetting layer due to surface reconstruction, this scenario would not change the energy state of the system during the initial phase of overgrowth. The surface area remains approximately the same as well as the composition and strain state of the dots.

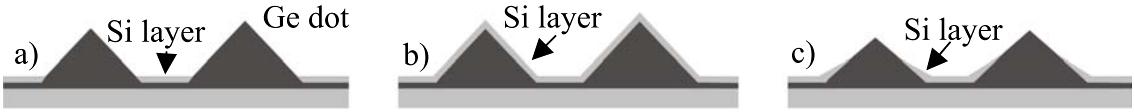

Fig. 6.1 Different scenarios for the incorporation of the Si during capping. a) Si is incorporated on the areas between the dots. Intermixing might occur. b) The Si forms a layer on top of the surface. Above the dots, the layer is tensile strained and introduces itself compressive strain into the dot. c) The Si intermixes with the dot. This leads to a reduction in strain. Consequently the dots can flatten to lower the surface energy.

The second scenario assumes the simple attachment of the Si everywhere on the surface without interdiffusion of Si with the underlying Ge dots and the wetting layer. Thus, this scenario would result in a simple replication of the surface after the deposition of a few monolayers of Si. But since the Si on top of the dot has to match the lattice constant of the partially relaxed Ge dot, it would be under tensile strain. At the same time the Si cap would also induce an increase of the compressive strain in the dot. Thus this scenario is from the energetic point of view rather unlikely.

In the third scenario Si and Ge are allowed to intermix. The Si arriving on the wetting layer may intermix with it due to Ge segregation as well as due to thermal diffusion of Ge. However, this intermixing of the wetting layer is of minor interest, since it is not changing the strain or the surface energy of the Ge dots. Both processes, segregation and interdiffusion, may also occur on the Ge dots. Here the incorporation of Si into the surface of the dot will lead to a change in lattice distortion, thus in strain energy. As has been discussed in chapter 4, the uncapped dot relaxes towards its apex, but even at the top, some compressive strain remains. Thus the incorporation of Si into the surface of the dot might be favoured, since its comprehensive strain might be further relaxed. In fact this relaxation mechanism might support Si/Ge-interdiffusion at the apex of the island. In turn the relaxation of strain energy by interdiffusion works against the stability of the dot. Originally the dots have formed to relax the strain in the Ge deposited to the expense of an increase in surface energy. If strain can be released by Si incorporation instead, this might lead to a rearrangement to minimize the sum of strain and surface energy. In this third scenario the intermixing of the dot might be initiated by Ge segregation, thermal diffusion or strain relaxation. All these processes depend strongly on the temperature. Thus we investigated sets of samples using a growth temperature for the capping layer of 620°C and 300°C

6.2 *High temperature overgrown dots*

As describe in paragraph 6.1, the temperature during overgrowth is expected to have a strong influence on the shape and composition of the dots. Since thermally activated process like interdiffusion might occur, we started our investigation by the overgrowth of Ge dots at high temperature. We focussed on the question, if the dots intermix at high temperature and which parts might be are affected. Besides this, the effect of capping on strain was studied.

6.2.1 Analysis by scanning tunnelling microscopy

STM gives an insight into the shape, and density of a large number of dots on the surface. As hut and dome clusters have different facets and different strain fields, a different influence of the cap layer is expected for the two types of dots. To study both at the same time, samples containing the two types, hut and dome clusters, were grown. For the samples, the typical buffer was grown as described in paragraph 3.2. Afterwards the Ge dots were grown on top of this buffer and they were capped by a few monolayers of Si at the same growth temperature. In this case clusters were

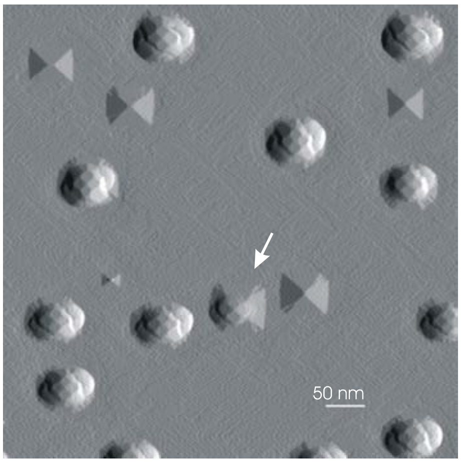

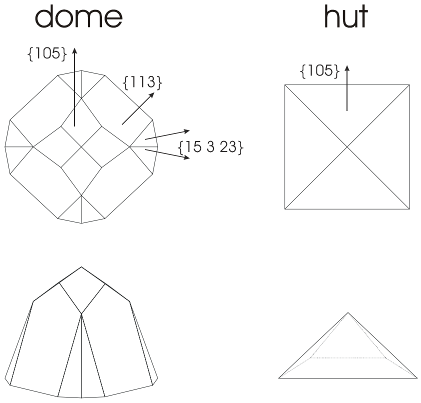

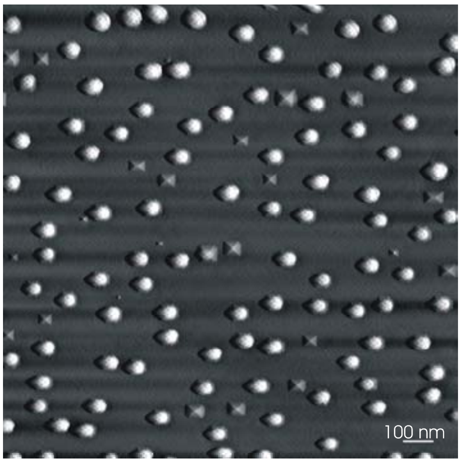

Fig. 6.2: Uncapped reference sample. The dots formed after the deposition of 6.5 ML of Ge at 620°C. Under these conditions, two types of dots, dome and hut clusters are found. In the upper picture an arrow marks an intermediate stage between a hut cluster and a dome cluster. (Empty state pictures, Bias 3V, Current 150pA (top), 270pA (bottom))

formed after depositing 6.5 ML of Ge on top of a Si buffer at 620°C. The growth rate for Ge was kept constant at 0.08 ML/s. To study the initial steps of capping, besides a reference sample without cap (introduced in chapter 4), a second sample was grown with a 5 ML thick Si-cap. The growth temperature for the Si cap was maintained at 620°C and the growth rate for Si was adjusted to 0.03 ML/s. The reference sample without Si cap has a density of clusters of $5.3\cdot10^{9}\,\mathrm{cm}^{-2}$, which is determined from Fig. 6.2.

Under the given growth conditions, the two types of clusters, domes and huts, are found. In the upper part of Fig. 6.2 the two types can be distinguished. The first one is a hut cluster with {105} facets and the second type is a dome cluster with {113}/{15 3 23} side facets and {105} top facets. The facets of these two types of clusters are typical and are known to be energetically favourable [38,101]. Besides these two types of clusters, also a transition stage between a hut and a dome cluster can be seen, marked by an arrow in Fig. 6.2. A hut clusters grows from the top downwards to its pedestal. When one layer is completed, the next one starts to grow. When the dot reached a certain volume, due to the ongoing relaxation, it might be energetically more favourable to start to grow a new layer on a facet, before the previous one is complete, as the lattice constant is larger at the top of the dot than at its pedestal. By this, the hut increases mainly in height and steeper side facets of a dome cluster are built. The occurrence of the huts and domes is also reflected in the bimodal height and diameter distributions. The intermediate stages are of low density and differ only slightly from the huts, so that they cannot be distinguished in the distributions and were not considered for the analysis.

		H030 no cap	***H034 5 ML @ 620°C***	***Changes***
domes rsp. huts	diameter [nm]	57.07 ±0.06	71.4 ±0.6	+ 25 % ± 1 %
	Height [nm]	9.64 ±0.02	7.8 ±0.05	- 19 % ± 0.5 %
huts	diameter [nm]	45 ± 2	59 ± 1	+ 31 % ± 6 %
	Height [nm]	4.51 ±0.06	5.7 ±0.2	+ 26 % ± 5 %

Tab. 6.1 diameter and height of uncapped and capped sample

For the capped sample, only hut clusters are found as depicted in Fig. 6.3. This made us conclude, that the capping initiates a shape transformation from dome to hut clusters. For the overgrown sample, a slightly higher density of $7.2\cdot10^{9}\mathrm{cm}^{-2}$ is determined. However, this is within the statistical variations of the dot density on the sample. Even though only hut cluster can be found on this sample, the analysis still reveals a bimodal distribution for the height and diameter of the dots, as shown in Fig. 6.4. This is indeed a hint for the different origins of the clusters. The clusters that belong to the peak at the lower range originate from the initially uncapped hut clusters, while the clusters of the peak at the higher range are attributed to initially uncapped dome clusters that have transformed into hut clusters due to the overgrowth. The height to diameter ratio of the clusters matches within the error limits again to the theoretical value of hut clusters, which is 1:10.

	H030 ***no cap***	***H034*** ***5 ML @ 620°C***
V_{dome} ***[nm³]***	$14,450 \pm 50$	$12,100 \pm 300$
V_{hut} ***[nm³]***	$3,000 \pm 400$	$7,100 \pm 400$
V_{total} ***[nm³] per cm²***	$6.55 \cdot 10^{13} \pm 4 \cdot 10^{11}$	$7.4 \cdot 10^{13} \pm 2 \cdot 10^{12}$

Tab. 6.2 Volume of clusters before and after capping.

The height distributions for the uncapped and capped samples show a shrinkage of the dome clusters in height while they transform to hut clusters. The shrinkage of height could not be explained by just filling up the wetting layer between the dots, as the amount of deposited Si corresponds only to 6 Å and the dots shrunk in height by 18 Å. Also the diameters of the new-formed huts are larger compared to the domes, as they have shallower facets. Both together indicate that during the shape transformation a material transport from the top of the dots to the pedestals occurs.

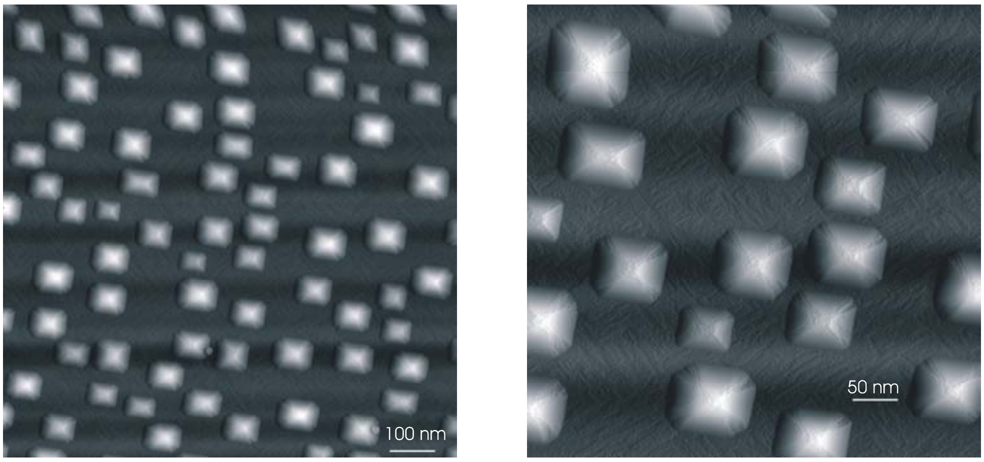

Fig. 6.3 Similar sample than in picture 6.2, but now kept by 5 ML of Si at 620°C. Only hut clusters are found, indicating a shape transformation from dome to hut clusters due to capping (Full state images, Bias 3V, Current 150pA).

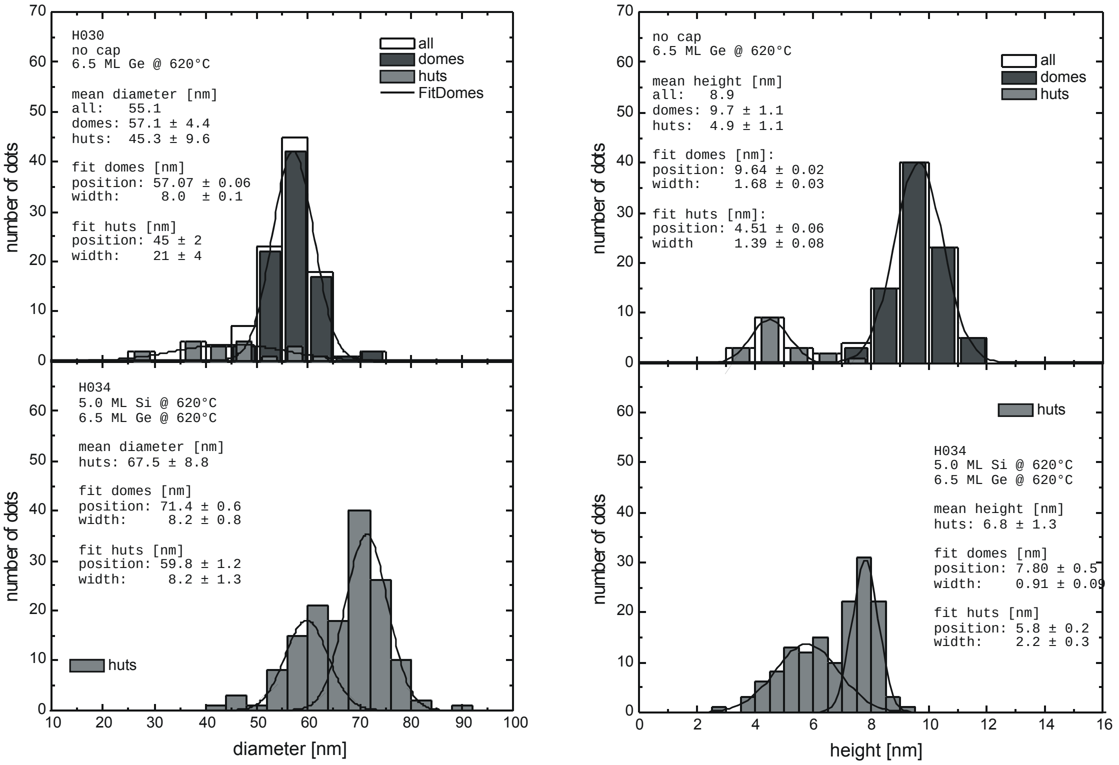

Fig. 6.4 Due to the different type of clusters, bimodal distributions of the uncapped reference sample are found. Slight volume-variations of the hut clusters lead to a broad diameter distribution, due to the fixed height to diameter ratio of 1:10. For dome clusters the ratio is just 1:5, this effect is less pronounced. The capped sample still reveals bimodal distributions for the diameter and the height, even though only hut clusters are found.

An average initially uncapped hut cluster increases in height and diameter, which shows again, that the dots are not simply covered by the cap. Indeed, the findings indicate, the hut clusters must have intermixed with the capping Si. Comparing the volumes of huts before and after the overgrowth, the increase by a factor of two shows a strong intermixing of Si with the hut clusters. If assumed, that no material from the wetting layer is consumed and that the Ge content is 100 percent before capping, this volume-increase by a factor of two indicates an average Ge content of 50 percent after overgrowing them with 5 ML of Si.

The change of total volume (huts and domes) of $8.5 \cdot 10^{12}$ nm^3 is in the range, which could be expected, if only the Si atoms deposited on the clusters themselves contribute to the volume increases and by assuming, that no significant uptake of Si from the wetting layer or the substrate occurs.

By our STM investigations we saw, that the shrinkage of the Ge dots in height cannot be explained by scenario one that was introduced in the previous paragraph. The reduction in height is larger than the thickness of the deposited Si film would be. As a shape transition from dome to hut cluster occurs, scenario two is also disproved, as it would only replicate the surface and dome cluster should be still present after capping with 5 ML of Si. As by scenario three a shape transition was possible, we found by the STM investigation a strong indication for the presence of thermal activated processes that changes the strain within the dot. The increase in volume for the initially uncapped hut clusters can also be explained by intermixing. No shape transformation was observed for these clusters, as the {105} facet has already a very low surface energy. To prove if the clusters are intermixed, TEM investigations were performed. Additionally EFTEM was performed to gather insights into the SiGe composition profiles of the dots.

6.2.2 Transmission electron microscopy

The STM investigations reveal a shape transformation from dome to hut clusters during the overgrowth of the dots with Si. The diameter and height distributions suggest that this can be attributed to an intermixing of the Ge dots with the deposited Si. To gather further insight on the details of the intermixing process, high resolution and energy filtered transmission electron microscopy were performed.

In cross-sectional TEM a limited number of clusters is observed. This restriction makes it more favourable to grow only one type of clusters, as the observed features than can be clearly attributed to the initial cluster-type. As a shape transformation has been obtained only for the dome clusters, we focussed on this type of cluster. Thus for

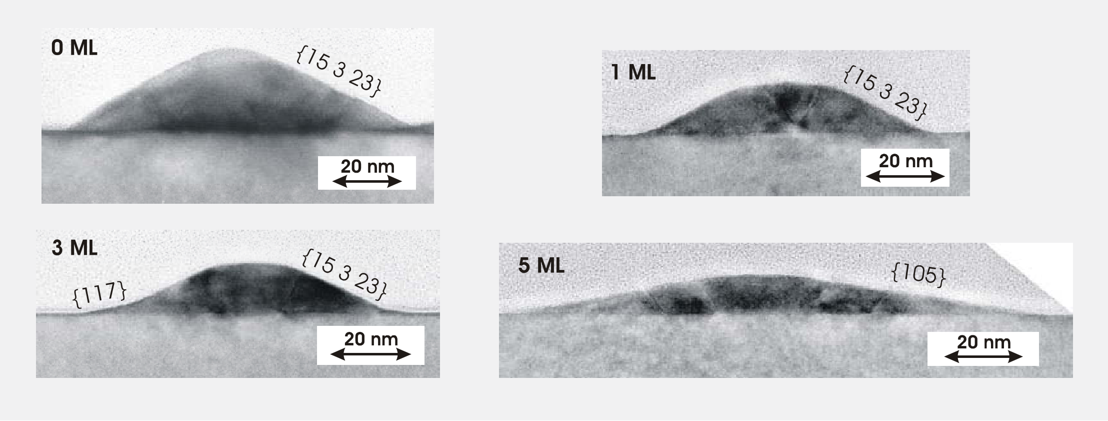

Fig. 6.5 High resolution TEM of the whole set. In the uncapped case predominantly dome clusters with dislocations are found. Capping with 1 ML of Si leads to a decrease in height while at 3 ML new facets are found at the pedestals of the former dome clusters. The overgrowth with 5 ML leads to shape transformations to hut clusters.

our TEM investigations a second set of samples was fabricated, which contained predominantly dome clusters. The growth rates for the formation of Ge dots and the capping-process with Si were again kept at 0.08 ML/s and 0.03 ML/s respectively, but the dots formed now after the deposition of 8.6 ML at 520°C. The growth temperature of the Si cap was also reduced to 520°C.

Fig. 6.5 shows for each sample of the set a high resolution TEM cross-section of a typical dot. In the uncapped case, predominantly large dome clusters with a diameter of about 100 nm are visible in the TEM cross section. Dislocations are found within some of these dome clusters, as it is typical for clusters of this size. The angle of 26 to 28° for the side facets correspondent to {113} and {15 3 23} side facets. The facets are commonly observed for dome clusters. No clear {105} top facet is detected in the TEM cross sectional view. A cap of just 1 ML of Si has no significant impact on the island shape. The dominant facets are the same as in the uncapped case. In addition, clearly {105} facets are now found at the top of the clusters. If the amount of deposited Si is increased to a value, corresponding to a layer thickness of 3 ML a new facet starts to grow at the pedestal of the former dome clusters. This facet has a surface with an angle of 11° towards the Si wafer surface, indicating a {105} or {117} facet. Besides this new facet at the pedestal, the rest of the cluster has still a dome-character. After the amount of Si increased to an amount corresponding to a 5 ML thick layer, the situation changes significantly. Besides a low density of dome clusters with typical facets, predominantly large hut clusters are found. The presence of these large hut clusters indicates that there is a non-abrupt transformation from the initially uncapped dome clusters to the new-formed hut clusters. Again, the changes in size show the material transport from the top of the clusters to its pedestal. So even the samples have been grown at a temperature of 520°C and those of the STM investigations at 620°C, a similar shape transformation of the domes is observed, with a decrease in height and an increase in diameter.

By this investigations it was found, that due the capping a material transport from the apex to the pedestal occurs and new facets start to grow at the pedestal, as this would be the case for the thermal activated interdiffusion. To study the distribution of Si, energy-filtered TEM was performed on the same set of samples. The method is described in detail in paragraph 3.5. Energy filtered TEM provides the elementary map of Si through a dot. Thus the qualitative insight into the Si distribution within the dot is obtained. Fig. 6.6 shows EFTEM images of three samples, having no, a

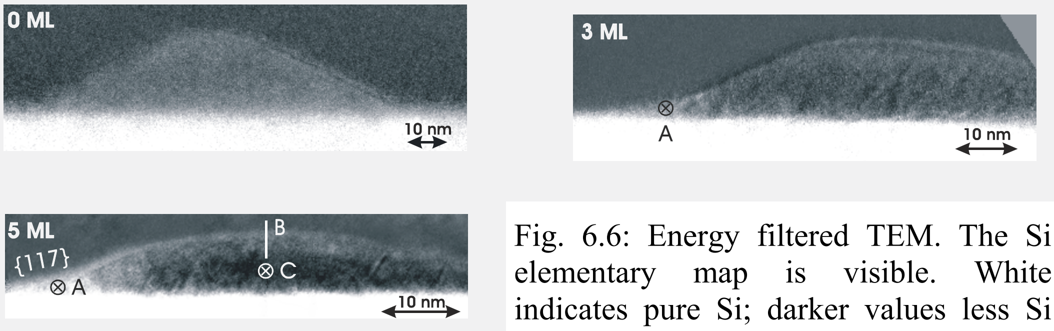

Fig. 6.6: Energy filtered TEM. The Si elementary map is visible. White indicates pure Si; darker values less Si and therefore more Ge. The pictures are not colour calibrated. The uncapped sample has a uniform Ge distribution, while the new formed facets at (A) of the 3 ML Si-capped sample show a strong intermixing with the capping Si. If the according cap layer thickness is increased to 5 ML, the Si start to penetrate into the dot as indicates at the line at (B), while the core of the dots remains Ge rich (C).

3 ML and a 5 ML thick cap. As the dots just consist of Si and Ge, the Ge composition is implied. These pictures are not colour calibrated, but white indicates a higher Si concentration. Darker areas indicate less Si and therefore a higher Ge concentration. Thus for the uncapped sample, the Si buffer mostly consisting of Si is white. The energy filtered TEM of the uncapped Ge islands reveal an almost uniform composition with an increase of the silicon concentration at the interface to the Si buffer layer. Even though, the pictures are not colour calibrated, a high Si content of 30% to 50% throughout the whole dot can be assumed, as it is typical for large domes grown in this temperature-regime [48, 54]. For the sample, which was capped by an amount of Si, which would correspondent to a layer thickness of 3 ML, the new formed parts, i.e. the pedestal of the dot are highly intermixed, as indicated by the grey colour at cross A. This intermixing is substantial, as the formation of the new-formed facets is deduced to the intermixing with the capping Si. If the amount of Si is increased to 5 ML, the highly intermixed areas at pedestal (A) are still found, but in addition, the colour gradient along line B shows that the Si now also penetrates into the Ge dot itself. Although the dark colour at C shows, that the core of the former dome clusters still has a higher Ge content.

The energy filtered TEM allows a qualitative insight into the process of intermixing. Intermixing changes the strain energy and therefore drives the shape transformation. The results reveal that the new formed side facets at the pedestal are highly intermixed with Si, some intermixing is also found at the top of the dot, while the core of the dot remained unchanged. As previously discussed in scenario 3 (page 74), apparently the intermixing at the apex of the islands leads to a further relaxation of the lattice. The driving force is the minimisation of the sum of surface and strain energy. In addition to the shape transformation by STM we found, that the transformation is non-abrupt. The transformation occurs via intermediate shapes, which contain strongly intermixed sections with shallower facets at the pedestal of the dot. As the dots and the capping layer for the TEM samples were grown at a different temperature (520°C) compared to the 620°C of the STM-investigation, the intermixing seems to be a general aspect of samples grown in this temperature regime.

6.2.3 X-Ray diffractometry

The STM and TEM investigations give a detailed insight into the shape transformation and also a qualitatively one into the intermixing between the Ge dot and the Si during the high temperature overgrowth. For a quantitative insight into the composition, x-ray diffractometry measurements were performed in collaboration with Anke Hesse from the group of Prof. Bauer, Johannes Kepler university of Linz. The x-ray diffractometry measurements are of special interest, as they also reveal the strain inside the dot, which should be the driving force for the observed shape transformation.

X-ray diffraction measurements averages over a high number of dots, as the spot size is in the range of several square millimetres and the densities of dots are roughly in the range of 10^{10} cm^{-2}. This makes it also desirable to have only one type of cluster.

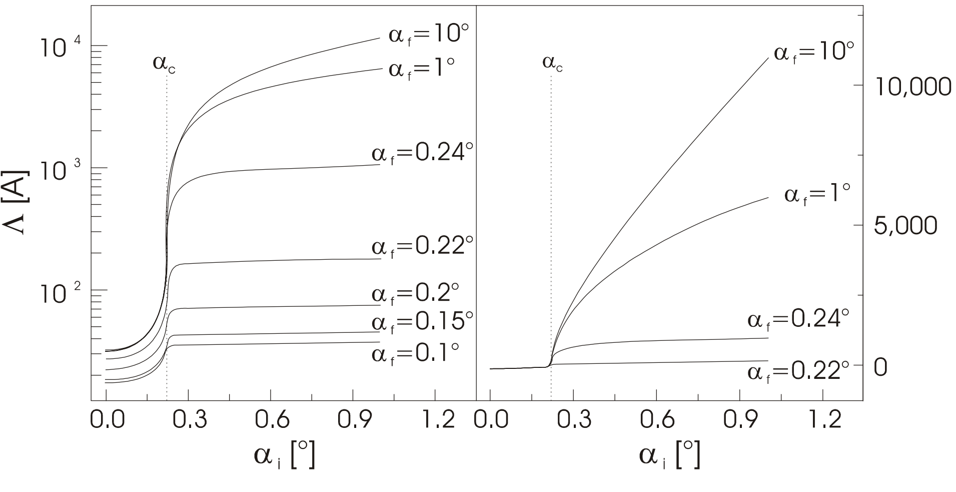

Fig. 6.7 Penetration depth Λ for various incidence- α_i and exit-angles α_f calculated for a CuKα_1 radiation source and Si as material. As long as α_i is below the angle of total reflection α_c, Λ is in the range of only 50 Å.

For this reason, a third set of samples containing only hut clusters was grown, to study this time also the influence of capping on huts. The dots formed after the deposition of 5.8 ML of Ge. The growth temperature for the Ge deposition and the Si cap were kept at 580°C, the growth rates at the same values as for the other series of samples. To study also the influence of capping on domes, besides this Xray-set, also another set of samples similar to the STM-set was investigated. It has a bimodal distribution of huts and domes, but as the influence of huts can be derived from the Xray-set, it is possible to determine the influence of capping on dome clusters as well.

The diffraction experiments were carried out at the European Synchrotron Radiation Facility (ESRF). X-ray diffraction (XRD) is the method of choice to measure strain and by this the composition of thin epitaxial films. However, to reveal the shape and composition of Ge dots from x-ray diffraction experiments is a difficult task, as most of the signal is a contribution of the substrate. Thus complex simulations are needed.

To reduce the contribution of the substrate, grazing incidence geometry is used. When the incident angle α_i of the incident x-ray beam is below the critical angle α_c, the penetration depth of the beam is in the range of about 50 Å for the CuKα_1 line, as shown in Fig. 6.7, and most of the signal originates from the Ge dots. For this reason, the samples were investigated under grazing incidence non-coplanar scattering geometry as described in paragraph 3.4. The in-plane lattice parameter and the lattice parameter in growth direction were determined to analyse the strain and composition of the dots. Reciprocal-Space-Maps (RSM) were measured with a momentum transfer component q_z along the growth direction ($q_z > 0$) and a component q_x perpendicular to it. Fig. 6.8 shows a contour plot of a RSM, where the intensity was measured around the (113) reciprocal lattice point for uncapped Ge dots on a Si(001) surface. The peak of highest intensity is attributed to the (113) reflex of the substrate. A vertical line starting at the peak goes to smaller q_z values, indicating an increasing vertical lattice constant. No change in q_x and therefore in the lateral lattice constant is observed. For this reason, the line must belong to the wetting layer which is fixed in lateral direction to the Si substrate and can only relax in vertical direction. The small variations due to relaxation by mixing dimers are within the line-width. For the islands the situation is different. The relaxation and therefore the change in elastic energy is the driving force for the two to three-dimensional transition in the Stranski-Krastanov-growth. For this reason, the maxima of the Ge-islands are found at lower q_x and q_z values compared to

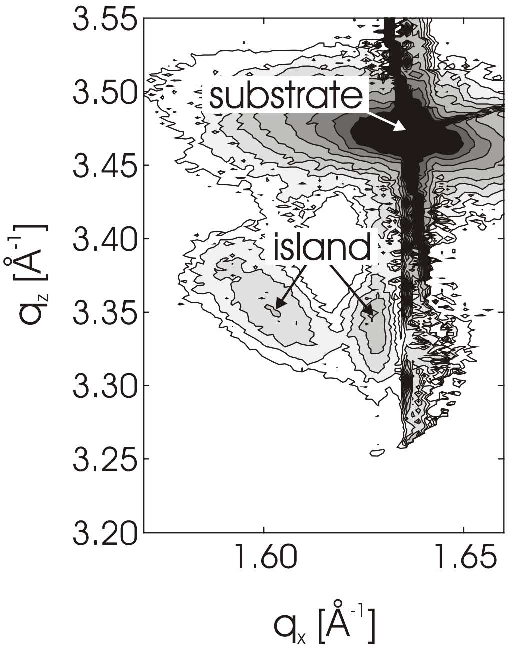

Fig. 6.8 Example of a measured reciprocal space map around the (113) reciprocal lattice point. The large peak belongs to the substrate. The halo comes from the non-infinity of the substrate. The vertical line to smaller q_z values belongs to the wetting layer. Two additional maxima at lower q_x values belong to the island.

the Si-substrate, since Ge has a larger lattice constant than Si. The signals, which can be attributed to the dots are at $q_x = 1.60$ and 1.63 Å^{-1}, as indicated in Fig. 6.8. As there is no ordering of the dots in a 2-d array on the surface, i.e. the dots are randomly distributed, all islands contribute to the diffraction signal.

Thus, the x-ray diffraction peaks of the dots can be considered as originating from a dot with size and composition reflecting the average values (“average dot”). In the contour plot depicted in Fig. 6.8, two maxima are found, indicating a partially relaxed state of the islands. The peak at $q_x = 1.63$ Å^{-1}, $qz = 3.34$ Å^{-1} is assigned to the part of the dot close to the substrate which is still under compressive strain, whereas the peak at $q_x = 1.60$ Å^{-1}, $qz = 3.35$ Å^{-1} is assigned to the relaxed portion close to the apex.

In a first step a rough method was used which gives an upper limit for the maximal Ge concentration within a dot. It determines the Ge concentration by the displacement of the island-maxima without taking the shape of the dots into account. It was used for both sets of samples, the X-ray set and the STM-set, to investigate the influence of capping on domes and huts. For the dome clusters, the intensity maxima of the islands shift with increasing thickness of the cap-layer to smaller q_z and higher q_x values, as shown in the upper part of Fig. 6.9. This shift indicates that the lateral lattice constant of the islands converges to the lateral lattice constant of Si. For the vertical lattice constant the opposite is the case (see Tab. 6.3). The unit cell becomes more distorted and the dots are more strained. Due to capping, the dome clusters become more

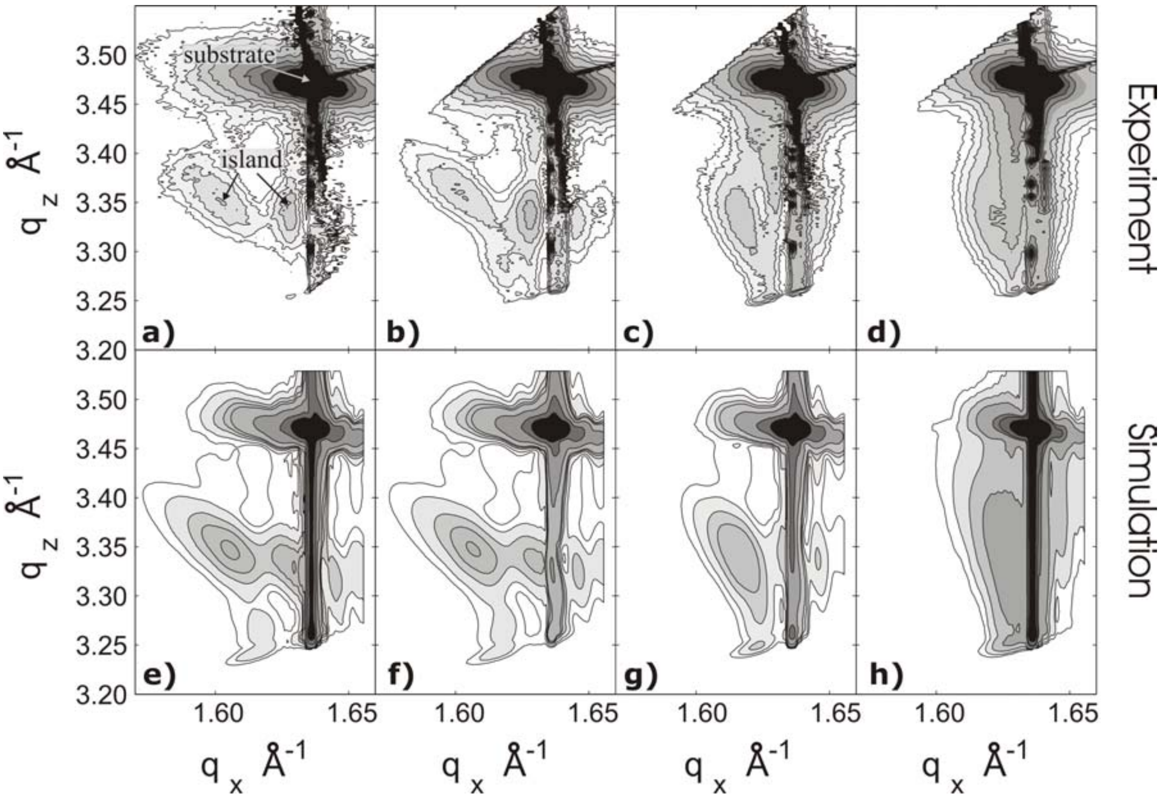

Fig. 6.9 Top: Reciprocal space maps of dome clusters on a Si(001) surface measured by x-ray diffractometry. The thicknesses of the capping layer are 0, 1, 3, 5 ML increasing from a) to d). The intensity maxima shift to higher q_x and lower q_z values, indicating the increase in strain due to capping. Bottom: Simulated reciprocal space maps, which were calculated with the fitting procedure, sketched in Fig. 6.10.

strained. The upper limit for the maximum Ge concentration only changes slightly and stays around 90 percent.

For the hut clusters, the intensity shift of the island is not uniform in x direction. For a capping layer thickness up to 3 ML, the maximum shifts to smaller q_x (increasing Δq_x), as shown in Tab. 6.3. When the thickness is increased to 5 ML, the process is inverted and the q_x value moves close to that of the Si substrate peak. In z direction, the maximum shifts in the direction of the Si substrate peak. Here, after capping with 5 ML of Si, the intensity maximum comes closer to the Si substrate peak showing the decrease in Ge content of the hut clusters, due to the capping by 5 ML of Si. The upper limit for the maximum Ge concentration inside the dots decreases from 100 percent to 51 percent due to the capping, as given in Tab. 6.3. As this method gives an upper limit for the maximum Ge concentration of the dot, the high intermixing of hut clusters, as it was already predicted from the STM results, is confirmed.

X-ray set 5.8ML @ 580°C	***uncapped huts***	***1ML-cap***	***3ML-cap***	***5ML-cap***
$\lvert\Delta q_x\rvert$ [Å^{-1}]	0.021	0.025	0.031	0.013
$\lvert\Delta q_z\rvert$ [Å^{-1}]	0.303	0.249	0.207	0.143
$\chi_{Ge\text{-}max\text{-}limit}$ [%]	100	86	75	51
STM set 6.5ML @ 620°C	***uncapped domes***	***1ML-cap***	***3ML-cap***	***5ML-cap***
$\lvert\Delta q_x\rvert$ [Å^{-1}]	0.036	0.033	0.019	0.014
$\lvert\Delta q_z\rvert$ [Å^{-1}]	0.115	0.114	0.140	0.133
$\chi_{Ge\text{-}max\text{-}limit}$ [%]	95	92	95	92

Tab 6.3 Displacement of island-maxima $|\Delta q_{xzy}|$ compared to the substrate, upper limit for the maximal Ge concentration $\chi_{Ge\text{-}max}$ within the dots.

Here we obtained two different results. For dome clusters we see that the dots are stronger strained due to the capping, but also that the upper limit of the Ge concentrations stays high. This is again in accordance with the EFTEM observations, showing that the Ge concentration of the core of the dots stays high and the strain is increased due to the increase of the base area and the decrease in height of the dome clusters. The hut clusters seem to intermix completely with the capping Si layer, reducing the maximum Ge concentration within the dots and increasing their size. It should be noted, that the strain, i.e. the lattice mismatch between dot and substrate, decreases due to the intermixing, but the integrated strain energy may stay the same.

For the dome clusters, we used in addition a more precise method to determine the concentration profile within the dots. This method is only useful for dome clusters, as they fit better to a radial-symmetric shape, as it is necessary for the simulation applied. The simulation fits the Ge concentration as well as the lateral and vertical lattice constant. For the Ge concentration only a dependence on the height can be treated, while for the lattice constant an axially symmetric distribution is assumed with the rotation axis through the centre of the parabol island. This shows also the limits of the simulation, as the etching experiments introduced in paragraph 2.5.2 reveal that the composition is not homogeneous within a slice parallel to the surface. A sketch of this fitting procedure is given in Fig. 6.10. In a first step the shape of the dot is approximated by a paraboloid. A typical Ge profile is chosen, which only depends on the height, as other symmetries cannot be treated. In a next step, this paraboloid is split into slices of constant Ge concentration, each slice having a height of 7.6 Å (5 ML). Subsequently, the finite element method (FEM) is used to calculate the displacement field resp. the lattice. From the displacement field and the composition, the lattice parameters are calculated, which are used to calculate the

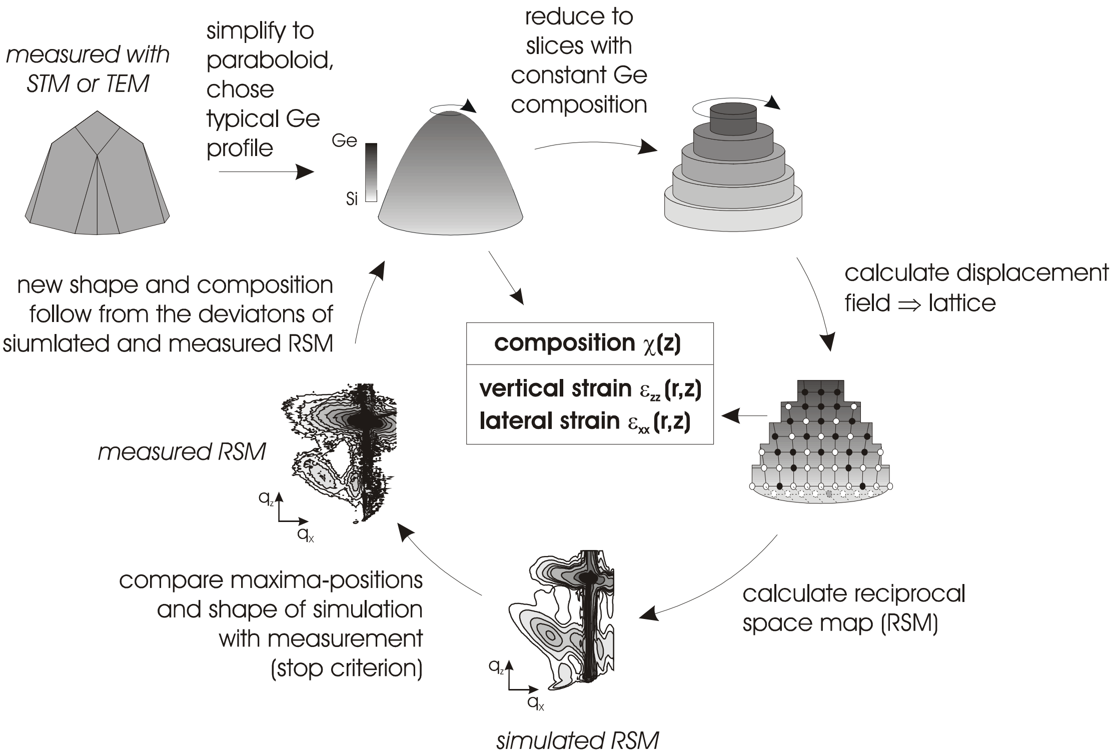
measured with STM or TEM
simplify to paraboloid, chose typical Ge profile
Ge
Si
reduce to slices with constant Ge composition
calculate displacement field ⇒ lattice
composition χ(z)
vertical strain ε_zz (r,z)
lateral strain ε_xx (r,z)
new shape and composition follow from the deviatons of siumlated and measured RSM
measured RSM
q_z
q_x
compare maxima-positions and shape of simulation with measurement (stop criterion)
calculate reciprocal space map (RSM)
simulated RSM

Fig. 6.10 Single-steps of fitting procedure to obtain the vertical Ge concentration profile and the strain fields.

diffraction patterned in a final step. The scattering process is described in the framework of the distorted Born approximation [52, 102]. The scattering potential in the wave equation is divided into a part dealing with the unperturbed system and the perturbation, while the intensity distribution along the truncation rode is not considered. Then a semi-infinite amorphous substrate with constant polarization can be chosen as unperturbed system while the crystalline structure of the surrounding matrix and the islands is included into the perturbation. In this approach the refraction of the primary and diffusely scattered beams at the sample surface are treated exactly. The waves propagating in the substrate are kinematically scattered by the crystal matrix and the islands. Dynamical effects did not affect the scattering signal from the islands and the surrounding strained Si. This allowed a simpler approach with the amorphous unperturbed system. Again, as the position of the islands is uncorrelated and the diffusely scattered intensity is proportional to the intensity originating from a single dot, the results can be treated as originating from a dot with average size and composition. For a more detailed description see reference [52]. The good accordance between experiment and simulation is shown in Fig. 6.9.

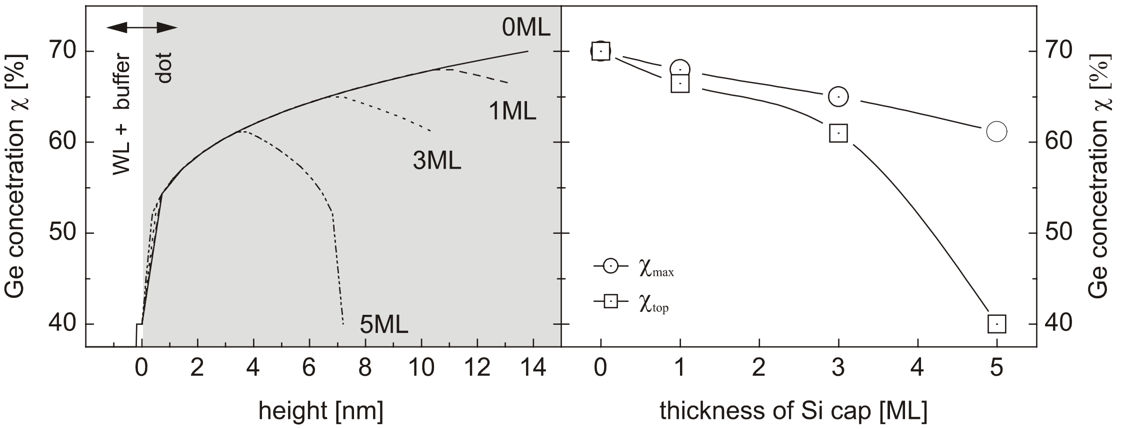

Fig. 6.11 Ge concentration profile through the centre of the dot, shown on the left side. With increasing amount of deposited Si an intermixing at the top can be observed, while the core remains Ge rich. This leads to a decrease of the Ge concentration down to 40 percent at the top and down to 60 percent for the maximum (right side).

The Ge concentration was determined with this more precise method and the result is depicted in Fig. 6.11. On the left side the Ge concentration profile through the "average dot" is shown for all samples. The zero at the x-axis corresponds to the base of the dots. Thus, the white area corresponds to the silicon buffer and the wetting layer. In the silicon buffer, the Ge concentration is zero and therefore not visible. The best fit was obtained by assuming a Germanium concentration of 40% in the wetting layer. For this reason, within the white area a jump from 0% in the Si buffer to 40% in the wetting layer is drawn. For the uncapped sample (solid line), the Ge concentration rises from 40% at the bottom to 70% at the top for the best fit. The shape of the curve follows an n^{th} root law. This shape of increase seems to conflict with the EF-TEM results. But as EF-TEM has only an accuracy of 5 to 10 percent for the composition, the change in concentration of only ten percent in the upper part of the dots (85% of the height) may look constant in EFTEM images. In addition, the dots investigated by TEM are higher and due to the n^{th}-law shape of the concentration profile, a larger part of the dots appears to have a constant composition.

The dotted lines are the profiles yielded for the best fits of the x-ray data for the capped samples. The profiles for the capped samples differ at the top of the dots from the uncapped sample, reflecting the intermixing, while the composition of the cores seems not to be affected, which is in accordance with EFTEM investigations. Also a reduction in height from 13 nm in the uncapped case down to 7 nm for the sample

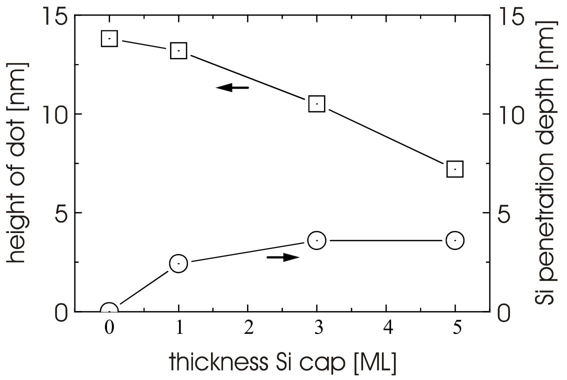

Fig. 6.12 Penetration depth and height of the average dot after capping. While the height shrinks continuously from 13.8 nm to 7.2 nm, the penetration depth saturates at 3.6 nm at a growth temperature of 620°C.

capped with 5 ML of Si is found. While, due to the intermixing, the Ge concentration at the apex strongly decreases from 70% for the uncapped islands to 40% for the islands capped with 5 ML of Si, this change is less pronounced for the maximum Ge content, as the core of the dot remains Ge rich, as depicted on the right side of Fig. 6.11. For this reason, the maximum Ge concentration is reduced only by 10%, while the concentration at the top decreases by 30%.

The penetration depth of Si is defined as the length, over which the Ge concentration of the dot is changed due to intermixing. The penetration depth of Si into the Ge dome cluster saturates at 3.6 nm after the deposition of a 3 ML thick cap, as shown in Fig. 6.12. The height of the dots still shrinks with increasing cap layer thickness. This is supported by the mass transport from the top of the dot down to the pedestals, as it was observed by TEM and STM.

Fig. 6.13 shows on the left side the lateral and vertical deviation of the lattice constant inside the Ge dots compared to the Si lattice for a cross section of the uncapped sample. It is a cross-section through half of a dot and the buffer, indicating the displacement by different grey levels. The displacements fields are defined in comparison to the Si lattice constant ($d = (a(r,z)-a_{Si})/a_{Si}$). The lateral displacement is monotonically increasing towards the top of the dot and its edges, showing the increase in relaxation in lateral direction. Below the dot in the Si buffer, the Si lattice is broadened in lateral direction, due to the strain induced by the dot. This tensile strain reaches down to a depth of 90 nm. As in the infinite the lateral displacement for Si has to be zero, a compensation effect occurs under the edge of the dot, leading to lateral displacement with opposite sign. Thus the Si in this area is under compression (white area in the contour plots of Fig. 6.13). The vertical displacement rises from the bottom of the dot up to 6 nm for all dots. There it reaches 3.9 % and decreases again towards the apex of the dot due to relaxation.

a) lateral displacement

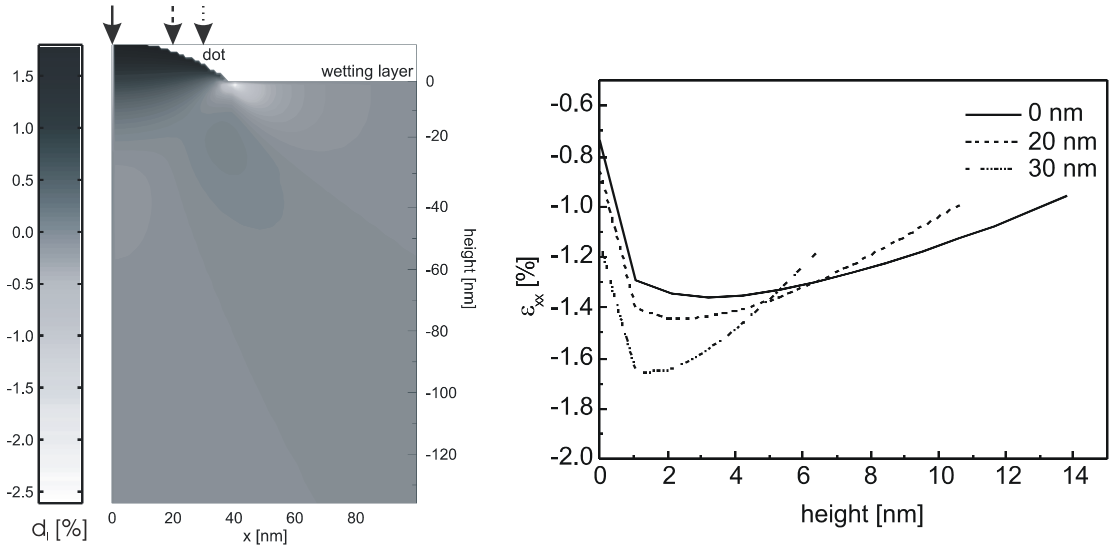

b) vertical displacement

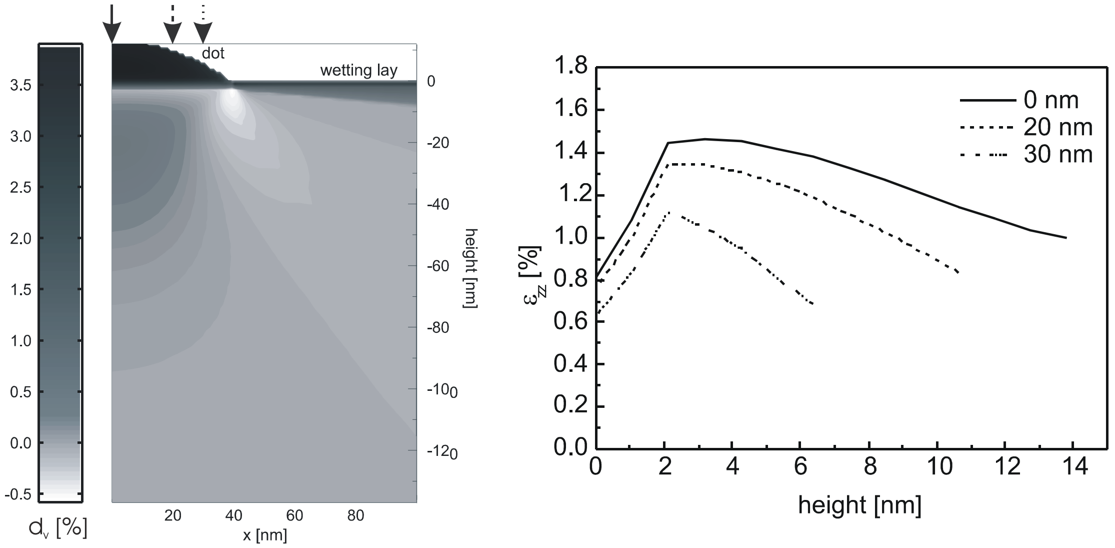

Fig. 6.13 Lateral and vertical lattice distortion. The deviations are given in percent with respect to the Si lattice. Negative values indicate lattice constants smaller than bulk Si, positive values indicate lattice constants larger than Si. On the right side the lateral and vertical strain through the dots are shown at the position, marked by an arrow on the left side.

On the right side of Fig. 6.13 the lateral and vertical strain through the dot are shown for certain points of interest, which are marked by arrows on the left side. All the parts of the dot are under tensile vertical and compressive lateral strain. The dot does not relax fully. Except for the outermost area at the basement of the dot, i.e. the region near the Si/SiGe interface, the lateral strain decreases towards the top, showing the increase in relaxation. Its minimum is found at the apex of the dot. Near the SiGe/Si

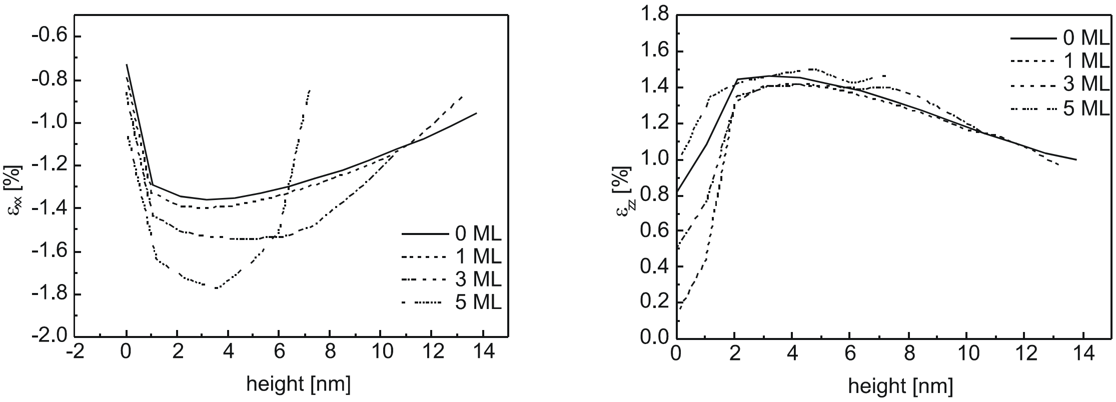

6.14 Lateral and vertical strain through the centre of the dot. While the lateral strain is reduced at the top of the dot and increase at the bottom due to the mass transport, no influence on the vertical strain is found.

interface of the dot and the Si buffer layer, the lateral strain increases from the centre towards the edge (compare lateral strain at height 1 nm), as due to a compensation effect, the Si below the edge of the dot is compressed, while it is stretched below the centre of the dot.

The vertical displacement field has a local maximum at a height of 6 nm within the dot due to the increasing Ge concentration (Fig. 6.11). The vertical strain increases in the dot up to a height of 2 nm and than decreases again. The difference can be explained by the change in composition of the dot. At the height of 6 nm, the relaxation process becomes more effective, as it goes with a power of two and the Ge concentration profile becomes flat due to its power of 1/n dependence (visualised in Fig. 6.11).

Near the substrate, the lattice constant is fixed to the Si substrate and therefore a deformation of the unit cell can only occur in vertical direction. This leads to a high tensile vertical strain of 1.45 %, while the lateral strain is of compressive type and is about -1.4 %. From the bottom to the top, the increase in Ge content still increases the vertical displacement, even though the dot can relax. The vertical strain at the top of the dot is just 1.0 %, while the lateral strain is of opposite type and decreases down to -1.0 %. The dot does not fully relax.

Fig. 6.14 shows the influence of capping on the strain. The left side represents the lateral strain through the centre of the dot down to the Si buffer, while the right side shows the vertical strain. The vertical strain is not significantly changing due to the capping, only the decrease in height of the dot can be observed. For the lateral strain it is different. Here an increase in strain is observed near the wetting layer, while at the

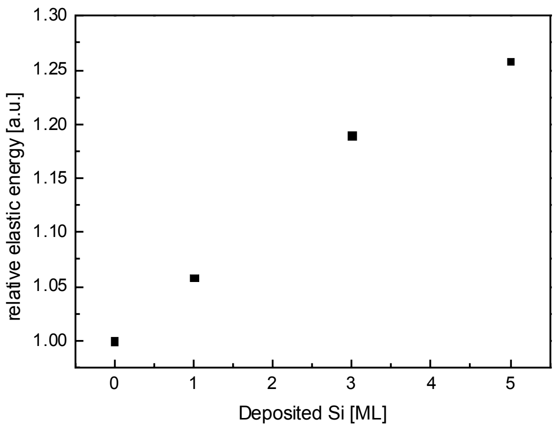

Fig. 6.15 Increase of elastic energy due to capping. The increase of strain at the bottom of the dots outweighs the release of lateral strain at the top of the dot. Consequently the elastic energy increases with the amount of deposited capping Si.

top a decrease is observed. As material is transported from the top of the dot down to its pedestal, the larger diameter leads to a less efficient relaxation and therefore to higher strain at the base. The top the dot can elastically relax and intermixing during capping further reduces the lateral strain. This intermixing and the increase in diameter was shown by TEM. Fig. 6.15 shows, that the total elastic energy stored in the dot is increased due to the capping process and the resulting material transport.

By the simulation of the x-ray measurements we found, that the dome clusters shrink in height due to the capping by Si, as it is the case for a shape transformation from a dome to a hut clusters. In addition, the Ge concentration at the apex is reduced, while the Ge core is unchanged, which is in agreement with the EFTEM images. The increase in lateral strain near the substrate and the decrease of lateral strain near the apex are the consequence of the mass transport from the material at the top down to the pedestal and intermixing with Si within the surface layer of the island respectively. In addition, it was shown, that due to the capping the elastic energy increases.

It was found, that for the dome cluster the penetration depth of Si into the dome is about 3.6 nm. By assuming a similar penetration depth for hut clusters, a total intermixing of hut clusters with the capping Si material can be concluded, as the height of clusters is in the range of the penetration depth. This intermixing of the Ge dots with a Si cap layer is much stronger than the intermixing which is typically obtained at the interfaces of pseudomorphic Si/SiGe quantum well structures grown in this temperature regime. For these quantum wells the intermixing is dominated by Ge segregation which would lead to a much lower Si fraction in the Ge wells, at least for distances as large as 3.6 nm away from the interface [106]. Moreover, annealing of these quantum wells in the temperature range from 520-620°C does not lead to a noticeable change in the interface abruptness. Thus our results let us conclude, that the interdiffusion of Si and Ge at the interface between dots and the Si capping layer has a reduced activation energy. Possibly this reduction is due to the lattice relaxation at the apex of the islands.

6.2.4 Summary

By Scanning Tunnelling Microscopy as well as by Transmission Electron Microscopy a transition from dome to hut clusters is detected, when these clusters are overgrown with silicon at temperatures in the range of 520° to 620°C. The reason for the formation of Ge dots on a silicon surface is the lattice mismatch of those materials of four percent, which leads to a Stranski-Krastanov growth mode. The explanation for the formation of the dot is the minimization of the sum of the surface and elastic energy, where the increase in surface energy of dots compared to a two-dimensional layer is intercepted by a more effective lowering of the strain energy. The Scanning Tunnelling Microscopy results let us assume, that an intermixing of the Ge dots occurs with the capping material, when they are overgrown by Si. This was verified by the Energy Filtered Transmission Microscopy that gave us qualitative concentration profiles. In addition, it was shown, that the shape transformation is non-abrupt and that in the first step material is transported from the top of the dot to its pedestal, where new facets start to grow. This material is highly intermixed with the silicon from the cap layer. When the new facets are formed, a penetration of the capping material into the surface of the entire dot is observed. By comparing the Si distribution within the dots and the strain fields with three different models, it was found, that most likely the interdiffusion at the interface between the dot and the Si cap has a smaller activation energy compared to the interdiffusion at the pseudomorphic Si/SiGe interfaces.

6.3 *Overgrowth of Ge dots at low temperatures*

The overgrowth of dots with Si in the high temperature regime of 520-620°C leads to alloying of the Ge hut and dome clusters with the capping Si. This intermixing is accompanied by a shape transition from dome to hut clusters as shown in the previous chapter. It was assumed, that the alloying and the shape transformation is due to thermal interdiffusion at the top of the Ge dot. Most likely this interdiffusion is thermally activated. To answer the question, if the interdiffusion has a rather small activation energy, we investigated samples that were overgrown at low temperatures, here below 300°C. In this temperature regime the interdiffusion and Ge segregation should be strongly reduced and the alloying should be suppressed. To keep all other experimental growth parameters the same, the dots were again deposited at 620°C. However, this requires a growth interruption after the dot deposition to lower the temperature before growing the Si cap. Depending on the start- and final temperature this interruption can take up to several minutes.

6.3.1 STM investigations

We studied the initial states of overgrowth by capping dots with 1, 3, and 5 ML of Si. The dots were grown under the same conditions as for the high-temperature overgrown samples. The growth rate amounted 0.08 ML/s and the dots formed again after the deposition of 6.5 ML of Ge at 620°C. For the overgrowth, the growth temperature was lowered within 400 s down to 300°C. Afterwards the samples were capped with Si at a growth rate of 0.03 ML/s. The uncapped sample was already presented in the previous chapter. The cap of 1 ML of Si seems to have no influence, as demonstrated in Fig. 6.16. Again dome and hut clusters are found as in the uncapped case. The ratio of dome to hut clusters of 1:14 is lower compared to the uncapped case, where the ratio is 2:9. The density is with $2.3 \cdot 10^{10}$ cm^{-2} a factor of 6 higher compared to the uncapped case with $5.3 \cdot 10^{9}$ cm^{-2}. After capping the dots with 3 ML of Si, still hut and dome clusters are found. The increase in diameter of the dots can be attributed to the statistical variations between different samples, in particular no new facets are found at the pedestals of the dome clusters, whereas this was the case for the high temperature overgrown TEM samples. The density of these clusters is again in the same regime ($1.9 \cdot 10^{10} cm^{-2}$) and the height to diameter ratio of 1:7 is comparable to the uncapped islands. But besides these hut and dome clusters, a new type of cluster was found. It has a squared base parallel to the <011> direction, thus rotated by 45° compared to base of huts, which are aligned along the <001> direction. For the sample, capped by 5 ML of Si, the dome clusters are found again. The density for domes and huts is in the same range again ($1.6 \cdot 10^{10} cm^{-2}$), while the ratio of domes to huts is 2 : 3. Here again no shape transformation from dome to hut clusters is found, in particular the mean diameter is lower compared to the diameter of the domes capped by 3 ML of Si. Besides the dome clusters, also the new clusters are again visible. Moreover, their density strongly increased.

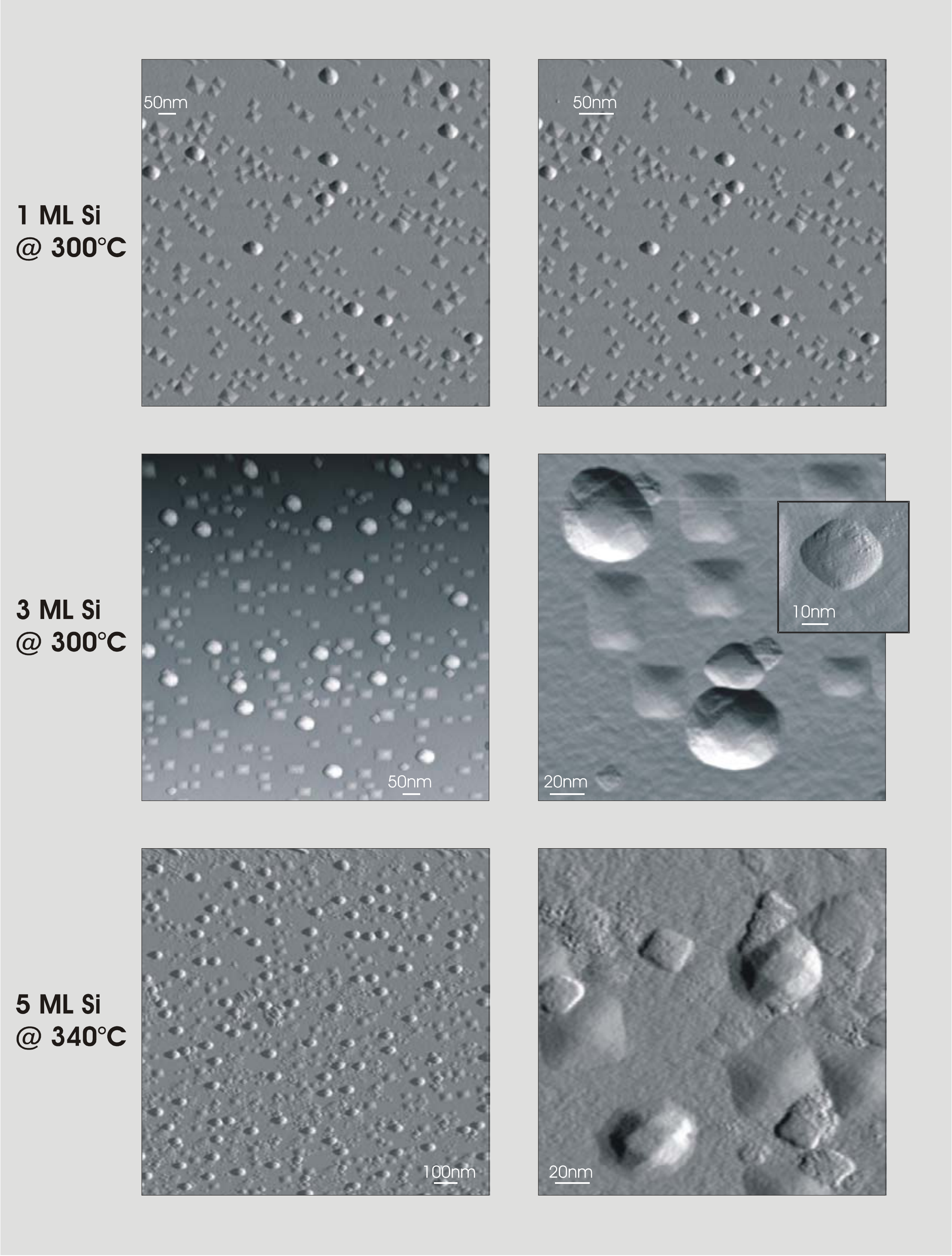
1 ML Si
@ 300°C
50nm
50nm
3 ML Si
@ 300°C
50nm
20nm
10nm
5 ML Si
@ 340°C
100nm
20nm

Fig. 6.16 STM overview of capped samples. A cap layer of 1 ML of Si at 300°C has no effect on the dome and hut clusters. 3 ML of Si lead to the formation of a new type of clusters. After 5 ML of Si at 340°C dome and hut clusters are still found. The shape transformation is prevented, but the new dots start to overgrow themselves.

The differences in size and density of the hut and dome clusters are still within the statistical variations. The mean diameter of the domes ranges between 33.4 nm and 59.2 nm (see table 6.4), while those for the huts ranges from 24.5 to 38.7 nm. Especially the diameter of dome is very sensitive to small variation of e.g. the growth temperature, as shown in chapter 4. The variations in height are not so pronounced, due to the shallow facets of the clusters. The density of hut and dome clusters is within the same range for all samples.

		1 ML Si @ 300°C	*3 ML Si @ 300°C*	*5 ML Si @ 340°C*
diameter [nm]	***domes***	33.4	59.2	39.5
	huts	24.5	35.6	38.7
	new		22.8	< 22.8
height [nm]	***domes***	7.0	11.5	7.0
	huts	3.1	3.7	3.9
	new		3.9	< 3.9

Tab. 6.4 Mean height and diameter of low temperatures-capped-samples

Here by lowering the overgrowth temperature, the shape transition from dome to hut clusters is prevented. Obviously the interdiffusion was suppressed. For this reason, another strong indication for the thermal activation of interdiffusion is found.

For the new clusters, which were found for the samples capped by 3 and 5 ML of Si, the height and diameter can only be determined for the sample capped by 3 ML of Si, as the new dots overlap for the sample covered by 5 ML of Si. Nevertheless, after capping with 5 ML (Fig. 6.16) it can be seen, that the new clusters are of the same size or even smaller than those of the sample covered by 3 ML of Si. In contrast to the sample capped by 3 ML, whole patches of new clusters are detected. These clusters are stacked so that their density is not to be quantified, but it is higher than for the sample capped by 3 ML of Si.

In scenario one it was assumed, that the Si should grow in layers between the dots, if no interdiffusion happens. Here we find that new clusters grow due to the capping. On the one hand side this is again an indication that the capping Si is deposited between the Ge dots and that the alloying of the Ge dots with the capping Si is suppressed. On the other hand the origin of the new clusters is not clear. As interdiffusion seems to be suppressed, the dots must consist up to a high fraction of the deposited Si. The dots start to grow where a nucleation point is given. In most of the cases they are found to

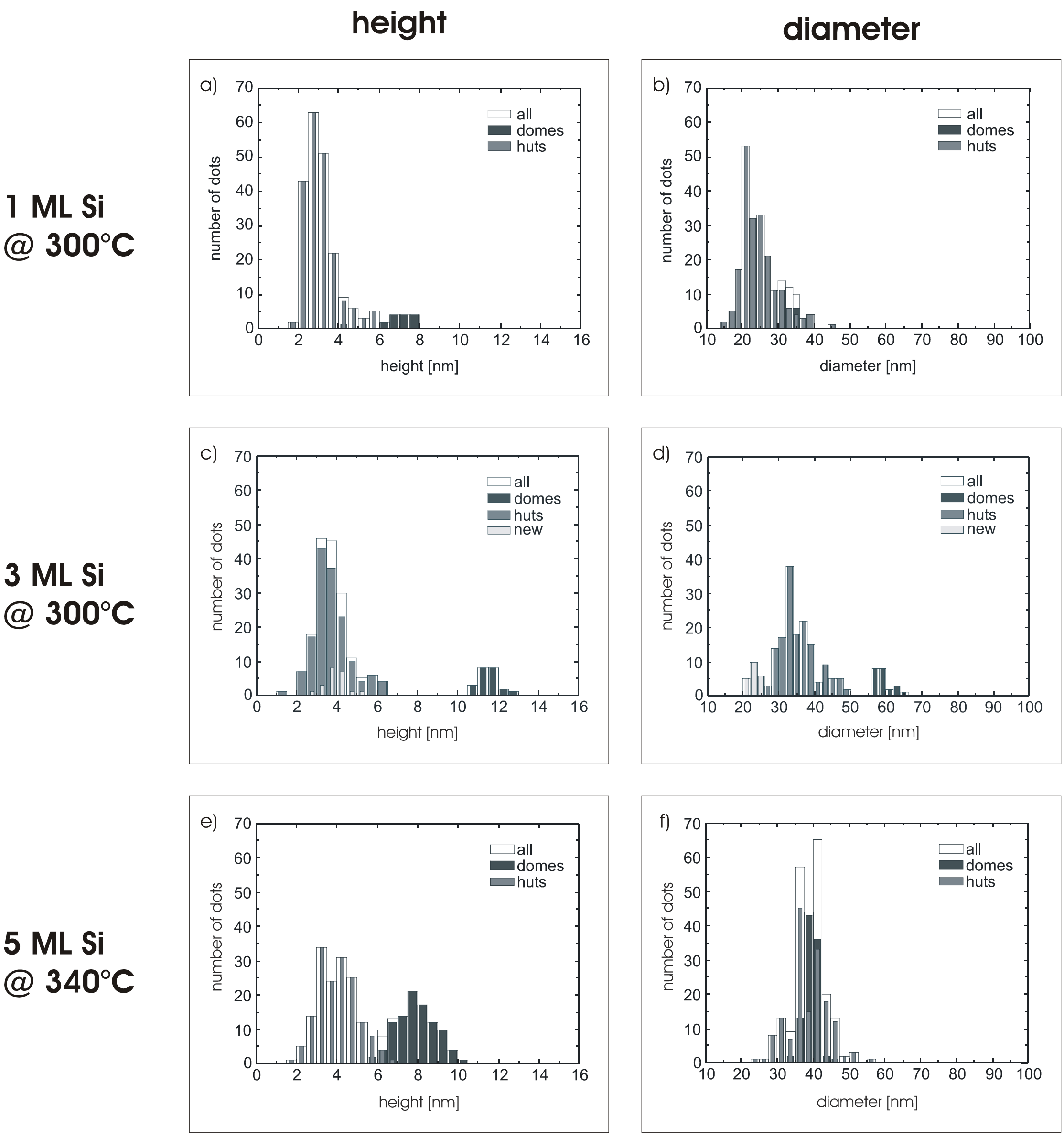

Fig. 6.17 Height and diameter-distributions of low temperature overgrown Ge dots. The strong dependence on small fluctuations during the growth of the samples is to be seen in the differences of the height and diameter distributions. Domes were found for all the samples, indicating the prevention of a shape transformation. It was still possible to create a height and diameter-distribution for the new clusters for the sample with a 3 ML thick Si cap. The high density and the fact, that the new clusters tend to overgrow themselves made this impossible for the sample overgrown by 5 ML of Si. The changes of mean diameter and height are given in table 6.4.

be near huts and domes. In addition, contaminations, e.g. carbon deposited during the growth interruption (necessary to lower the temperature for the overgrowth), might be nucleation sites for those new clusters that are not close to a hut or dome. We know from the x-ray simulations, that due to a compensation effect at the edges of the corner, the lattice constant of the wetting layer is smaller than that of pure silicon. If carbon is incorporated, the smaller lattice constant would lead to compressive strain in the wetting layer. In both cases, the lattice below the new huts would be smaller than that of the deposited pure silicon. The SiGe wetting layer has a larger lattice constant than pure Si. All that could lead to a similar formation process, as for Ge dots on carbon-modified surfaces. One can also speculate that the new clusters start to grow on those places, where formerly Ge dots existed. Coalescence of Ge dots grown at elevated temperature is a frequently obtained feature [106]. At places where formerly dots existed, the composition and the strain might be still different. Therefore they may also act as nucleation sites.

Finally it was found, that no shape transformation is observed for low temperature overgrown dome clusters indicating a pronounced reduction of the intermixing of the dot with Si. Whether the Si of the cap layer stays on top of the Ge islands, forming a Si film under tensile strain (scenario 2 in Fig. 6.1) or whether the Si diffuses to the base of the dot and is incorporated on top of the wetting layer (scenario 1 in Fig. 6.1) cannot be conclusively answered by the STM images.

6.3.2 Photoluminescence results

The aim of the reduction of the overgrowth temperature is to prevent the intermixing and the shape transformation during the overgrowth. Hence we studied the influence of growth temperature during capping on the optical properties of the dots. In order to observe intense PL signals, ten dots layers were stacked on top of each other. Subsequent to growth we investigated the composition and size by photoluminescence. The growth conditions were similar to those of the STM samples, to make the results comparable. Thus the same growth rates and temperatures were chosen. The amount of deposited Ge was again 6.5 ML to have the same initial

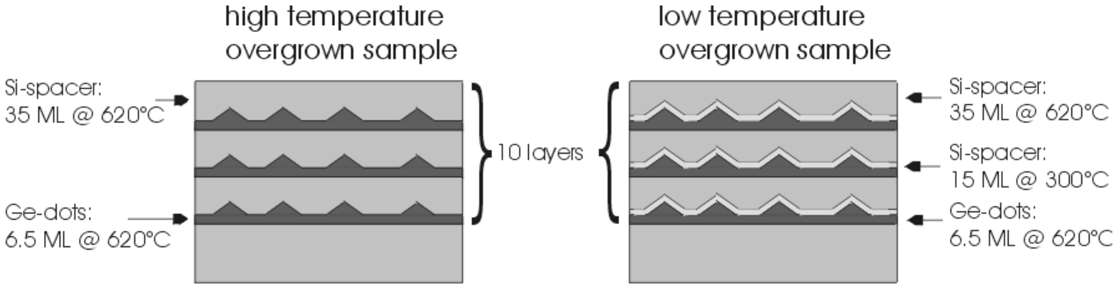

Fig. 6.18 Photoluminescence samples: Both samples have ten layers of Ge dots separated by 50 ML of Si. For the low temperature overgrown sample, the growth temperature was lowered to 300°C for the first 15 ML of the spacer, while the total thickness remained 50 ML.

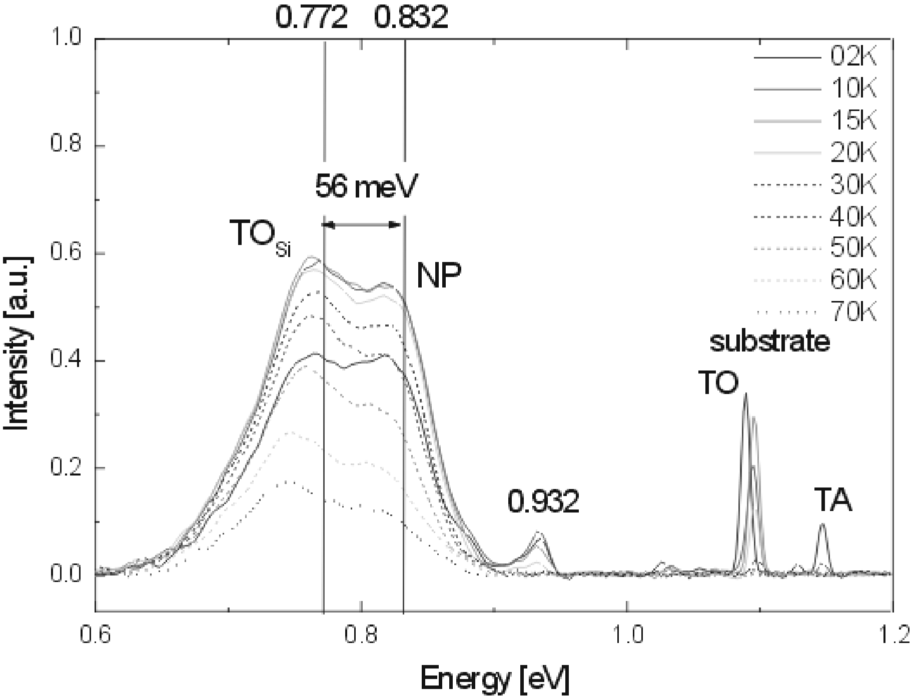

Fig. 6.19 Photoluminescence spectra of the high temperature overgrown sample. Besides the peaks that originate from the substrate, the island related no-phonon and To$_{Si\text{-}Si}$ phonon peaks are found. The peak at 0.932 eV might be related to the wetting layer. The peak position was determined by fitting the 2K spectrum.

formation of Ge dots before overgrowth. The samples consist of a stack of ten layers of Ge dots separated by Si spacers with a total thickness of 50 ML, shown in Fig. 6.18.

As a reference sample for high temperature overgrown dots, the Si-spacer-layers were grown at 620°C, at the same temperature as for the high temperature overgrown STM-samples of paragraph 6.2.1. For the second sample, the overgrowth temperature was decreased down to 300°C for the first 15 ML to establish low temperature overgrowth and afterwards increased to 620°C again, to obtain a smooth surface for the next layer of Ge dots.

Fig. 6.19 shows the photoluminescence spectra for the high temperature overgrown sample. Two peaks are at 1.15 eV and 1.11 eV found. They are 20 meV resp. 60 meV below the excitonic band-gap of Si with 1.17 eV. These values are close to those of the TA and TO phonons of Si with 18.4 and 58.0 meV. For this reason, these peaks are assigned to the phonon-assisted indirect recombination of the Si substrate. At the position of the excitonic-band-gap of Si no peak is found, as this is a forbidden recombination for an ideal crystal and therefore the probability for a no-phonon (NP)

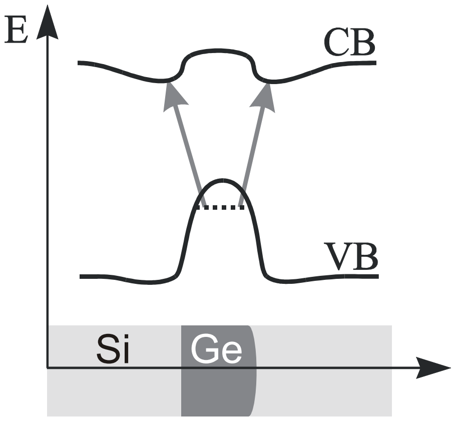

Fig. 6.20 Schematic band structure of a Ge dot embedded in a Si matrix. The dot forms a quantum well in the valence band, while it has only a slight influence on the conduction band. The Si that surrounds the dot is strained and therefore forms a quantum well for the electrons in the conduction band. Recombination between trapped holes of the dot and electrons of the strained Si are possible.

assisted recombination is always very small. Besides this, we have two broad peaks at 832 meV and 772 meV. These peaks belong to the islands. The first one is related to the NP assisted recombination of a hole confined in the Ge dot and an electron localised in the strained Si adjacent to the dot.

The band gap in real space is sketched in Fig. 6.20. Due to the broadening of the confined states in momentum space and broadening of the wave functions in real space, a phonon less recombination is possible. The occurrence of this peak is an indication for the existence of low dimensional confinement in these dots. The second

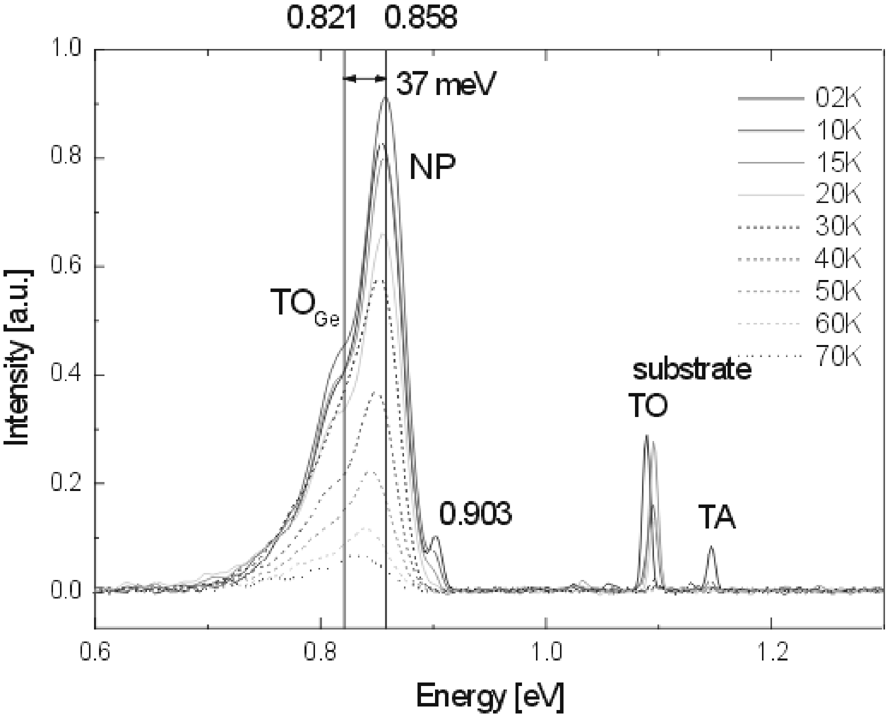

Fig. 6.21 Photoluminescence spectra of the low temperature overgrown sample. The island related peaks shifted to higher energy. Also the phonon of the island now belongs to a Ge-Ge oscillation. The peak position was determined by fitting the 2K spectrum.

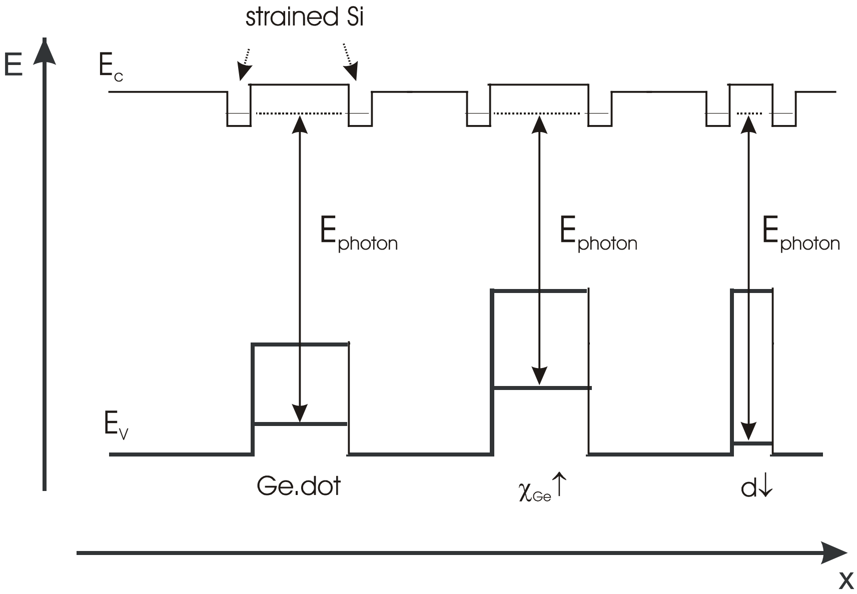

Fig. 6.22 When the Ge-content χ_{Ge} of a dot increases (center-picture), the well becomes deeper and the energy level shifts to higher energies. As a consequence, the photon-energy decreases. This can be compensated, when the dot shrinks in size (right picture). Then the energy level shift to lower energy and the photon energy increases again.

peak is at an energy 56 meV below the NP peak. The difference in energy correspondences with the energy of a Si-phonon. As the peaks are very broad and not well separated, TO-phonons like Si-Ge and Ge-Ge may occur as well, but with less intensity. All of the three types of phonons are possible for the indirect recombination, as the recombining electron is in the surrounding Si and the hole in the intermixed Ge dot.

Another very small peak is found at 932 meV and cannot be attributed absolutely sure to a recombination process, but there is a certain probability, that this peak is related to the wetting layer.

In Fig. 6.21 the results for the low temperature overgrown sample are shown. Here again, one can find the TO- and TA-phonon of the Si substrate at 1.1 and 1.14 eV. The peak for the Ge islands has shifted to a higher value of 858 meV. The reduced width of the peaks indicates a smaller size distribution of the clusters, as it might be the case, when the shape transformation is prevent. In addition the second peak is now found at 821 meV, just 37 meV below the NP-peak. Thus the phonon-assisted recombination is now done with a TO phonon of an oscillation between Ge atoms and the Si-Si and Si-Ge phonon assisted recombination is less strong. This Ge-TO phonon assisted recombination is normally only present in samples with a high Ge content.

Therefore we have an indication for the reduced intermixing during overgrowth, as expected by the lowering of the overgrowth temperature. On the other hand, a higher Ge content would mean, that the quantum well of the Ge in the surrounding Si-matrix should become deeper, as shown in Fig. 6.22. If the quantum well is deeper, the energy level responsible for the recombination should shift to higher energies and the observed photon energy should be smaller, than in a recombination process with lower Ge content. But here we observe the opposite. While for the high-temperature-overgrown sample the NP-peak is at 832 meV, the NP-peak of the low-temperature overgrown is at 858 meV. One possible explanation might be given again by the shape transformation together with the intermixing, that we have at the high temperature overgrown STM-samples.

As the intermixing and the shape transformation are prevented, the low temperature overgrown dot is smaller than the high temperature overgrown dot. The energy level responsible for recombination processes shifts to lower energies for smaller dots with the same Ge content, as schematically presented in Fig. 6.22. In our case, we have two diametrical processes. The higher Ge content of the low temperature overgrown sample would reduce the photon energy; on the other hand, the smaller size would increase it. This could explain why the NP-peak shifted to a higher energy, even though it has a higher Ge concentration. Here again, we can find a hint for a prevented

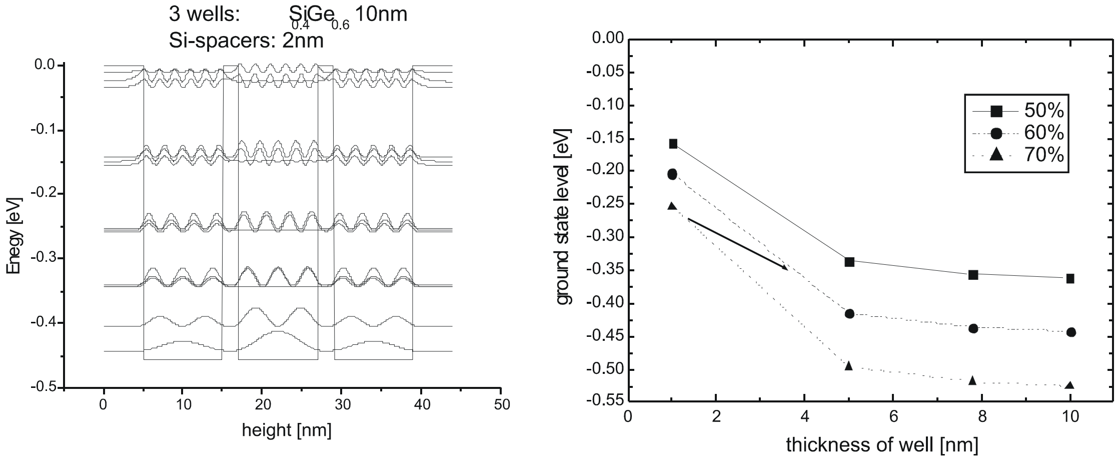

Fig. 6.23 Calculated energy levels of three couple quantum wells on the left side. On the right side there is the ground state level shown in dependence of the thickness and the Ge concentration. As indicated by the arrow, a lower Ge concentration together with an increase in thickness can lead to a deeper ground level state.

shape transformation and reduced intermixing during the overgrowth at low temperatures.

To proof the explanation, we calculated the energy states for three coupled quantum wells. Quantum wells were used, as due to the large diameter of the dome and hut clusters, a good confinement of the clusters is only given in height, which is similar to a quantum well. The energy levels were calculated for different compositions and thicknesses of the quantum wells. A comparison of the ground state level is given in Fig. 6.23. Here the energy levels are given with respect to the valence band. A lower energy in Fig. 6.23 would lead to a lower PL energy. For two samples with different Ge content (thin wells), the energy level of a sample with lower Ge content can have a

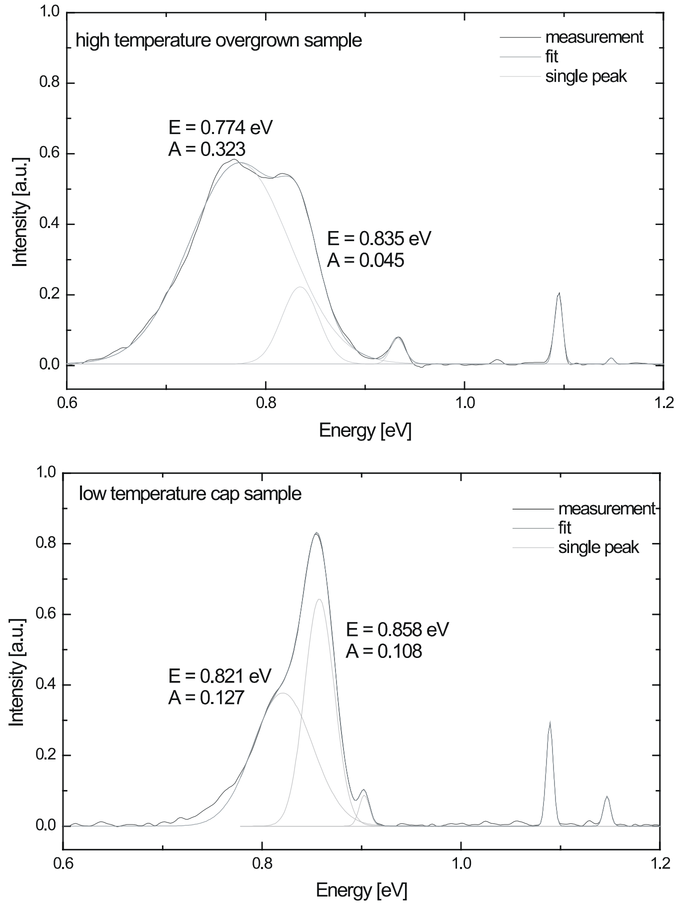

Fig. 6.24 Fits for the photoluminescence spectra measured at 2K. For the high temperature overgrown dots the ratio of the peak areas and therefore the intensity for no-phonon-assisted and indirect recombination is 0.14, indicating the bad confinement of the carriers within the dots. Even though, the double peak looks quite symmetric, the left peak is higher as the right one and therefore the fit parameters are not exchangeable. For the low temperature overgrown dot the ratio is already 0.85 showing the better confinement within the dots.

lower ground state level, when the well is of thicker size. This is equivalent to the scenario discussed above for the dot.

For the low temperature overgrown sample, the peak that could not clearly be attributed to the wetting layer, shifted to a lower energy (903 meV). If this peak belongs to the wetting layer, this is another indication for a lower intermixing due to the higher Ge content.

As the intensity of the no-phonon-assisted and indirect (NP and TO) recombination is an extend to get a qualitative information about the confinement and therefore again about the size of the dots, we have exemplarily fitted the curves of the PL measurements at 2K, to get the ratio of no-phonon-assisted to phonon-assisted recombination. The fits are shown in Fig. 6.24. For the sample that was overgrown at high temperature, the double peak looks quite symmetrically so one could expect, that the parameter of the fit are exchangeable for the two peaks. But as the left peak is slightly higher than the right one, this is not the case. The ratio of peak areas, which is the same as the ratio of the intensities, for the NP-assisted and indirect (TO-phonon) recombination, is just 0.14 for this sample. Thus, most of the recombination processes are phonon-assisted, indicating the inferior confinement of carriers within the dot.

For the low temperature overgrown sample, this ratio is 0.85. Here most of the carriers recombine without phonon assistance, indication an improved localisation of the involved carriers. Taking the confinement as criteria for the size of the dot, these results show again, that due to the low overgrowth temperature, the dot size is smaller and the Ge concentration is higher inside the dot compared to the reference sample.

6.3.3 Summary

In paragraph 6.2 we saw that already after the initial steps of overgrowth a shape transformation from dome to hut cluster occurs. This can be prevented, when the overgrowth temperature for the Si spacer is lowered to 300°C, as then still dome clusters can be found. In addition, a new type of clusters starts to grow after 3 ML of Si, looking like a rotated hut cluster with steeper facets. Its origin is still not clear. That the lowering of the overgrowth temperature prevents the shape transformation when the dots are embedded in a Si matrix, can be derivated from the photoluminescence measurements. A clear increase of no-phonon-assisted recombination is seen, reflecting a stronger localisation of the holes and electrons.

7 Summary

The embedding of Ge dots in a Si matrix is a promising way for the implementation of opto-electronic structures in silicon, as the confinement of carriers in dots increases the probability for a no-phonon assisted recombination. The crucial factors for the realization of such a device are the density, the dimensions, and the composition of the dots. Here, we studied the modification of a silicon surface and its influence on the size and density of the dots. The modifications were done by carbon, as previous results showed, that the pre-deposition of submonolayers of carbon leads to c(4x4) reconstructed areas on silicon and that Ge tends to grow on areas without this reconstruction. This changes the growth mode of Ge from Stranski-Krastanov mode to a Volmer-Weber mode, that allows achieving smaller Ge dots even at high growth temperatures [15, 38]. As Ge grows on c(4x4) free areas, the size of the Ge dots and their density is determined by the carbon influenced areas. Consequently, the amount of deposited carbon is a crucial factor to control the shape and density of dots. Up to now, the modification of the Si surface was studied for an amount of up to 0.11 ML of carbon. In the present study the carbon pre-deposition was increased up to 0.3 Ml. Our investigations showed, that already after an increase of up to 0.2 ML of carbon, most of the surface is c(4x4) reconstructed.

Kaxiras and Remediakis took different models into account. One builds a sub-surface β-SiC cluster with 5 carbon atoms is the most promising candidate for explaining the results after a low amount of deposited carbon. This model is able to simulate the observed STM pictures and the configuration is stable, too. But when the amount of carbon is increased to more than 0.11 ML of carbon, the model comes to its limits. It cannot explain, that after the deposition of 0.2 ML of carbon nearly the whole surface is covered by the c(4x4) reconstruction. In addition, some small areas with a p(4x2) reconstruction are observed now. They often occur at domain boundaries of the c(4x4) islands. It is possible, that the configuration suggested by Remediakis has become instable and another configuration including only up to two carbon atoms per unit cell, as it was e.g. suggest by Kelires for high amounts of carbon, must have become energetically more favourable. One possible reason for the reconfiguration can be the strain, as Remediakis configuration for low amounts of carbon is not containing missing dimers and therefore no strain can be released. Finally, the c(4x4) reconstruction becomes instable and after the deposition of 0.3 ML of carbon, only the new p(4x2) reconstruction is found.

When Ge dots are grown on such carbon modified surface, the achieved size of the dots is smaller and the density of clusters is higher compared to Ge dots, grown on pure silicon. Photoluminescence spectra show, that the luminescence intensity of carbon induced Ge dots is by an order of magnitude higher than those of dots on pure Si. One reason (besides the size of the dot) is the confinement of electrons in the carbon rich areas. These areas form a quantum well in the conduction band and lead to a better confinement of the electrons. On the other hand, the separation in real space reduces the overlap of the wave-functions of the electrons and the holes. Therefore it was found, that when enough Ge is deposited and the dots start to overgrow also the carbon rich areas, the photoluminescence intensity becomes highest, as a competing process between size of dots and the separation of carriers in real space exist.

The crucial factor, the composition of the Ge-dots deposited on pure Si surfaces was investigated by STM, TEM, x-ray diffractometry, and PL before and after the overgrowth. It was found, that the overgrowth at high temperatures (here higher than 600°C), leads to pronounced intermixing of the Ge hut clusters with Si. As a consequence they increase in volume. For the dome clusters, a shape transition from a dome back to a hut cluster was found after capping with more than 3 ML of Si. Our TEM and x-ray investigations showed, that the capping Si intermixes with the Ge-dot. This intermixing is thermally activated and is able to explain the observed shape transformation from dome to hut clusters due to intermixing.

To prevent the alloying during the overgrowth, the growth temperature was lowered down to 300°C for the capping Si. This indeed prevents the transformation from dome to huts and supported our assumption of the thermal activated intermixing. In addition a new type of cluster was found, which has of pyramidal shape and a round top. Its base is rotated by 45° compared to a normal hut. As this hut appeared after the deposition of Si, the question is how they are composed. This is not clear yet and has to be studied in the future. One possible explanation for their formation is, that they consist of Si and formed due to strain induced by the wetting layer. As these new dots are very often besides a Ge dot, the strain of their corners can also have acted as a nucleation site for the new dots.

To determine, if the lowering of the overgrowth temperature prevents the shape transformation completely, we also embedded Ge dots in a Si-matrix by growing stacks of dots. The photoluminescence data give reason to believe, that the intermixing is lowered enough to prevent a shape transformation.

In the end, it was found, that the predeposition of carbon increases the radiative recombination probability, and the capping of Ge dots at low temperatures is reasonable to keep a high Ge-content within the dots. The origin of the new dots, that formed during the initial steps of overgrowth at low temperature, is not clear yet and has to be studied in the future.

Our investigations showed, that the formation of small dots to obtain no-phonon assisted recombination is possible. Also the question if they could be integrated in possible devices by embedding while keeping the necessary high Ge content was proved and found to be possible.

References

[1] R. Kuntz, J. Dziesiaty, *Physica Status Solidi A* **124**, 149 (1991)

[2] H. Kakinuma, M. Mohri, M. Sakamoto, H. Sawai, *Phys. Rev. B* **43**, 4871 (1991)

[3] R. Singh, R.S. Srivastava, *Solid-State Electronics* **25**, 227 (1982)

[4] A. Gold, *Phys. Rev. Lett.* **54**, 1079 (1985)

[5] L. Han-Sheng, *J. App. Phys.* **53**, 4250 (1982)

[6] J. Faist, F.Capasso, D.L. Sivco, C. Sirtori, A.L. Hutchinson, A.Y. Cho, *Science* **264**, 553 (1994)

[7] G. Dehlinger, L. Dieh, U.Gennser, H. Sigg, J. Faist, K. Ensslin, D. Grützmacher, E. Müller, *Science* **290**, 2277 (2000)

[8] M. Diani, D. Aubel, J.L. Bischoff, L. Kubler, D. Bolmont, *Surface Science* **291**, 110 (1993)

[9] C. Kohler, *Journal of Physics* **15**, 133 (2003)

[10] O.Leifeld, E. Müller, D. Grützmacher, B. Müller, K. Kern, *Phys. Rev. B* **66**, 125312 (2002)

[11] E. Bauer, *Zeitschrift für Kristallographie* **110**, 372 (1958)

[12] R.J. Asaro, W.A. Tiller, *Metall. Trans.* **3**, 1789 (1972)

[13] M.A. Grinfeld, Sov. Phys.-Dokl. **31**, 831 (1989)

[14] H. Neddermeyer, *Rep. Prog. in Phys.* **59**, 701 (1996)

[15] E. A. Wood, *J. Appl. Phys.* **35**, 1306 (1964)

[16] S. J. Jenkins and G. P. Srivastava, *Journal of Physics: Condensed Matter* **8**, 6641 (1996)

[17] O. L. Alerhand and E. J. Mele, *Phys. Rev. B* **35**, 5533 (1987)

[18] R. J. Hamers, R. M. Tromp, and J. E. Demuth, *Phys. Rev. B* **34**, 5343 (1986)

[19] D. J. Chadi, *Phys. Rev. Lett.* **59**, 1691 (1987)

[20] C. J. Chen, Introduction to Scanning Tunneling Microscopy (Oxford University Press, 1993).

[21] Oliver Leifeld, Ge Quantum Dot Formation on the C-alloyed Si(001) Surface – a Scanning Tunneling Microscopy Study, (1999).

[22] Y. W. Mo, R. Kariotis, B. S. Swartzentruber, M. B. Webb, and M. G. Lagally, J. *Vac. Sci. Technol. A* **8**, 201 (1990)

[23] B. S. Swartzentruber, Phys. *Rev. B* **55**, 1322 (1997)

[24] X. Chen, F. Wu, Z. Zhang, and M. G. Lagally, *Phys. Rev. Lett.* **73**, 850 (1994)

[25] B. Voigtländer and M. Kästner, *Phys. Rev. B* **60**, 5121 (1999)

[26] R. Tromp, *Phys. Rev. B* **47**, 7125 (1993)

[27] F. Wu, X. Chen, Z. Zhang, and M. G. Lagally, *Phys. Rev. Lett.* **74**, 574 (1995)

[28] H. Hammar, F. LeGoues, J. Tersof, M. Reuter, and R. Tromp, *Surf. Sci.* **349**, 129 (1996)

[29] J. Tersof and R. M. Tromp, *Phys. Rev. Lett.* **70**, 2782 (1993)

[30] K. C. Pandey, in Proceedings of the International Conference on the Physics of Semiconductors, edited by J. D. Chadi and W. A. Harrison, p. 55, New York, 1985, Springer-Verlag

[31] M. Copel, M. C. Reuter, M. Horn von Hoegen, and R. M. Tromp, *Phys. Rev. B* **42**, 11682 (1990)

[32] K. Nakajima, A. Konishi, and K. Kimura, *Phys. Rev. Lett.* **83**, 1802 (1999)

[33] H. J. Kim and Y. H. Xie, *Appl. Phys. Lett.* **79**, 263 (2001)

[34] F. Liu and M. Lagally, *Phys. Rev. Lett.* **76**, 3156 (1996)

[35] M. Tomitori, K. Wanatabe, M. Kobayashi, and O. Nishikawa, *Appl. Surf. Sci.* **76**, 322 (1994)

[36] I. Goldfarb et al., *J. Vac. Sci. Technol. A* **16**, 1938 (1998)

[37] M. Zinke-Allmang, L.C. Feldman, M. Grabow, *Phys. Rev. B* **39**, 7848 (1989)

[38] F.M. Ross, R.M. Tromp, M.C. Reuter, *Science* **286**, 1931 (1999)

[39] G. Medeiros-Ribeiro, A. M. Bratkovsky, T.I. Kamins, D.A.A. Ohlberg, R.S. Williams, *Science* **279**, 353 (1998)

[40] Y.W. Mo, D.E. Savage, B.S. Swartzentruber, M.G. Lagally, *Phys.Rev.Lett.* **65**, 1020 (1990)

[41] Z. Atzomon et al, *Appl. Phys. Lett.* **65**, 2559 (1994)

[42] L.D. Lanzerotti, A.S. Amour, C.W. Liu, J.C. Sturm, *Int. Electron Devices Mett. Tech. Dig.*, 930 (1994)

[43] K. Rim, S. Takagi, J.J. Welser, J.L. Hoyt, J.F.Gibbons, Mater. Res. Soc. Symp. Proc. 397 (1995)

[44] M. Todd, P. Matsunaga, J. Kouvetakis, D. Chandrasekhar, D.J. Smith, *App. Phys. Lett.* **67**, 1247 (1995)

[45] A. Rastelli, H. Von Känel, B.J. Spencer, J. Tersoff, *Phys. Rev. B* **68**, 115301 (2003)

[46] M. W. Dashiell, U. Denker, C. Müller, G. Costantini, C. Manzano, K. Kern, and O. G. Schmidt, *Appl. Phys. Lett.* **80**, 1279 (2002)

[47] T. I. Kamins, E.C. Carr, R. S.Williams, and S. J. Rosner, *J. Appl. Phys.* **81**, 211 (1997); T. I. Kamins, G. Medeiros-Ribeiro, D. A. A. Ohlberg, and R. S.Williams, *Appl. Phys. A* **67**, 727 (1998).

[48] X. Z. Liao, J. Zou, D. J. H. Cockayne, J. Qin, Z.M. Jiang, X.Wang, and R. Leon, *Phys. Rev. B* **60**, 15605 (1999).

[49] G. Capellini, M. De Seta, and F. Evangelisti, *Appl. Phys. Lett.* **78**, 303 (2001).

[50] A.V. Kolobov, K. Morita, K.M. Itoh, and E. E. Haller, *Appl. Phys. Lett.* **81**, 3855 (2002)

[51] A. V. Kolobov, H. Oyanagi, K. Brunner, P. Schittenhelm, G. Abstreiter, and K. Tanaka, *Appl. Phys. Lett.* **78**, 451 (2001)

[52] J. Stangl, A. Daniel, V. Holy, T. Roch, G. Bauer, I. Kegel, T. H. Metzger, T.Wiebach, O.G. Schmidt, and K. Eberl, *Appl. Phys. Lett.* **79**, 1474 (2001)

[53] A. Hesse, J. Stangl, V. Holy, T. Roch, G. Bauer, O.G. Schmidt, U. Denker, and B. Struth, *Phys. Rev. B* **66**, 085321 (2002)

[54] S. A. Chaparro, J. Drucker, Y. Zhang, D. Chandrasekhar, M. R. McCartney, and D. J. Smith, *Phys. Rev. Lett.* **83**, 1199 (1999)

[55] Y. Zhang, M. Floyd, J. Drucker, and G. L. Kellogg, *J. Appl. Phys.* **90**, 4748 (2001)

[56] U. Denker, O.G. Schmidt, N.Y. Jin-Philipp, and K. Eberl, *Appl. Phys. Lett.* **78**, 3723 (2001)

[57] U. Denker, M. Stoffel, and O.G. Schmidt, *Phys. Rev. Lett.* **90**, 196102-1 (2003)

[58] O.G. Schmidt, U. Denker, S. Christiansen, and F. Ernst, *Appl. Phys. Lett.* **81**, 2614 (2002)

[59] Z. M. Jiang, H. J. Zhu, F. Lu, J. Qin, D. M. Huang, X. Wang, C.W. Hu, Y. F. Chen, Z. Q. Zhu, and T. Yao, *Thin Solid Films* **321**, 60 (1998)

[60] J. A. Floro, E. Chason, L. B. Freund, R. D. Twesten, R. Q. Hwang, and G. A. Lucadamo, *Phys. Rev. B* **59**, 1990 (1999)

[61] T. I. Kamins, G. Medeiros-Ribeiro, D. A. A. Ohlberg, and R. S. Williams, *Appl. Phys. A: Mater. Sci. Process.* **67**A, 727 (1998)

[62] B. Voigtländer and M. Kästner, *Phys. Rev. B* **60**, R5121 (1999)

[63] O.G. Schmidt, C. Lange, and K. Eberl, *Appl. Phys. Lett.* **75**, 1905 (1999)

[64] N. Liu, J. Tersoff, O. Baklenov, A. L. Holmes, Jr., and C. K. Shih, *Phys. Rev. Lett.* **84**, 334 (2000)

[65] A. Rastelli, M. Kummer, and H. von Känel, *Phys. Rev. Lett.* **87**, 256101 (2001)

[66] P. Sutter, and M.G. Lagally, *Phys. Rev. Lett.* **81**, 3471 (1998)

[67] O.G. Schmidt, U. Denker, K. Eberl, O. Kienzle, and F. Ernst, *Appl. Phys. Lett.* **77**, 2509 (2000)

[68] F. Boscherini, G. Capellini, L. Di Gaspare, F. Rosei, N. Motta, and S. Mobilio, *Appl. Phys. Lett.* **76**, 682 (2000)

[69] R. M. Tromp, Phys. Rev. B 47, 7125 (1993); A. J. Hoeven, J. Arts, and P. K. Larsen, *J. Vac. Sci. Technol. A* **7**, 5(1989)

[70] S. J. Jenkins and G. P. Srivasta, *Phys. Rev. B* **57**, 8794 (1998)

[71] P. C. Kelires and J. Tersoff, *Phys. Rev. Lett.* **63**, 1164 (1989)

[72] C. Schelling, G. Springholz, and F. Schäffler, *Phys. Rev. Lett.* **83**, 995 (1999)

[73] G. Binnig, H. Rohrer, C. Gerber, and E. Weibel, Appl. Phys. Lett. 40, 178 (1982)

[74] C. J. Chen, Introduction to Scanning Tunneling Microscopy (Oxford University Press, 1993)

[75] J. Tersoff, D.R. Hamann, Phys. Rev. Lett **50**, 1998 (1983)

[76] M. Schmidbauer, Th. Wiebach, H. Raidt, M. Hanke, R. Köhler, and H. Wawra, *Phys. Rev. B* **58**, 10523 (1998)

[77] Th. Wiebach, M. Schmidbauer, M. Hanke, H. Raidt, R. Köhler, and H. Wawra, *Phys. Rev. B* **61**, 5571 (2000)

[78] I. Kegel, T.H. Metzger, P. Fratzl, J. Peisl, A. Lorke, J.M. Garcia, and P.M. Petroff, *Europhys. Lett.* **45**, 222 (1999)

[79] D. Shindo, K. Hiraga, High-Resolution Electron Microscopy for Materials Science, Springer Verlag Tokyo (1998)

[80] A. Goeldel, U.S. Schubert, C.D. Eisenbach, *J. Microscopy* **186**, 67 (1997)

[81] O.Leifeld, E. Müller, D. Grützmacher, B. Müller, K. Kern, *Phys. Rev. B* **66**, 125312 (2002)

[82] Cardona, G. Harbeke, O. Madelung, U. Rossler, in Landolt-Bornstein: Numerical Data and Functional Relationships in Science and Technology, edited by O. Madelung (Springer Verlag, New York, 1982) vol.III/17a

[83] J.R. Chelikowsky, M.L. Cohen, *Phys. Rev. B* **10**, 5095 (1974)

[84] Handbook on SemiconductorsVolume 1, edited by W. Paul (North-Holland, Amsterdam, 1982), p. 229f.

[85] W. Weber, *Phys. Rev. B* **15**, 4789 (1977)

[86] R. Braunstein, A.R. Moore, and F. Herman, *Phys. Rev.* **109,** 695 (1958)

[87] J. Weber, M.I. Alonso, *Phys. Rev. B* **40**, 5683 (1989)

[88] Properties of Silicon Germanium and SiGe:Carbon, edited by E. Kasper and K. Lyutovich (INSPEC, London, 2000) p. 128

[89] P.J. Dean, J.R. Haynes, and W.F. Flood, *Phys. Rev.* **161**, 711 (1967)

[90] G. Davies, Physics Reports (Review Section of Physics Letters) 176 (1989) 83-188, p. 94

[91] P.C. Kelires, *Int. J. Mod. Phys. C* **9**, 357 (1998)

[92] O. Leifeld, D.Grützmacher, B. Müller, K. Kern, E. Kaxiras, P.C. Kelires, *Phys. Rev. Lett.* **82**, 972 (1999)

[93] J. Tersoff, F.K. LeGoues, *Phys. Rev. Lett.* **72**, 3570 (1994)

[94] Ph. Sonnet, L. Stauffer, A. Selloni, A. De Vita, R. Car, L. Simon, M. Stoffel, and L. Kubler, *Phys. Rev. B* **62**(11), 6881 (2000)

[95] S. J. Jenkins and G. P. Srivastava, *Journal of Physics: Condensed Matter* **8**, 6641 (1996).

[96] M.L. Shek, *Surf. Sci.* **353**, 414 (1998)

[97] M. Stoffel, L. Simon, D. Aubel, J.L. Bischoff, L. Kubler, **Surf. Sci.** *201*, 454 (2000)

[98] I.N. Remediakis, C. Guedj, P.C. Kelires, D. Grützmacher, E. Kaxiras, Surf. Science 2004 (in press)

[99] Y.W. Mo, J. Kleiner, M.B. Webb, and M.G. Lagally, *Phys. Rev. Lett.* **66**, 1998 (1991)

[100] O. Leifeld, E. Müller, and D. Grützmacher, B. Müller, and K. Kern, *App. Phys. Lett.* **74**, 994 (1999)

[101] Z. Gai, X. Li, R.G. Zhao, W.S. Yang, *Phys. Rev. B* **57**, R15060 (1998)

[102] S.K. Sinha, E.B. Sirota, S. Garoff, H.B. Stanley, *Phys. Rev. B* **38**, 2297 (1988)

[103] O. Leifeld, B. Müller, D.A. Grützmacher, K. Kern-K, *Appl. Phy. A* **66**, 993 (1998)

[104] M.A. Makeev, W. Yu, and A. Madhukar, *Phys. Rev B* **68**, 195301 (2003)

[105] D.A. Grützmacher, T.O. Sedgwick, A. Powell, M. Tejwani, S.S., Iyer, J. Cotte, F. Cardone, Appl. Phys. Lett. 63, 2531 (1993)

[106] S.M. Prokes, A.K. Rai, *Journal of VacuumScience &Technology A* **12**, 1148 (1994)

Curriculum vitae

Personal:

Name: Olaf Kirfel
Address: Lindenhof 5
5430 Wettingen
Switzerland
Date of birth: 23.10.1971, Haselünne, Germany
Nationality: German

Education:

1978 – 1982 Primary school in Streekermoor
1982 – 1984 “Orientierungsstufe” in Hatten
1984 – 1991 Grammar school in Oldenburg

1991 – 1992 military service

1992 – 1999 Study of physics at the Faculty of Physics, University of Oldenburg (Carl v. Ossietzky Universität Oldenburg)
Diploma thesis in the group for Energy- and Semiconductor-Research, Prof. Dr. J. Parisi, entitled: “Beleuchtungsabhängige Hallmessungen zur Untersuchung der Persisten Photoleitung in Gallium-Nitrid” (Illumination dependent hall measurements for the investigation of the persistent photoconductivity in GaN), grade “sehr gut”

since Sep. 99 Ph.D. thesis about the formation and overgrowth of Ge quantum dots on modified Si surfaces at the Paul-Scherrer-Institut, 5232 Villigen, Switzerland, Laboratory for Micro- and Nanotechnology, supervisor: Dr. habil. Detlev Grützmacher
University and supervising professor: Swiss Federal Institute of Technology Lausanne (École Polytechnique Fédérale de Lausanne), 1015 Lausanne, Switzerland, Department of Physics, Laboratoire de science à l'échelle nanométrique, group of Prof. Dr. Klaus Kern

Paper

- Shape and composition change of Ge dots due to Si capping
  O. Kirfel, E. Müller, D. Grützmacher, K.Kern, A.Hesse, J. Stangl, V. Holý, G. Bauer, *Appl. Surf. Science*, in print

- Influence of capping on strain, composition and shape of SiGe islands
  A. Hesse, J. Stangl, V. Holy, G. Bauer, O. Kirfel, E. Müller, D. Grützmacher, *Mat. Sci. Eng. B* **101**, 71-76 (2003)

- Structural properties of SiGe islands: Effect of capping
  J. Stangl, A. Hesse, V. Holy, G. Bauer, U. Denker, O. G. Schmidt, O. Kirfel, and D. Grützmacher, *Materials Research Society Symposium Proceedings* **749**, W21.3.1 (2003)

- Successful shape-preservation of Ge-clusters during Si-coverage at low temperature
  E. Müller, O. Kirfel, A. Rastelli, H. von Känel, D. Grützmacher, *Mat. Sci. Eng. B* **101**, 142 (2003)

- Fabrication of SiGe/Si/Cr bent cantilevers based on self-rolling of epitaxial films
  S.V. Golod, D. Grützmacher, C. David, E. Deckardt, O. Kirfel, S. Mentese, B. *Ketterer, Mircoelectronic Eng.* **67**, 595 (2003)

- Shape transformation of Ge quantum dots due to Si overgrowth
  O. Kirfel, E, Müller, D. Grützmacher, K., Kern, *Physica E* **16**, 602 (2003)

- Investigation of the early stages of Si-overgrowth of Ge-dots on Si (001)
  E. Müller, O. Kirfel, A. Rastelli, H. von Känel, D. Grützmacher, *Inst. Phys. Conf. Ser.* **169**, : 163 (2001)

- Interface effects on the persistent photoconductivity in thin GaN and AlGaN films
  O.P. Seifert, O.Kirfel, M.Munzel, M.T. Hirsch, J. Parisi, M. Kelly, O. Ambacher, H. Stutzmann, *MRS Internet Journal of Nitride Semiconductor Research* **4**: Art. No. G5.5 Suppl. 1 (1999)

- Photoquenching of persistent photoconductivity in n-type GaN
  M.T. Hirsch, O. Seifert, O. Kirfel, J. Parisi, J.A. Wolk, W. Walukiewicz,
  E.E. Haller, O. Ambacher, M. Stutzmann, *Nitride Semiconductors Symposium*,
  531 (1998)

Conference Contributions

- Talk: Ge dots on Si and modified Si surfaces
  O. Kirfel, A. Beyer, E. Müller, D. Grützmacher, K. Kern,
  NATO Advanced Researchers Workshop, 2003, Heraklion, Crete

- poster: Low temperature molecular beam epitaxy of Ge quantum dots
  O. Kirfel, A. Hesse, E. Müller, O. Stukalov and D. Grützmacher,
  ICSI3, 2003

- Talk: Shape and composition changes of Ge dots due to Si capping
  O. Kirfel, E. Müller, D. Grützmacher, K. Kern, A. Hesse, J. Stangl, V. Holý, G. Bauer, *International SiGe Technology and Device Meeting*, 2003, Nagoya, Japan

- Talk: Shape Transformation of Ge Quantum Clusters Due to Si Overgrowth
  O. Kirfel, E. Müller, D. Grützmacher, K. Kern,
  E-MRS spring conference, 2002, Strasbourg, France

- Talk: Si Overgrowth of Ge clusters on Si(001)
  O. Kirfel, E. Müller, D. Grützmacher, A. Hesse, J. Stangl, G. Bauer,
  2nd Lion Symposium on Nanostructures at Surfaces and Interfaces, 2002, Villigen, Switzerland

- Poster: Shape Transformation of Ge Quantum Islands During Si Overgrowth
  O. Kirfel, E. Müller, D. Grützmacher, K.Kern, A. Hesse, J. Stangl, G. Bauer,
  12th International Winterschool on New Developments in Solid State Physics, 2002, Mauterndorf, Austria

- Talk: ELS/SPA-RHEED: In-situ-Charakterisierung der Oberflächenmorphologie und der elektronischen Eigenschaften von SiGe-Nanostrukturen
  O. Kirfel, D. Grützmacher, B. Müller, M. Escher und M. Merkel,
  Spring Meeting of the Deutsche Physikalische Gesellschaft, 2000, Regensburg, Germany

- Poster: Hall-Effekt-Experimente zu persistenter Photoleitung in n-leitendem GaN
  O. Kirfel, M.T. Hirsch, O. Seifert, J. Parisi, O. Ambacher und M. Stutzmann,
  Spring Meeting of the Deutsche Physikalische Gesellschaft, 1998, Regensburg, Germany

Danksagung

An dieser Stelle möchte ich mich bei allen bedanken, die zum Gelingen der Arbeit beigetragen haben. Ohne die umfangreiche Unterstützung zahlreicher Personen wäre die hier vorgestellte Arbeit nicht in dieser Form möglich gewesen.

Mein besonderer Dank gilt Herrn Prof. Dr. Klaus Kern für die Übernahme der Arbeit. Neben seinem regen und steten Interesse an den gewonnenen Ergebnissen und den anschließenden Diskussionen, die zu neuen Impulsen führten, hat er auch bei verwaltungstechnischen Aspekten hilfreich eingegriffen und erst ein Gelingen der Arbeit möglich gemacht.

Weiterhin gilt mein Dank Herrn Prof. Dr. Hans von Känel und Herrn Prof. Dr. Andrea Fiore für die freundliche Übernahme des Koreferates.

Zu besonderem Dank fühle ich mich meinen Betreuer Priv. Doz. Dr. habil. Detlev Grützmacher verpflichtet. Zum einen ermöglichte er mir eine eigenständige Arbeit am Laboratorium für Mikrotechnologie (LMN), zum anderen stand er aber auch immer mit Rat und Tat zur Seite, wenn es nötig war. Seine Anregungen und die Diskussionen haben wesentlich zum Gelingen der Arbeit beigetragen. So waren seine Kenntnisse im Bereich der Probenherstellung mit der MBE aber auch auf Gebieten wie der Röntgenspektroskopie, der Photolumineszenz und der Elektronentransmissionsspektroskopie von großer Hilfe. Weiterhin danke ich ihm für die Unterstützung bei den Veröffentlichungen und insbesondere für seine Unterstützung und Motivation, wenn es mal wieder nicht so gut lief. Auch hat die Zusammenarbeit mit ihm viel Spaß gemacht, so dass er nicht unwesentlich zu der guten Arbeitsatmosphäre beigetragen hat.

Ebenfalls möchte ich mich bei Herrn Prof. Dr. Günther Bauer von der Universität Linz und seinen Mitarbeitern für die Zusammenarbeit bei der Röntgenspektroskopie bedanken. Mein besonderer Dank gilt hier Frau Dipl. Phys. Anke Hesse, die wesentlich für die Simulationen verantwortlich zeichnet und diese größtenteils am Paul Scherrer Institut durchführte, so dass eine gute Zusammenarbeit gewährleistet war.

Auch möchte ich mich bei Frau Dr. Elisabeth Müller für die umfangreiche Charakterisierung der Proben mittels Elektronentransmissionsspektroskopie bedanken. Diese habe haben den entscheidenden Hinweis auf die Durchmischung der Proben mit Silizium geliefert und sind somit unverzichtbar für die Arbeit.

Ganz herzlich möchte ich mich bei Dr. Hans Sigg bedanken, der mich bei den PL-Messungen unterstützte und in aufschlussreichen Diskussionen mein Verständnis für diese Spektroskopie verbesserte.

Bei Dr. Oliver Leifeld und Dr. Andre Beyer möchte ich mich für die Einführung in die Molekularstrahlepitaxie sowie die Reinigung der Proben danken. Dr. Oliver Leifeld hat mich insbesondere in die Rasterelektronenmikroskopie eingeführt und stand mir auch nach seinem Wechsel zu MBE-Komponenten immer wieder mit Rat und Tat zur Seite.

Mein Dank gilt auch allen Technikern des Laboratoriums für Mikrotechnologie. Besonders möchte ich mich bei Thomas Neiger bedanken, der immer zur Stelle war, wenn mal wieder Not am Mann war und auch an Wochenenden kurzfristig half, wenn die MBE oder der Reinraum Probleme verursachten. Stefan Stutz danke ich für die tatkräftige Unterstützung bei den PL-Messungen, während Fredy Glaus und Dieter Bächle für die unterschiedlichsten Hilfestellungen und die Einführungen in den Reinraum gedankt sei.

Der gesamten Abteilung des LMN danke ich für die angenehme Arbeitsatmosphäre. Dr. Jens Gobrecht danke ich für die Aufnahme ins LMN und Edith Meisel für die Unterstützung bei organisatorischen Angelegenheiten. Allen Mitdoktoranden und Postdocs im LMN danke ich ganz besonders für das angenehme Arbeitsklima, insbesondere nach Feierabend.

Ganz besonders danke ich auch meinen Eltern für deren Unterstützung.

Die finanzielle Unterstützung der Dissertation erfolgte durch den Schweizer Nationalfonds (Projekt Nr. 21-55531.98).